POLITECNICO DI MILANO

School of Industrial and Information Engineering

Master of Science in MECHANICAL ENGINEERING

Mechanical performance of metal tubes filled with metal foams: prototype parts for machine tools and helicopters

Supervisors:

Prof. MATTEO STRANO

Prof. PHILIPPE BOCHER (ÉTS de Montréal)

Master of science Thesis of:

ANDREA BELFIGLIO

Registration n°: 765060

ACADEMIC YEAR 2012-2013

Dedico questa tesi a mio padre Carlo,
mia madre Angela e mio fratello Matteo,
che con il loro supporto mi hanno
permesso di raggiungere questo
importante traguardo con serenità.

Acknowledgements

At the end of this journey I would like to express my gratitude to all of you who have supported me over the past 5 years of my studies. In particular sincere thanks go to all those people who have permitted the development of my internship, result of the collaboration between MUSP and university ÉTS (*École de technologie supérieure*) *de Montréal.*

I would like to begin by thanking my supervisor Professor Matteo Strano for his guidance, patience and support while completing all stages of my thesis including my internship at the ÉTS in Canada.
I would also like to thank engineers Valerio Mussi, Andrea Rossi and Massimo Goletti for their technical expertise and availability.
I extend my gratitude to all staff of the research laboratory MUSP, in particular to Professor Michele Monno for the opportunity to use the laboratory structures necessary to advance and perform my analysis.

My special thanks go to Professor Philippe Bocher for his hospitality, instruction and assistance during my stay at ÉTS.
Moreover, I thank Serge Plamondon and engineers Mourad Kedadouche, Nicolas Vanderesse and Alexandre Vigneault for their consistent help during the experimental tests.

My profound gratitude also goes to Alan R. Colle, Mathieu Ruël and Eric Thibault of the Bell Helicopter Textron Canada Company for their availability and interest shown during the presentation of my work.

Last but certainly not least, I would like to thank my family whose permanent support, trust and love have been fundamental throughout these years. In

particular, a very special thanks to my parents for their encouragement and their help, without you I would not be the person I am today.

Index

List of the figures

List of the tables

Abstract

The aim of this work, executed through a partnership between MUSP (*Macchine utensili e sistemi di produzione*) and university ÉTS (*École de technologie supérieure*) de Montréal, is to study the mechanical performances of steel and titanium tubes filled with different types of metal foams, focusing the attention on the following aspects: energy absorption, damping capacity and fatigue behaviour. The study is divided in two main parts relating to two different application fields: machine tools and helicopters.

In particular three models of machine tool portal, constituted by three steel samples, have been submitted to a dynamic analysis before and after the filling in order to understand the dynamical effect of different types of metal foam (aluminum foam and hybrid foam polymer-aluminum). Moreover after this first analysis all samples have been subjected to cyclic three-points bending tests simulating a certain number of work cycles, after which, they have been dynamically analysed again to understand what was the influence of work cycles on metal foam properties. Titanium samples filled with aluminum foam have been instead submitted to cyclic three-points bending tests and quasi-static compression tests in order to analyse their performances when subjected to these conditions of load. Particular attention has been given to the cyclic bending tests executed to investigate the behaviour of metal foam when subjected to “fatigue” tests (low number of cycles).

During the bending tests the acoustic emission (AE) of the samples, supposed to be strictly connected with any damages or cracks developing inside the specimens during the tests, has been monitored. The last step has been the microscopic inspection for the samples for which the trend of the AE parameters had indicated an internal damage developed during the bending tests. All the

results obtained have been finally shown to the company *Bell Helicopter Trexton Canada* in order to propose the use of metal foam filled tubes in helicopters field and find in which direction it is possible to proceed towards a specific application.

Keywords: metal foams, energy absorption, damping capacity, fatigue behaviour, machine tools, helicopters, dynamical analysis, three-points bending tests, acoustic emission.

Estratto

L'utilizzo delle schiume metalliche, come riempimento di componenti strutturali, è volto al miglioramento delle caratteristiche dei componenti stessi, in particolare riguardo l'assorbimento dell'energia e la capacità di smorzamento. Lo scopo di questo lavoro, eseguito grazie ad una collaborazione tra il laboratorio MUSP (*Macchine utensili e sistemi di produzione*) e l'università ÉTS (*École de technologie supérieure*) de Montréal, è quello di studiare le prestazioni meccaniche e dinamiche di tubi in acciaio e in titanio, riempiti con differenti tipologie di schiume metalliche. In particolare, lo studio è diviso in due parti principali riguardanti due differenti campi applicativi: le macchine utensili e gli elicotteri.

Nella prima fase sperimentale tre modelli di portale di macchina utensile, costituiti ognuno da tre campioni in acciaio a sezione quadrata, sono stati sottoposti ad analisi dinamica prima e dopo essere stati schiumati, al fine di comprendere l'influenza dei diversi tipi di riempimento (schiuma di alluminio e schiuma ibrida alluminio-polimero) sulle caratteristiche dinamiche dell'intera struttura prima e dopo un certo numero di cicli di lavoro. In particolare, successivamente alla prima analisi dinamica, tutti i campioni sono stati sottoposti a prove di flessione ciclica su tre punti, al fine di simulare i cicli di lavoro, monitorandone la deflessione, il segnale di vibrazione e l'emissione acustica, al fine di avere la certezza di far lavorare in modo significativo i campioni senza danneggiarli, per poter ripetere l'analisi dinamica effettuata precedentemente e valutare, se e come, varia il contributo dei riempimenti.

La seconda fase del lavoro ha invece riguardato l'analisi del comportamento di tubi in titanio riempiti con schiuma di alluminio sottoposti a compressione quasi statica e prove di flessione ciclica su tre punti, alle quali è stata data particolare

attenzione, al fine di studiare il comportamento della schiuma di alluminio in condizioni di fatica a flessione per un basso numero di cicli. I test di flessione sono stati seguiti da un'analisi al microscopio finale, eseguita su quei campioni per i quali i parametri relativi al segnale di emissione acustica fornivano indicazioni particolari suggerendo lo sviluppo di possibili danneggiamenti interni. Tutti i risultati ottenuti sono stati infine presentati alla compagnia *Bell Helicopter Trexton Canada* al fine di proporre l'utilizzo dei materiali studiati nel campo elicotteristico e individuare una direzione in cui procedere nelle ricerche future verso applicazioni specifiche.

Parole chiave: schiume metalliche, assorbimento dell'energia, capacità di smorzamento, macchine utensili, elicotteri, analisi dinamica, prove di flessione su tre punti, comportamento a fatica, emissione acustica.

Nomenclature

x_f	Generic property of the foam
x_s	Generic property of the material of the cell wall of the foam
k	Constant comprised between 0.1 and 4 depending on the structure of the foam.
z	Constant comprised between 1.8 and 2.2 depending on the structure of the foam.
E	Young's modulus
G	Shear modulus
ρ	Density
σ_y	Elastic limit
σ_{pl}	Plateau stress
ε_D	Densification strain
η	Mechanical loss coefficient
C_P	Specific heat
λ	Thermal conductivity
W	Energy absorbed per unit volume
δ	Damping
$\dot{\varepsilon}$	Strain rate

N	Number of vibrations
σ_u	Upper boundary stress
σ_l	Lower boundary stress
σ_a	Semi-amplitude of stress applied in fatigue tests
c	Damping coefficient
c_c	Critical damping coefficient
b	Base of the cross-section of steel square tubes
h	Height of the cross-section of steel square tubes
t	Thickness of the wall of steel square tubes
l	Distance between the lower supports of the fixture for the three-points bending tests [ISO 7438]
a	Diameter of the circle inscribed inside the cross-section of the empty square tubes - Diameter of the test piece [ISO 7438]
D	Diameter of the former and the lower supports of the fixtures [ISO 7438]
d	Distance between the axes of the lower supports of the fixture for the three-points bending tests
n	Number of three-points bending cycles
F_x	Cutting force in direction x
F_y	Cutting force in direction y
F_z	Cutting force in direction z

k_{mp} Stiffness of the model of the portal composed by the three steel samples

k_s Stiffness of the model representing the simplification of the real tool machine considered as reference

D_e External diameter of titanium tubes

D_i Internal diameter of titanium tubes

I Second moment of area

L Length of the sample

P_{cr} Critical load

L_c Effective length of the samples subjected to static compression tests

μ Parameter depending on the type of constraints

Chapter 1

Metal foams:
production, properties and applications

The metal foams are part of the big family of cellular materials, that are biphasic materials within which a solid phase and a gas phase coexist. A cellular solid is one made up of an interconnected network of solid struts or plates which form the edges and faces of cells, and appear widely in nature: examples include wood, cork, corals and bones. Man has made use of these natural cellular materials for centuries: the pyramids of Egypt have yielded wooden artefacts at least 5000 years old, and cork was used for bungs in wine bottles in Roman times. More recently man has made his own cellular solids and nowadays almost any solid can be foamed, to the point that techniques now exist for making three-dimensional cellular solids out of polymers, metals, ceramic and even glasses. Man-made foams (recyclable and non-toxic) are used for different applications due to their properties, such as absorption of the energy of impacts (in packaging and crash protection), thermal and acoustic insulation, lightweight structures, marine buoyancy and water-repellent membranes. [1]

Most commercially available metal foams are based on aluminum or nickel but methods exist for foaming magnesium, lead, zinc, copper, bronze, titanium, steel and even gold, available on custom order. [2]

1.1 Making

Nine distinct kind of process have been developed to make metal foams, but only five are now established commercially. They fall into four broad classes:

1. Foam formed from the vapor phase;
2. Foam electrodeposited from an aqueous solution;
3. Foam depending on liquid-state processing;
4. Foam created in the solid state.

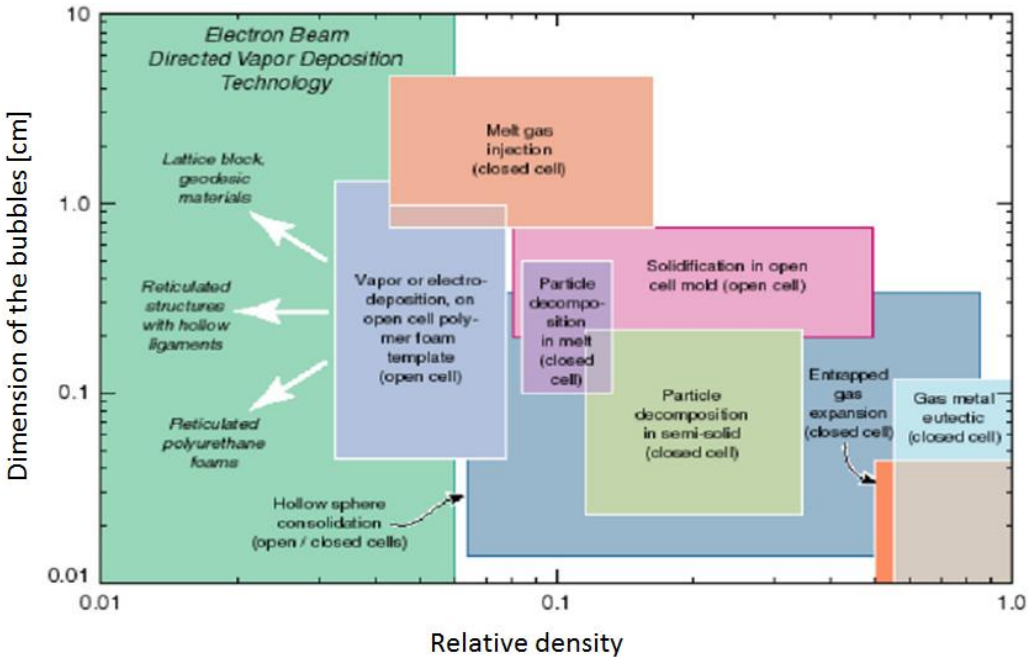

Figure 1.1: Relative density and dimension of the bubbles depending of the process used. [3]

Each method can be used with a small subset of metals to create a porous material with a limited range of relative densities and cell sizes; however some produce open-cell foams, others produce foams in which the majority of the cells, are closed.

Our process used to realize metal foam is the *particle decomposition in semi-solid* highlighted in light green in Figure 1.1. This kind of production gives the possibility to realize a foam characterized by closed cells, a limited relative density and a limited dimension of the bubbles. This gives advantages in terms of weight and performances, in fact the properties of metal foams, as for other cellular metal structures, depend upon the properties of the metal, the relative density and the cell topology. As already said foams are made by one of the nine processes listed synthetically below:

1. Bubbling gas through molten Al-SiC or Al-Al_2O_3 alloys [Al, Mg].
2. By stirring a foaming agent (typically TiH_2) into a molten alloy (typically an aluminum alloy) and controlling the pressure while cooling [Al].
3. Consolidation of a metal powder (aluminum alloy are the most common) with a particulate foaming agent (TiH_2 again) followed by heating into the mushy state when the foaming agent releases hydrogen, expanding the material [Al, Zn, Fe, Pb, Au].
4. Manufacture of a ceramic mold from polymer-foam precursor, followed by a heating, to let the polymer evacuate and fill the mold with molten metal in pressure [Al, Mg, Ni-Cr, stainless steel, Cu].
5. Vapor phase deposition or electrodeposition of metal onto a polymer foam precursor [Ni, Ti].
6. Trapping of high-pressure inert gas in pores of a pressed powder sample, followed by the expansion of the gas at elevated temperature [Ti].
7. Sintering of hollow spheres, made with a modified atomization process, or from metal-oxide, or hydride spheres followed by reduction or dehydration, or by vapor-deposition of metal onto polymer spheres [Ni, Co, Ni-Cr alloys].

8. Co-pressing of a metal powder with a leachable powder, or pressure-infiltration of a bed of leachable particles by a liquid metal, followed by leaching to separate soluble and insoluble elements and obtain the metal-foam skeleton [Al, with salt as the leachable powder].
9. Dissolution of gas (typically, hydrogen) in a liquid metal under pressure, allowing it to be released in a controlled way during subsequent solidification [Cu, Ni, Al].

Only the first five of these are in commercial production.[2] Figure 1.2 summarizes all of them, in particular is highlighted the method used in our experimental tests.

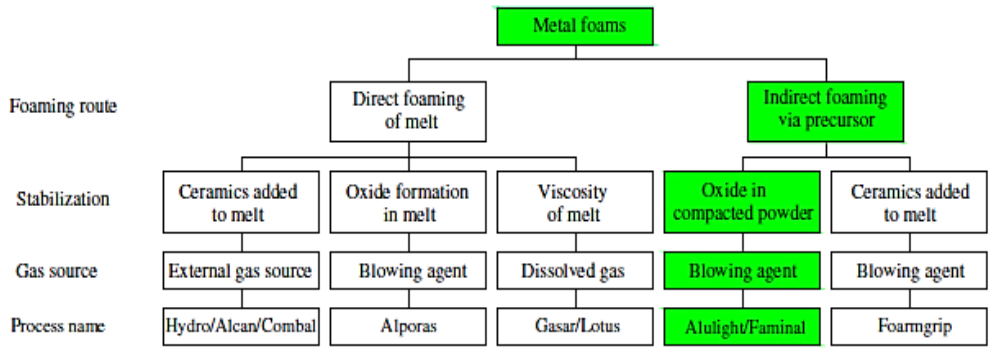

Figure 1.2: Summary diagram in which are described the five methods used in commercial production to manufacture metal foams. The highlighted process is the one used in our experimental tests. [3]

As described in Figure 1.2 in the process used for our experimental tests, a foaming agent is introduced in the solid metal, through the mixing and consolidation of powders. This mix is then extruded obtaining round or square precursors with density similar to the pure aluminum one. The precursor is finally inserted into apposite molds and reheated in furnace as represented in Figure 1.3.

Figure 1.3: Example of precursors inserted in a mold for the production of cylindrical foam samples.

The Titanium hydride (TiH_2) normally used as foaming agent, starts to decompose at about 465 °*C*, lower temperature than the melting temperature of pure aluminum (660 °*C*) and its alloys, releasing hydrogen and letting the semi-solid expand in order to permit the making of the foam. The final cooling gives stability to the product. [2]

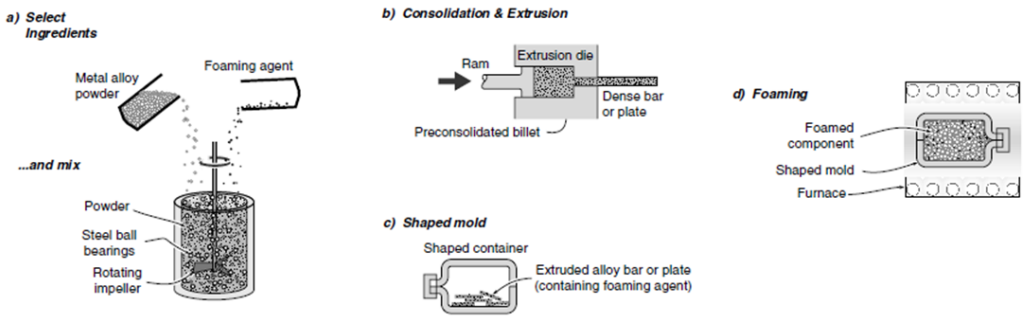

Figure 1.4: Steps representing the manufacture of metal foams, by gas realising particles in semi-solids. [2]

The most suitable method to create the precursor is the utilization of a hot press represented in Figure 1.5.

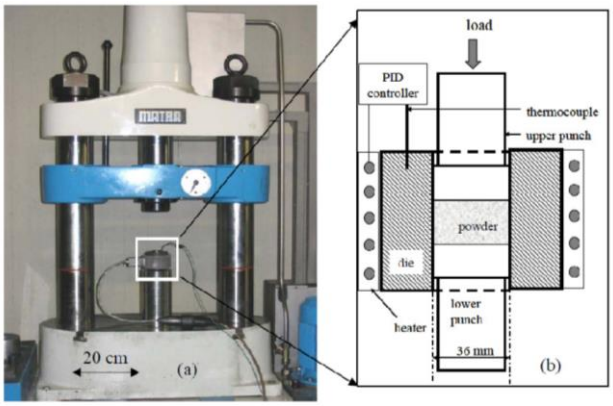

Figure 1.5: Hot press for the production precursors. [3]

This technique permits to obtain precursors homogeneous in characteristics but with limited length because of the limited maximum load of the machine, which doesn't allow to do a continuous process.

Note how, not having this equipment in our laboratory, we usually buy precursors from the supplier Alulight, which produces them in bars of diameter of 10.5 *mm* containing 99.2% of AlMg1Si0.6 and 0.8% of TiH_2, with a linear density, experimentally calculated, of 0.227 *g/mm*. The process followed by Alulight is different from the one described before: the powders mix is inserted in a particular device, dragged into rotation and pushed in the area of extrusion, permitting a continuous production of the precursor to the detriment of homogeneity of the characteristics (Figure 1.6).

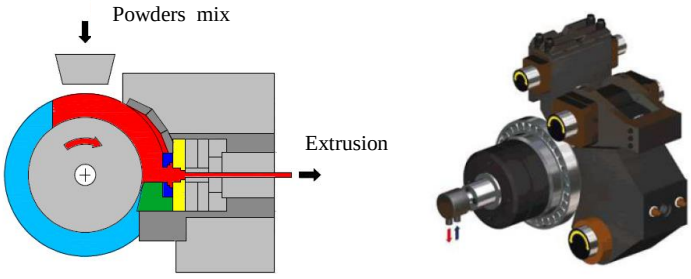

Figure 1.6: Alulight process for the production of precursors. [3]

Figure 1.7: Example of Alulight precursors obtained with the Alulight procedure described above.

1.2 Properties: an overview

The characteristics of metal foams are best summarized by describing the material from which they are made, their relative density ρ/ρ_s (where ρ is the foam density and ρ_s is the density of the material of the cell wall) and stating whether they have open or closed cells (Figure 1.8). According with what just said, foams are usually subdivided in two big classes:

- Close-cell foams;
- Open-cell foams. [21]

Close-cell foams are constituted by closed adjacent spheres containing gas. The material of the cell wall is principally confined between three or more adjacent spheres conferring high mechanical properties because the cell walls, although thin, give an additional contribution to rigidity. In open-cell foams the spheres are instead interconnected because the thin membrane typical of the closed cell structure is perforated during the process of expansion and stabilization.

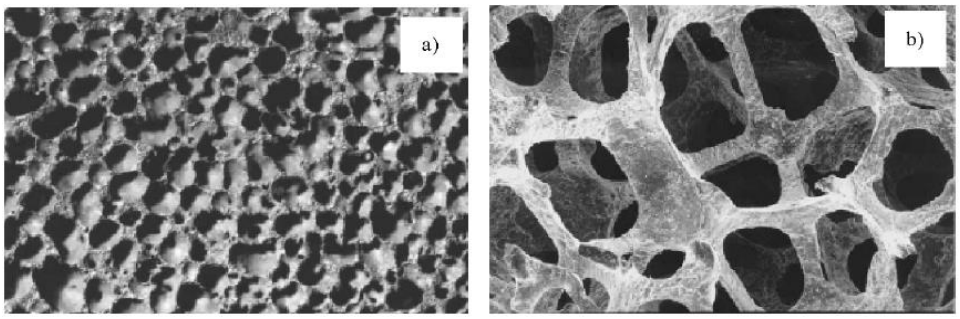

Figure 1.8: a) Close-cell foam. b) Open-cell foam. [9]

In reality most of the foams has an intermediate morphology. For that reason one speaks of the degree of openness of the cells. Of course with a different structure (different degree of openness of the cells due to the process used for the foaming process), the physical characteristics and the mechanical properties of the foam, change independently from the intrinsic properties of the base material. In Figure 1.9 is possible to see how changing the degree of openness of the cells, changes the application of reference.

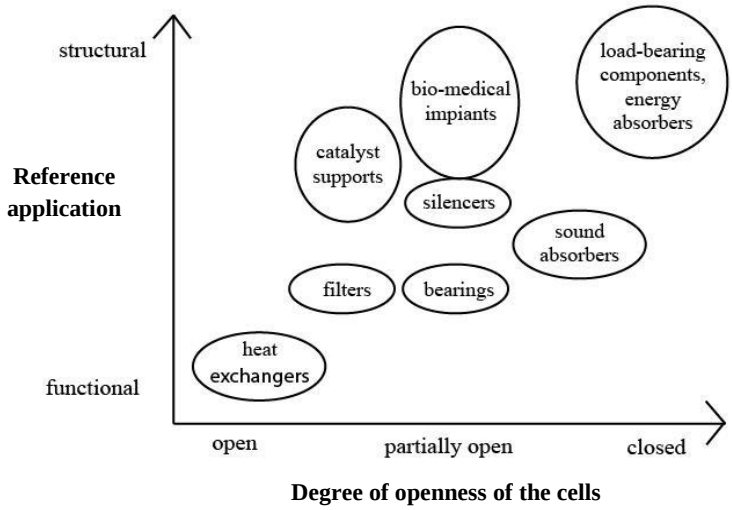

Figure 1.9: Application depending on the degree of openness of the cells. [5]

However most of the properties of the foams follows a general law, which is function of the relative density and the structure of the metal foam, and can be written as follows:

$$\frac{x_f}{x_s} = k \cdot \left(\frac{\rho}{\rho_s}\right)^z$$

Where x_f and x_s represent respectively a generic property of the foam and the correspondent solid, k and z are constants whose values, respectively comprised between 0.1 and 4 and 1.8 and 2.2, depend on the structure of the foam. For example considering E and G:

$$\frac{E_f}{E_s} = k \cdot \left(\frac{\rho}{\rho_s}\right)^z$$

$$\frac{G_f}{G_s} = \frac{3}{8} k \cdot \left(\frac{\rho}{\rho_s}\right)^z$$

Performance indices help identify the applications in which a material might excel. An important instrument of comparison is represented by the Ashby charts which show on the same graph a series of different materials as a function of two variables of interest (for example E vs ρ - Figure 1.10). These charts have the following characteristics:

- Logarithmic scale to permit the comparison between very different materials;
- Envelopes, group together materials of the same family (for example wood - glass - metal);
- The bubbles show the range of variability for each particular material;
- Each chart contains design guidelines: materials on the same guideline have the same value of the index considered.

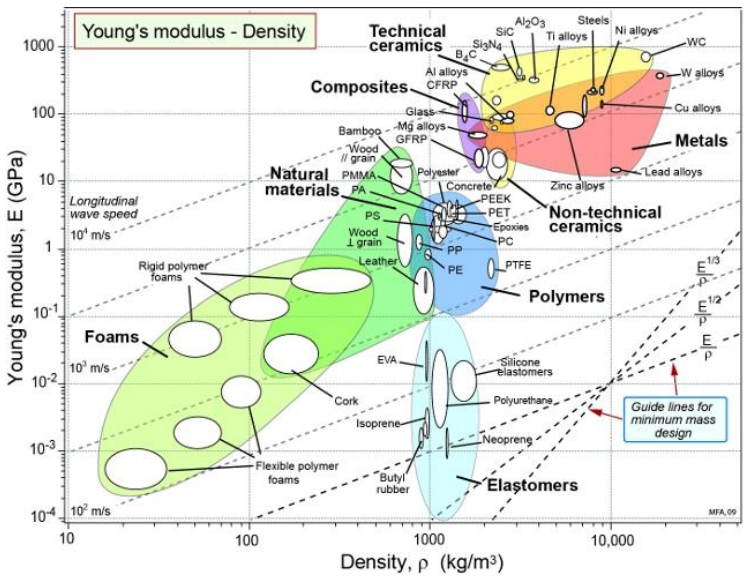

Figure 1.10: Ashby chart Young's modulus - Density. [45]

The comparison between metal foams and other engineering materials reveals that metal foams have interesting value for the following indices:

1. The index $E^{1/3}/\rho$ which characterizes the bending-stiffness of lightweight panels. A foam panel is lighter, for the same stiffness that one of the same material which is solid.
2. The index $\sigma_y^{1/2}/\rho$ which characterizes the bending-strength of lightweight panels (σ_y is the elastic limit). A foam panel is stronger, for a given weight, than one of the same material which is solid.
3. The exceptional energy-absorption ability of metal foams is characterized by the index $\sigma_{pl} \cdot \varepsilon_D$ which measures the energy absorbed in crushing the material up to its 'densification' strain ε_D (σ_{pl} is the plateau stress).
4. The index $\eta \cdot E^{1/3}/\rho$ which measures the ability of a panel to damp flexural vibrations (η is the mechanical loss coefficient). High values of this index capture both high natural flexural vibration frequencies of metal

foams (suppressing resonance in the acoustic range) and the ability of the material to dissipate energy internally.

5. The index $C_P \cdot \rho \cdot \lambda$ which characterizes the time-scale for penetration of a thermal front through an insulating layer of a given thickness and also the total thermal energy lost in the insulation of an oven in a thermal cycle (C_P is the specific heat and λ is the thermal conductivity). In both case low values are sought and foams offer these. [2]

Because of the reference applications considered in this project (machine tools and helicopters fields), in the following paragraphs we focus on absorption of energy and damping capacity of metal foams.

1.3 Absorption of energy by plastic work

The fundamental characteristic for a good energy absorber is the ability to withstand high strain at an almost constant level of stress. Considering the schematic curve stress - strain for a metal foam submitted to compression (Figure 1.11) , we can see how the behaviour meets the characteristic indicated above:

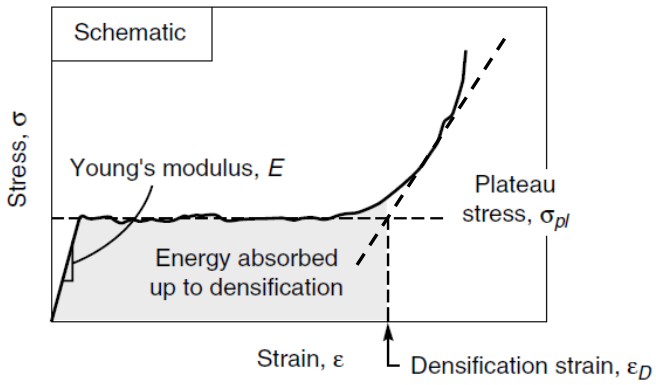

Figure 1.11: Schematic compression curve for a metal foam. [32]

The area under the curve, roughly $\sigma_{pl.}\,\varepsilon_D$, measures the energy that the foam can absorb, per unit initial volume, up to the end of the plateau. Note how σ_{pl} is the first peak in strength which represents the first cell band collapse and ε_D is the onset of densification identified by the intersection of tangent to the stress - strain curve for the cell wall collapse regime and the densification regime.

Note also how the stress - strain response of the foam exhibits *three distinct regimes*; a linear elastic regime at very low stresses, followed by a long stress - strain plateau wherein localized plastic collapse propagates from one cell to another. When all the cell collapse we reach the third regime which manifests in the curve in truncation of the plateau region and a rapid rise in stress with further strain (begin of the densification of the foam). [12]

Theoretically in order to have the best energy absorption we need a trend of the curve stress - strain as rectangular as possible, so the best behavior for an energy absorber is the one of an elastic material perfectly plastic. For that reason foams have excellent energy absorption ability because show a very similar trend with just a small slope of the curve.

The behavior of the foam depends from different factors such as for example the density, the strain rate and the direction of application of the load respect to the direction of foaming.

1.3.1 Influence of density

From different studies carried out by many authors is clear how the absorption of energy increases with an increment of density and this dependence is not linear.

Hall et al. [11] have studied the dependence of the curves stress-strain obtained submitting cylindrical specimens of aluminum foam to quasi-static compression tests conducted using a displacement controlled machine at an initial strain rate of 1.5 x 10^{-3} s^{-1} and high strain rate compression tests conducted at a strain rate of ~ 2.0 x 10^{-3} s^{-1}. The foam was prepared using 6061-Al alloy powder and TiH_2 as foaming agent and supplied as rectangular plate (50 *mm* thick and 100 *mm* wide) with a typical closed cell structure.

Quasi - static compression tests

Figure 1.12 shows the quasi-static compressive engineering stress-strain curves obtained from 3 samples of each of the lowest and highest density foams, respectively 0.82 g/cm^3 e 0.34 g/cm^3.

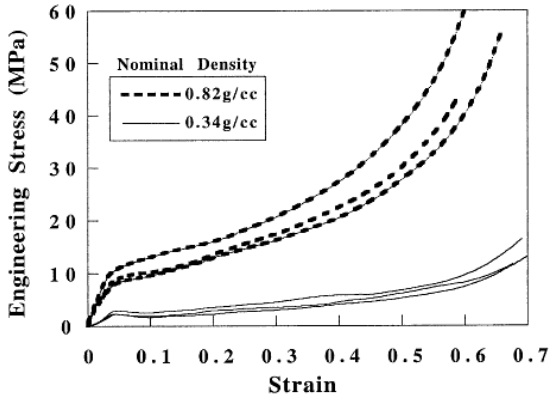

Figure 1.12: Quasi-static stress vs. strain curves for samples of two different nominal density. [11]

It is clear how the curves show the typical shape which may be divided into *three distinct regimes* previously defined for the schematic representation. Looking at the figure it is possible to observe that:

- The flow stress and the rate of densification are function of the relative density and particularly they increase with an increment of density ;

- The energy absorption too depends from the density, increasing with an increase of it;
- For the low density foams a load drop occurs after the initial elastic extension while the higher density ones exhibited no load drop;
- Stress oscillations occur in the collapse region of low density samples while the higher density ones showed an essentially monotonic increase in stress throughout the tests.

High strain rate compression tests

Figure 1.13a shows the high strain rate compressive engineering stress-strain curves obtained from 3 samples of respectively 0.84 g/cm^3, 0.45 g/cm^3 and 0.31 g/cm^3.

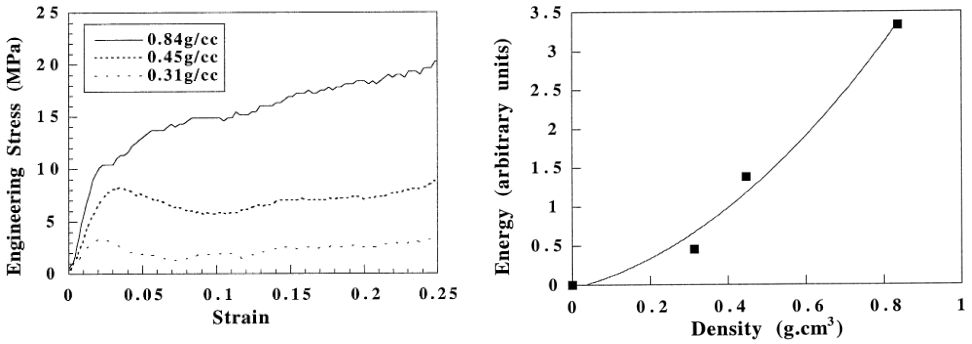

a) b)

Figure 1.13: a) Stress vs. strain curves at 2.0 x 10-3 s^{-1} for samples of three different densities, b) Energy absorbed as a function of density, between 5% and 25% of strain. [11]

Looking Figure 1.13a it is clear how again, the flow stress values and the energy absorption, represented by the area under the stress - strain curve, are strong function of relative density. Furthermore, calculating the areas under the curves between 5% and 25% of strain and plotting the values in function of density, it is possible to obtain the results showed in Figure 1.13b from which we can

observe how the dependence of the energy absorption from the density it is not linear.

Flexural tests

Yu et al. [16] have studied the flexural strength as function of the foam density. The tests were carried out in three-points bending tests with rectangular samples (200 *mm* long x 25 *mm* wide x 20 *mm* thick). The resulting bending strength, and so the absorption of energy, was found to vary linearly with the density in a logarithmic plot as shown in Figure 1.14.

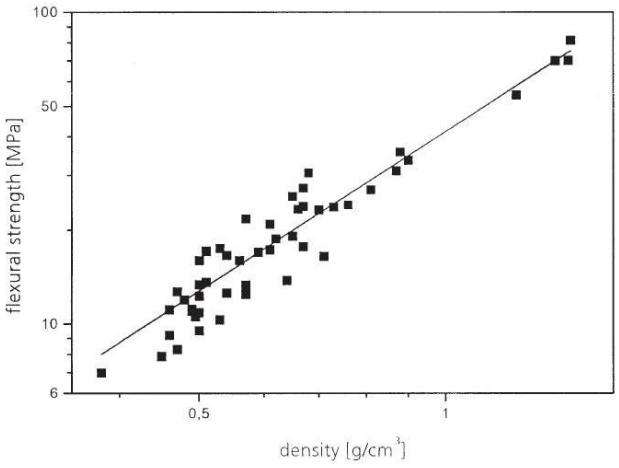

Figure 1.14: Dependence between the flexural strength and the density on logarithmic scale. [16]

1.3.2 Influence of strain rate

Regarding the influence of the strain rate, there is not an univocal opinion. In fact in literature it is possible to find studies developed by several authors whose conclusions are very different because of the different test parameters used.

In particular Figure 1.15a shows the results obtained by Hall et al. [11], who have tested in compression foam samples of individual measured density of 0.52 g/cm^3, over a range of strain rates from $1.5 \cdot 10^{-3}\ s^{-1}$ (quasi - static) to 2 x $10^3\ s^{-1}$. As we can see there is no unequivocal effect of strain rate within this strain range and the areas under the curves are approximately equal. The same result has been obtained by Deshpande et al. [31] through compression tests on Alulight foam at strain rates of $10^{-3}\ s^{-1}$ and 3000 s^{-1} (Figure 1.15b). The absence of marked strain rate sensitivity is in agreement with other studies on this and other aluminum alloys such as the one developed by Youn et al. who have obtained the same results using lower strain rates (0.01 s^{-1} and 10 s^{-1}).

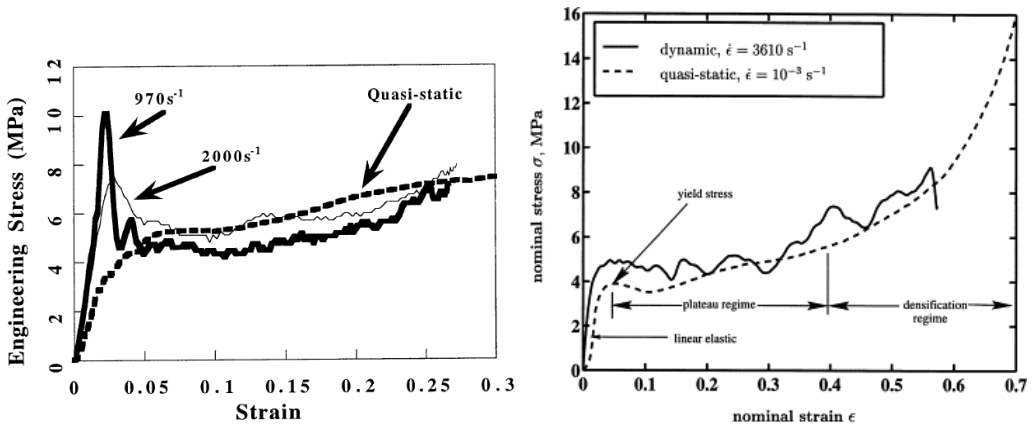

a) b)

Figure 1.15: a) Typical stress-strain curves for 3 samples of 0.52 g/cm^3 of density, submitted to different strain rate [11], b) Comparison between quasi-static and dynamic compression of Alulight, density 0.17 g/cm^3. [31]

Paul et al. [12] have instead obtained different results from their studies executed submitting rectangular samples of Alporas aluminum foam to compression tests characterized by strain rates from $3.3 \cdot 10^{-5}\ s^{-1}$ to $1.6 \cdot 10^{-1}\ s^{-1}$. As shown in Figure 1.16a and Figure 1.16b, σ_{pl} and the absorption of energy are function of the strain rate.

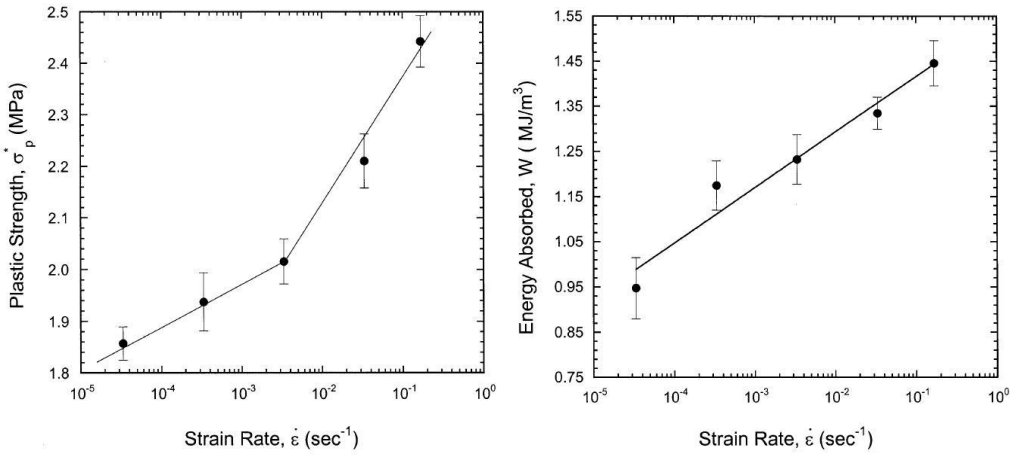

a) b)

Figure 1.16: a)Variation in the plastic strength σ_{pl}, with the nominal strain rate. b)Variation in the energy absorbed with the nominal strain rate. [12]

Obviously because the plateau strength increases with the strain rate, the energy absorbed per unit volume (W) also increases with the strain rate because of an increase in area under the σ - ε curve. However the W - $log(\dot{\varepsilon})$ plot doesn't exhibit the same bilinearity shown by the σ_{pl} - $log(\dot{\varepsilon})$ plot because of the different mechanism of deformation of the cells for different strain rates.

Analogous results for Alporas foams have been obtained also by Mukai et al. [32] and Cady et al..[33]

1.3.3 Influence of direction of load

Banhart et al. [13] have instead conducted a study regarding how the testing direction influences the deformation characteristics. The aluminum foam samples used for compression tests (dimensions 40x40x40 mm^3 and density between 0.2 and 0.8 g/cm^3) were manufactured using precursors produced through the powder-metallurgical Fraunhofer process.

In a first series of measurement were tested samples which had two closed outer opposite surfaces originating from the foaming process and four sides where the porosity was open owing to cutting. The testing direction of the compression tests was chosen in parallel and perpendicular to the closed outer surfaces as represented in Figure 1.17a and 1.17b just above the curve stress - strain obtained:

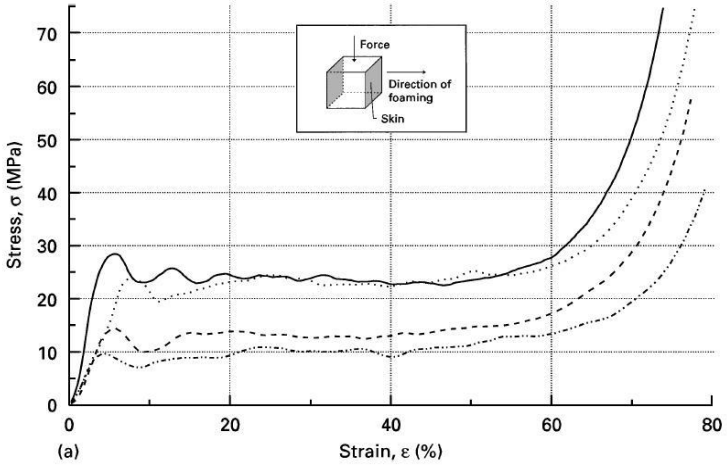

a)

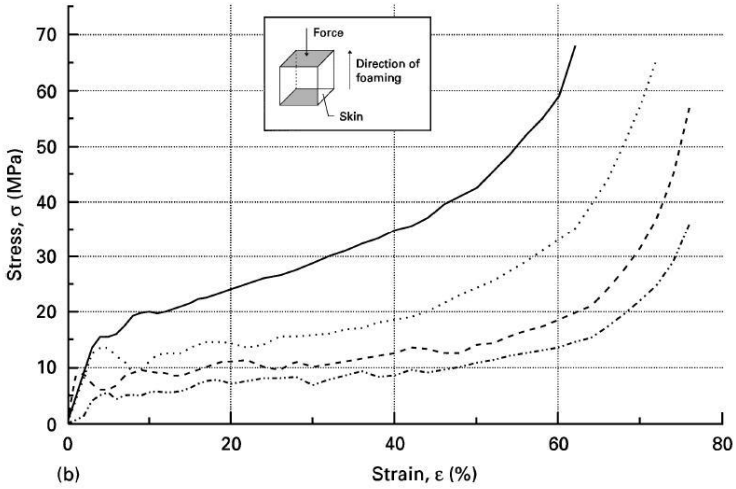

b)

Figure 1.17: Stress-strain curves resulting from the compression tests a) Testing direction parallel to the closed outer surfaces b) Testing direction perpendicular to the closed outer surfaces. [13]

As one can see easily, the orientation of the closed skin with respect to the testing direction influences the deformation characteristics in a very pronounced way. In Figure 1.17a the stresses before the onset of strong plastic deformation and therefore the compression strength are much higher than in Figure 1.17b. Moreover, in the plateau regime the stress curve is nearly horizontal in Figure 1.17a, while no range of constant stress can be observed in Figure 1.17b except for the foams with very low densities.

The reason for the observed stress-strain curve of the samples tested with a load parallel to the closed skin is the supporting effect of the vertically arranged densified outer foam sections, which would show a typical buckling behavior (characterized by a high initial strength peak and a subsequent drop in strength) without the connected foam. The combination of these outer sections with the foam results in a superposition of this buckling behavior with the properties of the bare foam.

A further possible reason for the observed difference between the two stress-strain curves could be also the anisotropy of the foam itself. For that reason Banhart et al. have tested also foam samples without any closed surfaces again in both directions, perpendicular and parallel respect to the direction of foaming (Figure 1.18).

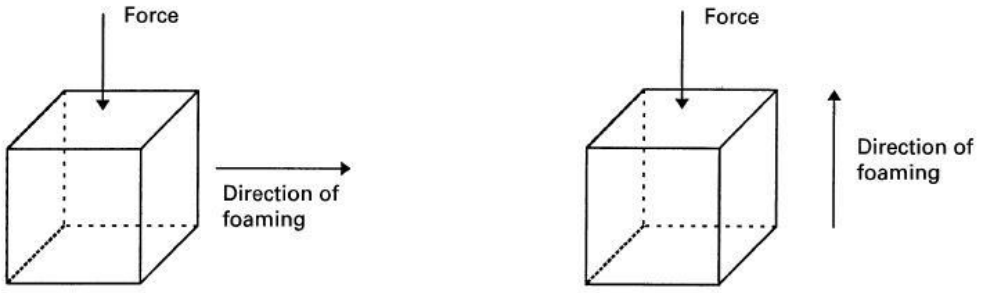

a) b)

Figure 1.18: Samples of aluminum foam without any closed surfaces a) Force perpendicular to the direction of foaming, b) Force parallel to the direction of foaming. [13]

The resulting compression strengths are compared with each other in Figure 1.19 where we it is possible to observe how the samples with a parallel orientation of foaming and testing direction show a slightly higher compression strength than the sample with alternative orientation. The reason for the slight anisotropy is probably the deviation of pore sizes from sphericity obtained during the foaming process.

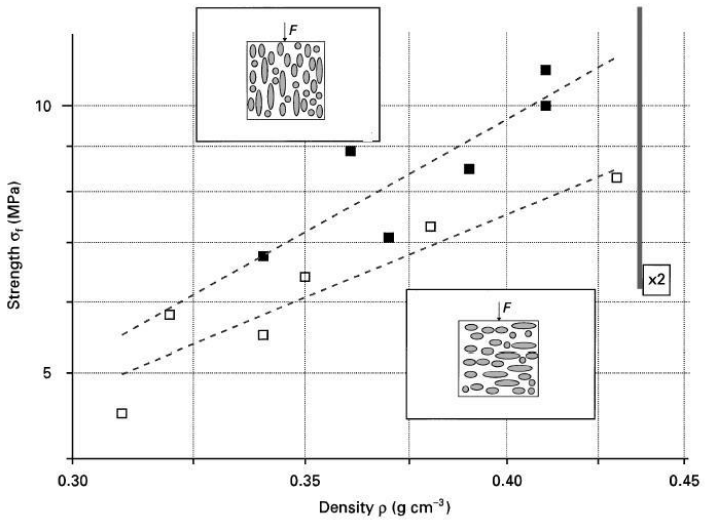

Figure 1.19: Compression strength of aluminum foam with the foaming direction oriented in parallel and perpendicular to the force orientation.

However the difference between the two orientations of load is not as pronounced as between the two skin orientations compared before. [13]

1.3.4 Influence of geometry

Furthermore Pan et al. [14] have studied the influence of geometry on energy absorption ability of closed-cell metal foams. In particular they have carried out

the compression tests on cubic and cylindrical samples obtaining the results showed in Figure 1.20.

They have concluded that the strain and the absorbing energy value decrease with the geometry size increasing. Moreover, with the increasing of material diameter, the compressive strength increases quickly while the strain reduces.

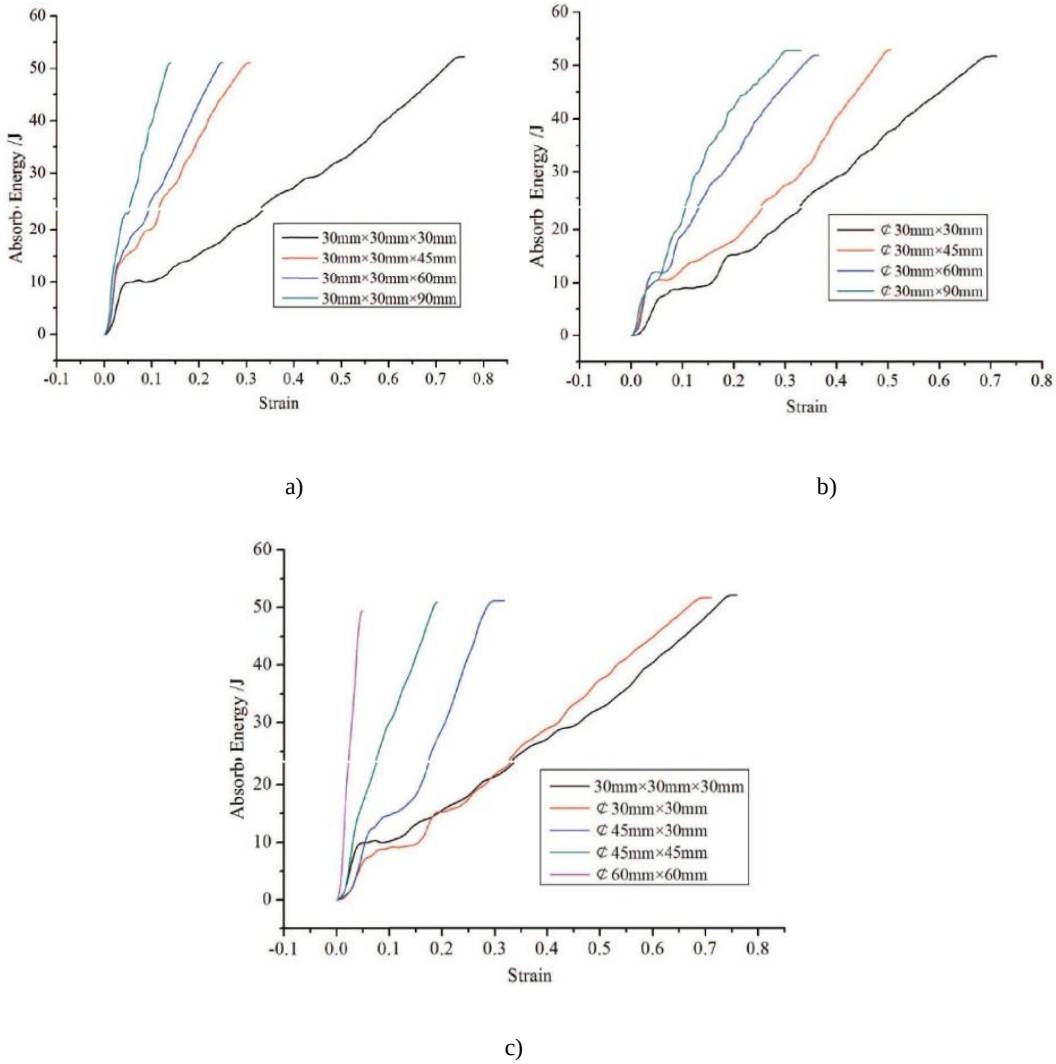

Figure 1.20: Energy absorption for samples of different length a) Cube, b) Cylinder, c) Comparison of energy absorption for different dimensions. [14]

1.4 Damping capacity

From the commercial viewpoint, aluminum foams have already found their application for sound and energy absorption when weight minimization is demanded. Very limited information is available as yet about mechanical damping and mechanism of internal friction in any type of cellular metals but it is known how most of the internal friction mechanism acting in dense metal, contribute to damping in cellular metallic materials.

As already said in *paragraph 1.3* when a compressive force increases, foams exhibit elasticity, elasto-plasticity and densification. In case of tension, a softening takes place instead of the plateau. Energy absorption due to compression is an advanced characteristic of cellular materials and, in particular, Al foams: energy is absorbed as the cell walls bend plastically, or buckle, or fracture, while the stress is limited by the long flat σ-ε plateau. If foams or other cellular metallic materials are applied for damping of mechanical vibrations, the energy losses in the first (elastic) and in the second (elasto-plastic) ranges of deformation are the most important. [19]

A explained by Bertolino et al. [22] to evaluate the possible utilization of foams as components in damping applications, it is important to know how the cycle frequency as well as the vibration amplitude affects the damping capacity of the material. When pseudoelastic foams are solicited in constrained compression, the deformation cycle is composed by an elastic deformation part and a region where the material deforms transforming to martensite. When the strain amplitude grows, the deformation associated with the martensitic transformation increases as compared to the elastic one, thus increasing the damping capacity. In particular Bertolino et al. have concluded that the specific damping capacity of the material remains independent of the cycling frequency between 0.01 *Hz*

and 20 *Hz* at fixed strain amplitudes between 0.1% and 0.6%. This is a useful frequency range when considering structural damping applications. In addition, they have found that the specific damping capacity increases with the increment of the applied strain amplitude, reaching around 40% at a strain amplitude of 1.6%.

Moreover Golovin et al. [19] [20] have shown how for cyclic tension-compression tests on Alporas aluminum foam the energy dissipated per cycle, represented by the area enclosed between the loading and unloading curves (Figure 1.21), depends from the number of cycles *N*.

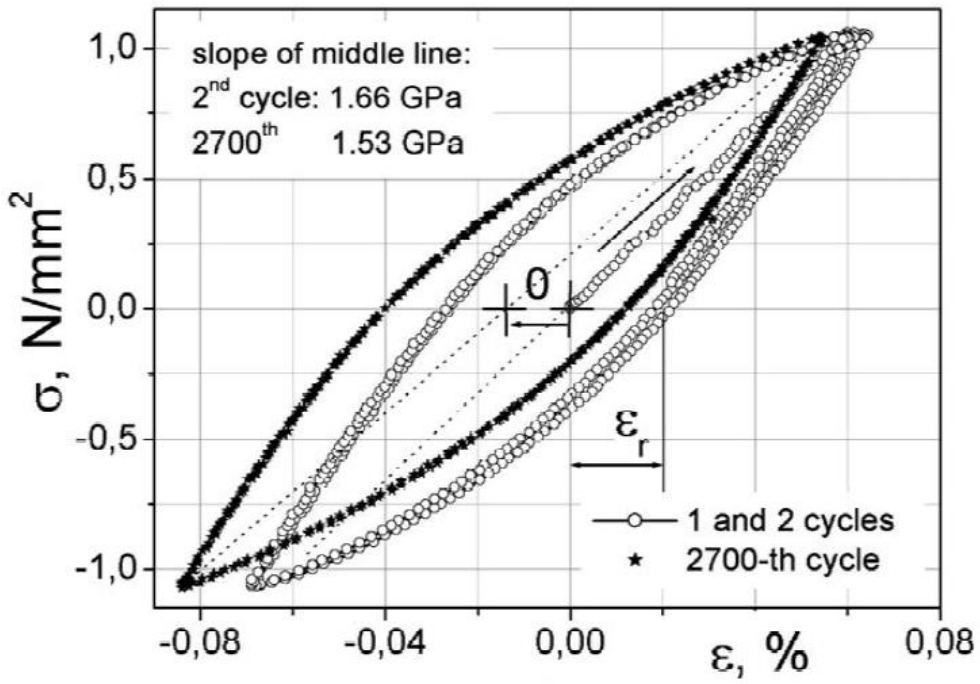

Figure 1.21: Cyclic tension and compression tests for 1, 2 and 2700 cycles. [19]

Similar dependencies are observed in damping tests (Figure 1.22): the damping δ increases both with the amplitude (ε) and number of vibrations (N).

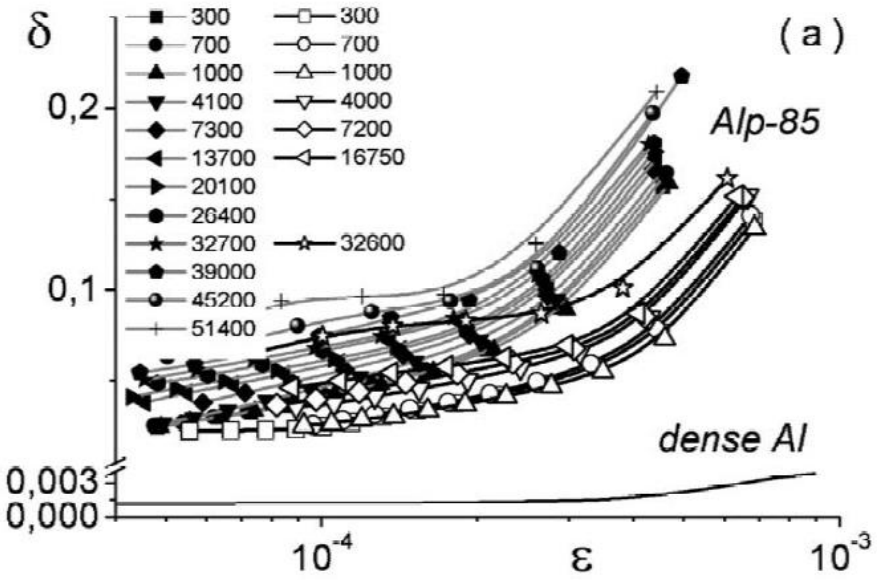

Figure 1.22: Diagram δ-ε for Alporas aluminum foam. [19]

Golovin et al. have studied damping in cellular metallic materials in a wide range of deformation amplitude concluding that it can sometimes be comparable with dense high damping metals, while their density is much lower. Moreover metal foams present also some advantages compared to the dense material they are made from. It can be also stated that density, pore size and other structural parameters, chemical composition, pre-deformation, time of vibration and air pressure inside the cells can influence the damping capacity via different structural mechanism.

1.5 Benefits due to the filling of empty tubes with metal foam

Not necessarily a simple structure of metal foam has excellent energy absorption capacity. Sometimes is possible to fill empty tubes of traditional materials, for

instance steel or aluminum, obtaining a final structure able to absorb energy in a better way.

Is known that thin-walled metal tubes are efficient energy absorbers when crushed axially where by “efficient” is meant that the energy absorbed per unit volume or per unit weight is high. When a foam is compressed, its cell walls bend and buckle at almost constant stress until the cell faces impinge. The tube behaves in a different way: it buckles into a series of regular folds until the fold faces come into contact (Figure 1.23). [4]

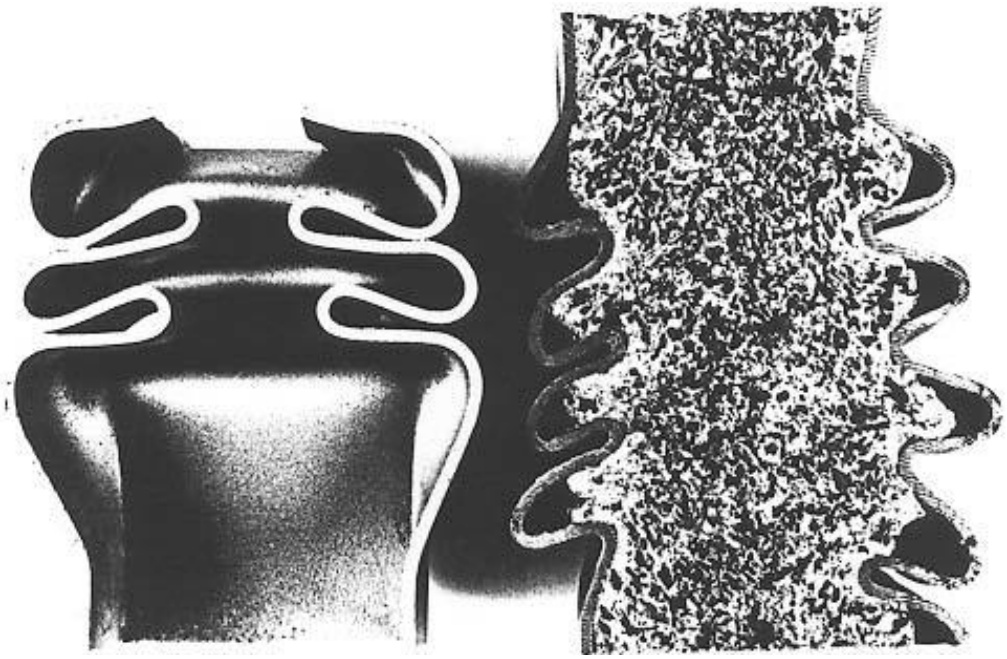

Figure 1.23: Sections of tubes with and without foam fillings, after partial crushing. [2]

Considering the load-deflection curves obtained by Ashby et al. [2] for the compression of foam, a tube and a foam filled tube (Figure 1.24), we can clearly see a different behaviour between the empty tube and the foam as previously said. In particular the tubes show regular wave-like oscillations of load, each

wave corresponding to the formation of a new fold, while the foam shows the typical behaviour already described in *paragraphs 1.3*. Figure 1.24 shows the gain in energy absorption made possible by filling tubes with metal foam. This synergistic enhancement is described by:

$$W^{Filled\ tube} = W^{Tube} + W^{Foam} + W^{Interaction}$$

Where $W^{Interaction}$ represent the additional energy absorbed, and arises from the interaction between the tube and the foam. This is because the foam provides internal support for the tube wall, shortening the wavelength of the buckles and thus creating more plastic folds per unit length. The same results have been obtained for instance by Banhart et al. [13] and Peroni et al. [35] in their studies on compression tests.

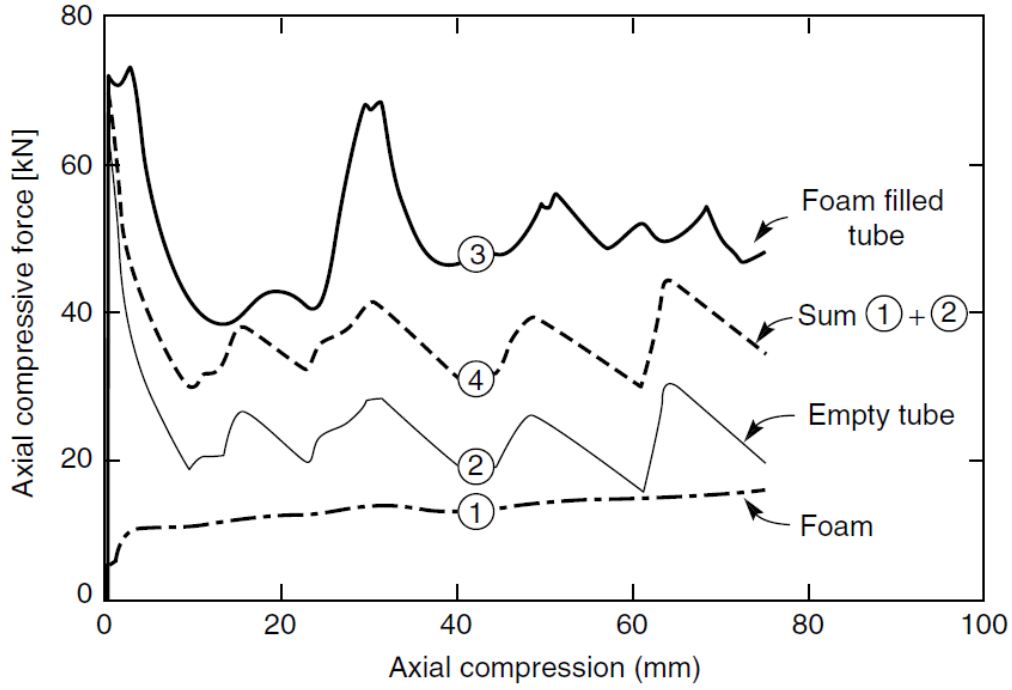

Figure 1.24: Load-deflection curves for a foam, a tube and a foam-filled tube in compression tests. [2]

In flection Peroni et al.[35] have obtained similar results. As shown in Figure 1.25 in fact, the sample of foam absorbs less energy respect to the tube and the foam filled tube but the filling, in this condition of load, changes the collapse mechanism of the tube. Even if the foam breaks, the tube acts as a constraint and avoids the collapse of the foam owing to the bending. However the new mechanism due to the filling increases the stress traction on the wall of the tube, so the tube breaks, and load and energy absorbed both decrease (behaviour clear in Figure 1.25).

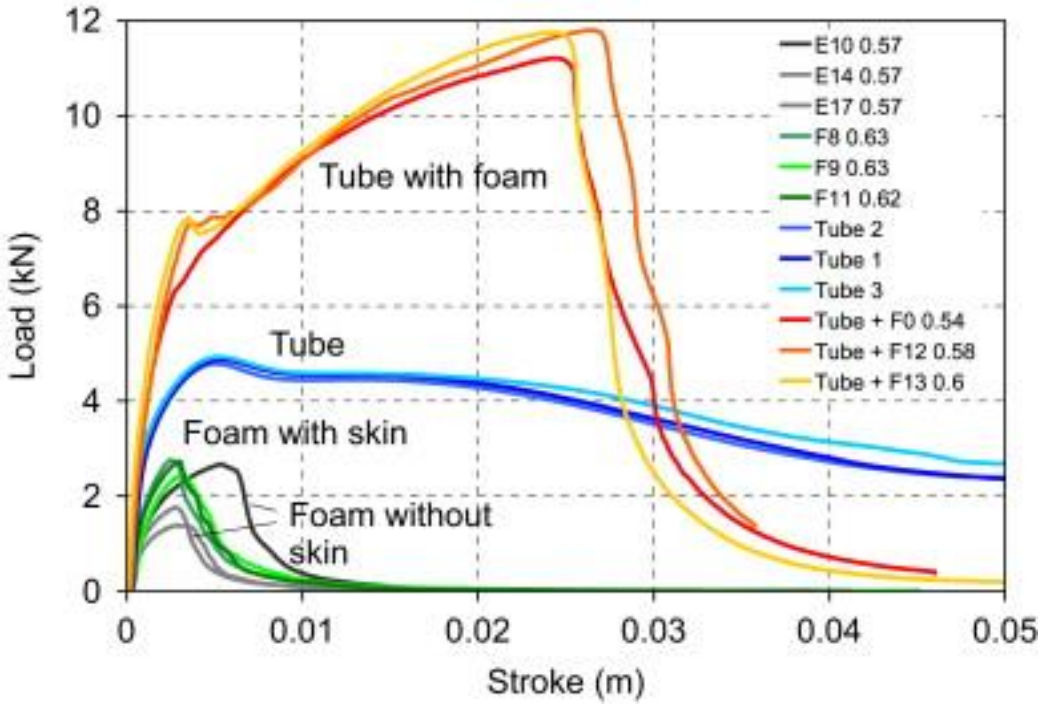

Figure 1.25: Load-Stroke curves for foam, empty tubes and foam-filled tubes submitted to flection. [35]

1.6 Examples of applications

The projections of the future fuel crisis, the requirements of achieving high fuel efficiency along with higher passenger safety in the automobile industry, and the

needs of creating light weight construction materials have attracted tremendous consideration for ultralight weight metallic foams. The use of metallic foams in these industrial sectors depends to a large extent upon their manufacturing cost, the environmental durability, and fire retardancy. In general, metallic foams possess a range of thermomechanical properties that suggest their application in areas demanding impact/blast amelioration, heat dissipation, acoustic isolation and heat exchange.

We can say that the existing applications of metallic foams cover a wide field and new uses are continually arising. It is difficult to list all the present and potential applications but it is possible to identify some examples to indicate the wide range of circumstances in which the metallic foams can be utilized. [15]

1.6.1 Energy absorbers and dampers

Application in impact-absorbing systems offer the greatest potential for the use of foamed metals. The possibilities range from automobile bumpers to clamping fixtures, protective envelopes for airborne equipment (crash recorders, for instance) and landing “feet” for space vehicles.

In many cases aluminum foam has proved itself a good energy absorbing material. It can be used for safety pads in system for lifting and conveying. In high-speed grinding machines (Figure 1.26a) by using it as an energy absorbing lining for the protective covers excellent results have been obtained. Aluminum foam is also suitable for forming the deformable zones of car bodies in front and behind the passenger compartment in order to improve the safety of car occupants (Figure 1.26b). Moreover it can be used for limiting vibrations in applications such as machine tools where high precision is required.

a)

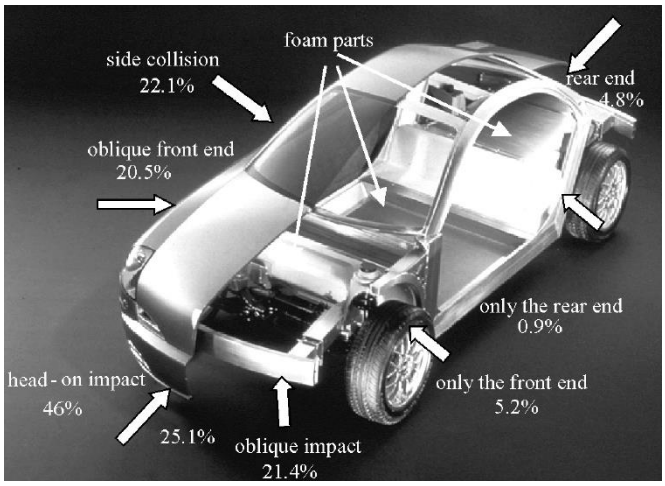

b)

Figure 1.26: a) High-speed grinding machine, [47] b) Karmann car with parts made of aluminum foam [10]

1.6.2 Filters

Porous filters are used for filtration of solid particles from streams of liquid, such as oil, gasoline, refrigerants, polymer melts, aqueous suspensions or from streams of air or other gases. The most widely used metallic filter materials are porous bronze and porous stainless steel. In some cases where exceptionally

high resistance to corrosion is required, precious metals can be used to advantage. For example, gold foam made by metallic deposition can be used for the coarse filtration of corrosive liquids.

Figure 1.27: Example of porous filters. [46]

1.6.3 Silencers

The acoustic properties of metallic foam are utilized in noise prevention. For example, the operation of reducing the pressure of gas being transported over long distances by high pressure pipe lines in order to feed the gas into local networks, produce very high-intensity noise which can travel along the pipe lines and reappear at long distances. Arrangements of metal foam have been designed which diffuse the gas gently, almost completely eliminating the noise, without serious interference with gas flow.
Metal foams have also been used in other cases of pressure reduction, such as in steam power station and exhaust mufflers for air tools and motor cars.

Figure 1.28: Example of a gas pipeline.

1.6.4 Thermal management and heat transfer

The thermal conductivities of metal foams are at least an order of magnitude greater than their non-metallic counterparts, so they are generally unsuited for simple thermal insulation though they can provide some fire protection. The thermal conductivities of closed-cell foams are, however, lower than those of fully dense parent metal by a factor of between 8 and 30, offering a degree of fire protection in, for instance, an automobile bulkhead between engine and passenger compartment. More important, open-cell metal foams can be used to enhance heat transfer in applications such as heat exchangers for airborne equipment, compact heat sinks for power electronics, heat shields, air-cooled condenser towers and regenerators.

Moreover metal foam, as previously mentioned, is significantly used as flame arrester in preventing, for instance, flame propagation along pipes and ventilating enclosures in dangerous atmospheres. It is an excellent material for this purpose because it is fire-proof and highly permeable which is consistent with flame stopping power.

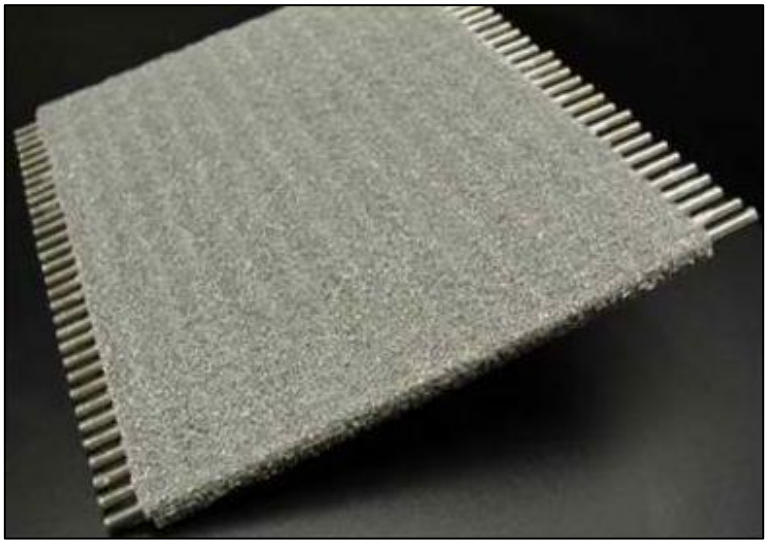

Figure 1.29: Lightweight metal foam heat exchanger. [48]

1.6.5 Other applications

To give an overview about other applications, we can say that:

- In the *chemical industry* metal foam is a highly absorbent material which combines lightness and strength with chemical inertness;
- The distinctive structural and other physical properties of metal foams make them useful as light weight *constructional materials*, especially where temperatures are in excess of 200 *°C*;
- For *electrochemical applications* porous metal is used to produce electrodes for alkaline batteries and for fuel cells;
- In *turbine constructions*, metal foam is of value as an abradable seal. To allow for small variations in the dimensions of the turbine case the abradable seal can be fitted so that the turbine blades can bite into it without excessive wear.

1.6.6 Future developments

Significant progress has been achieved in developing metal foams. As new materials with many unique properties, metallic foams may have far reaching use. New areas can be expected to be found in which metallic foams will constitute key elements enabling special devices or parts of unique properties to be constructed. However, foams have a lot of competition, many of which are lower in cost. It seems important to improve the manufacturing processes in order to be able to furnish a wider variety of products of metallic foam at lower cost. This would permit a more large-scale industrial use of these materials.

Srivastava et al. [10] have reported a survey, both in industries and in research institutions, made by the National Physical Laboratory (UK) to have an idea about the potential expectations from metallic foams.

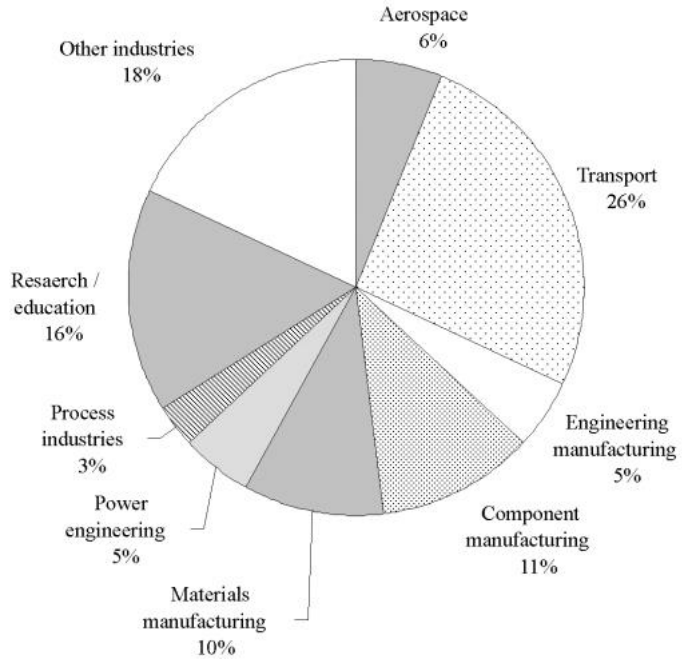

Figure 1.30: Break-up of projected industrial sector requirements for metallic foam applications. [10]

The survey results (Figure 1.30) show how the major applications of metallic foams, around 32%, in the near future would be directed towards automotive and aerospace industries. In addition to this, 26% of the demand would go to materials, engineering and component manufacturing.

1.7 Fatigue behaviour of metal foams

Considering the analysis that will be described in *Chapter 2* and *Chapter 3*, the last fundamental aspect that has to be introduced is the fatigue behaviour of metal foams. Previous studies have been executed regarding the behaviour of metal foams when subjected to cyclic compression - tension tests obtaining not univocal results.

In particular, Banhart et al. [23] have exposed to the purely compressional loading defined in Figure 1.31, cylindrical aluminum foam samples (Figure 1.32), produced through the powder metallurgical route, characterized by a density of 550, 630 and 940 kg/m^3.

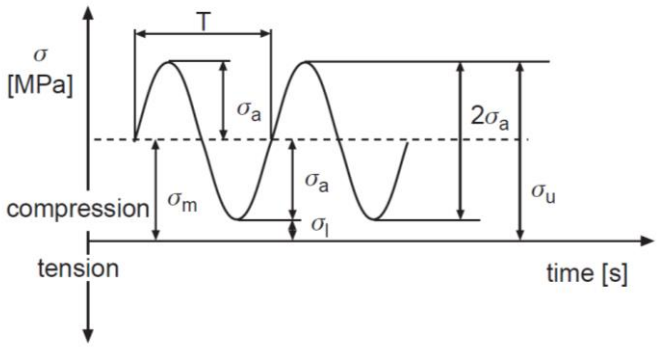

Figure 1.31: Definition of forces applied in fatigue tests. [23]

As represented the stress was varied between an upper boundary σ_u and lower boundary σ_l with an amplitude of $2\sigma_a$. Moreover a load ratio $\sigma_u/\sigma_l = 10$ was chosen and stresses were calculated assuming a constant apparent area of the

sample, pre-loaded with an initial stress of 0.1 *MPa*, throughout the experiment. Furthermore the testing frequency was 3 to 10 *Hz*.

Figure 1.32: Unfoamed aluminum alloy precursor material (left); corresponding foamed part as used for the tests (right). [23]

All samples were cycled up to $3 \cdot 10^6$ times with maximum stresses chosen to be between 50% and 80% of the measured averaged compression strength obtained through the extrapolation method (no. 3, Figure 1.33) after the preliminary quasi-static tests.

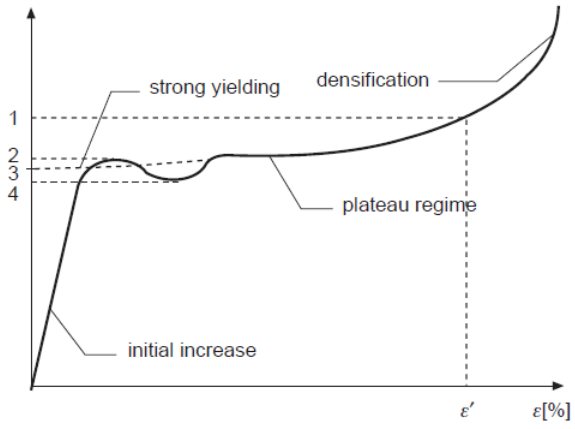

Figure 1.33: Schematical stress - strain diagram of a foam. The numbers denote the various compression strengths. 1: compression under a given load. 2: upper yield strength. 3: strength extrapolated to $\varepsilon = 0$ from the stress - strain curve in the plateau regime. 4: lower yield strength. [23]

Banhart et al. have obtained similar failure pattern in all cases. An example of the gradual deformation under cyclic compression load is shown in Figure 1.34a where it is possible to observe how the initial deformation due to preloading is about 1 *mm* and there is a very gradual compaction for some 10^4 or 10^5 cycles. Then, within a few hundred cycles, the foam starts to yield strongly and is strained by a few millimeters. After this initial yielding, the rate of straining decreases, but the destruction of the foam continues.

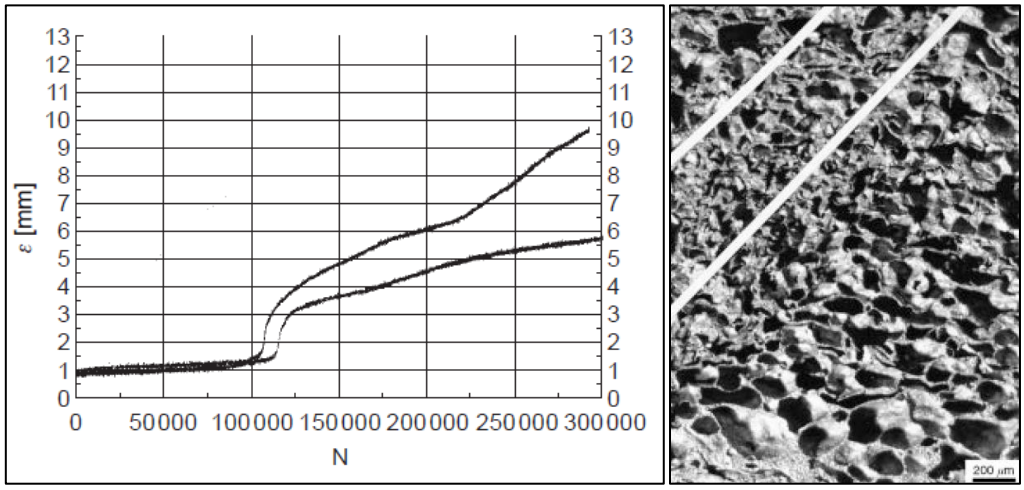

a) b)

Figure 1.34: a) Deformation of foams of density 550 kg/m^3 under cyclic loading with σ_u. 4.6 MPa , b) Example of a deformation plane bounded by the white lines. [23]

Moreover they conclude that is very difficult to detect the features leading to fatigue failure in the foam because the unloaded foam is already full of cracks, and crack propagation is hard to observe. Furthermore the foams seem to fail in a similar way under static and cyclic loading: certain regions with a disadvantageous cell wall arrangement, or possibly holes or cracks in their walls, collapse first, causing the subsequent failure of neighboring cells obtaining final deformation planes as shown for instance in Figure 1.34b. Finally one can somewhat arbitrarily define a failure criterion and determine the number of cycles up to failure for various maximum stresses to obtain a Wöhler-like curve for the foam as shown in Figure 1.35. In that case Banhart et al. have

assumed failure after more than 2 *mm* (3%) of deformation (including the initial deformation due to preload). Most of foam samples failed between 10^4 and $2 \cdot 10^5$ cycles for the stresses applied.

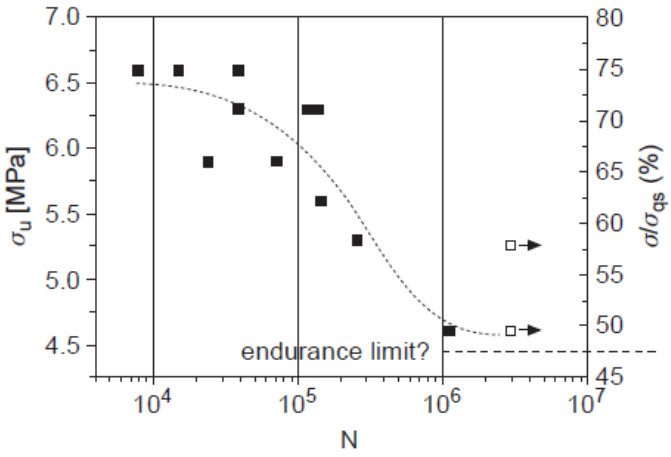

Figure 1.35: Wöhler-like curve obtained for foam samples of density 630 kg/m^3. [23]

The scatter of the results is considerably higher than for the quasi-static tests, as expected and only in two cases the samples survived the maximum number of cycles ($3 \cdot 10^6$) at stress levels between 50% and 60% of the quasi-static compression strength. From the results obtained, it isn't possible to derive an endurance limit in a reliable way, but it can be estimated that it is below 50% of the static compression strength. In conclusion trying to characterize the fatigue behavior of foams, Banhart et al. have encountered various difficulties: in fact the static compression strength varies even when the density of various foams is the same and this applies even more to fatigue failure because fatigue properties depend more sensitively on cell arrangements or crack densities in the foam. Moreover when having to relate stresses in fatigue tests to static compression stresses, the two sources of error are even combined. They therefore conclude that more samples (perhaps a hundred or more) are needed to obtain reliable estimates for the endurance limit, many more than used in their study.

Zettl et al. [26] have instead investigated the fatigue properties of different chemical compositions of aluminum foams rods of density 500 kg/m^3 (160 *mm* length and 17 *mm* diameter, produced from powder metallurgical precursors), when subjected to fully reversed tension-compression loading. The fatigue data obtained are subjected to pronounced scatter, which is typical for inhomogeneous materials. However all foams, as represented in Figure 1.36, show a fatigue limit and cycles to failure above 10^7 are rare.

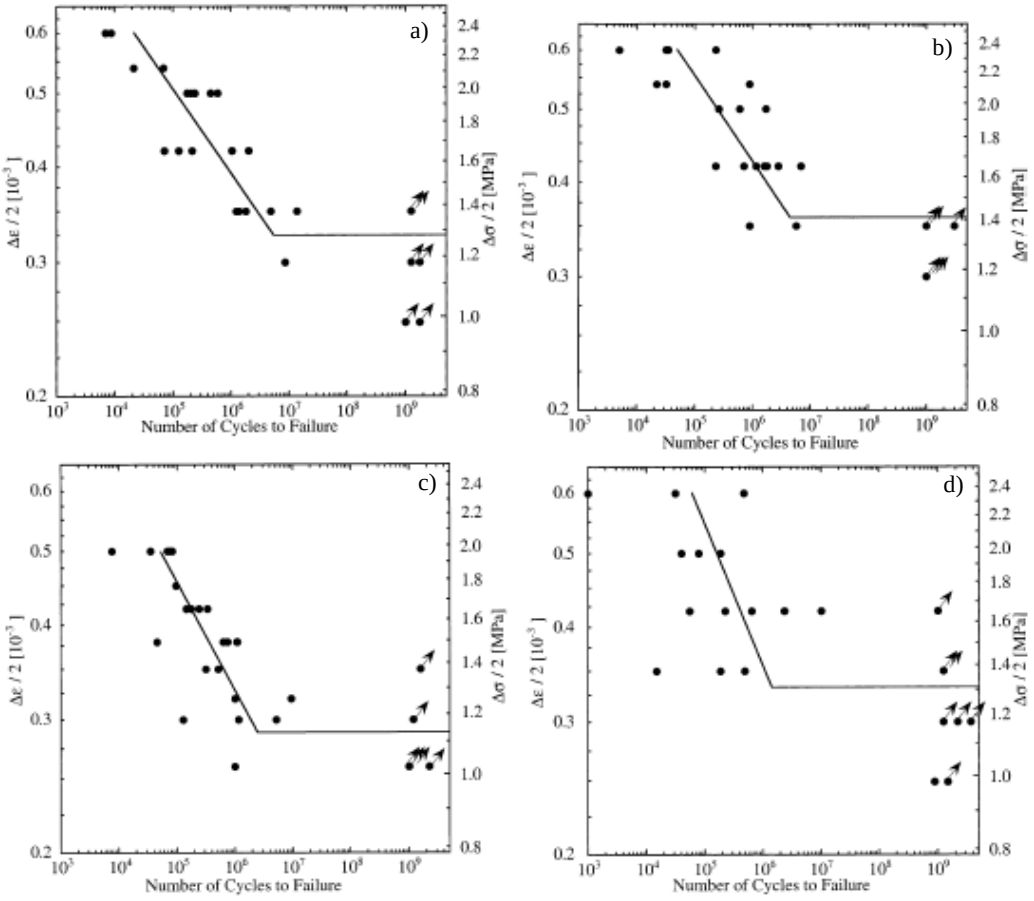

Figure 1.36: Results of endurance fatigue tests under fully reversed tension compression cycling of AlMg1Si0.6 foam (a), AlMg1Si0.6-T5 foam (b),AlMg0.6Si0.3 foam (c), and AlSi12 foam (d). [26]

The median endurance limits are 1.1–1.4 *MPa* which represents the 16–23% of the plateau stress (corresponding to the compression strength calculated again

through method 3 - Figure 1.33). Moreover they have observed how fatigue damage under fully reversed tension compression loading is governed by the formation of cracks. Preferential areas for crack initiation, according with the results obtained by Banhart et al., are initial defects like precracks or holes in the interior sections of cells. Final fracture can be frequently found in areas with low material density or large cells and no strain localization or formation of deformation bands were found. Fatigue cracks preferentially grow in the inner sections of cell walls where wall thickness is small. Furthermore below the endurance limit eventual cracks are trapped at the nodes of cells. In conclusion Zettl et al. state that a limited size of initial defects, small cell size and a homogeneous material density is of beneficial influence on the high cycle fatigue properties.

No studies have instead been found regarding the behaviour of metal foam or foam filled tubes when submitted to bending cycles which represents for sure a worst working condition for metal foams with respect to compression. For that reason, as described in detail subsequently, in this work the attention will be in focused on the behaviour of titanium and steel tubes filled with metal foam when subjected to cyclic bending tests. In particular the objective won't be to establish the effective fatigue limit of our samples but to observe if and how the mechanical and dynamical performances of the structures get worse.

Chapter 2

Foam filled steel tubes

The use of aluminum foam as a filling for structural components is intended to improve their dynamic behaviour, increase impact energy absorption, *etc.*. In the machine tools field, the structures are generally designed by means of finite elements models (FEM) of the whole machine to obtain the desired dynamic behaviour, the desired material savings and to avoid unwanted vibrations. If the virtual model is taken as a starting point the technological problems for the realization of the designed structure must be solved. In the realization of a ram with aluminum foam filling, for instance, the component must be grinded and heat-treated. As the foaming process needs to take the ram to up to 650 *°C*, it is difficult to obtain the required tolerances. Therefore the use of aluminum foam fillings adds degree of freedom to the structure design but also introduces some technological issues. [18]

This part of the work regards the analysis of the performance of steel square tubes (whose main mechanical properties are listed in Table 2.1) filled with different types of foam fillings.

Parameter	***Value***
ρ [kg/m^3]	7850
E [MPa]	200000
Yield point [MPa]	250

Table 2.1: Main mechanical properties of the structural steel used. [56]

The samples used for the tests are parts of models machine tool portal. In particular each structure, which represents a model of portal grounded by its free ends as shown schematically in Figure 2.1, is composed by three steel tubes with a welded flange at both ends connected by means of eight M8 steel bolts (torque of 25 *Nm*), with an aluminum washer placed between the flanges in order to ensure the linearity of the joint (at least constant contact surface). The analysis splits into three different steps:

- *Dynamic analysis* of each model of portal, whose aim is to evaluate the effect of the different fillings on the dynamic behaviour of the structures, by establishing if and how the filling changes it;
- *Cyclic three-points bending tests* carried out on each single sample, simulating a certain number of work cycles;
- *New dynamic analysis* of the structures in order to evaluate if the influence of the foam on their dynamic behaviour, changes after a certain number of work cycles.

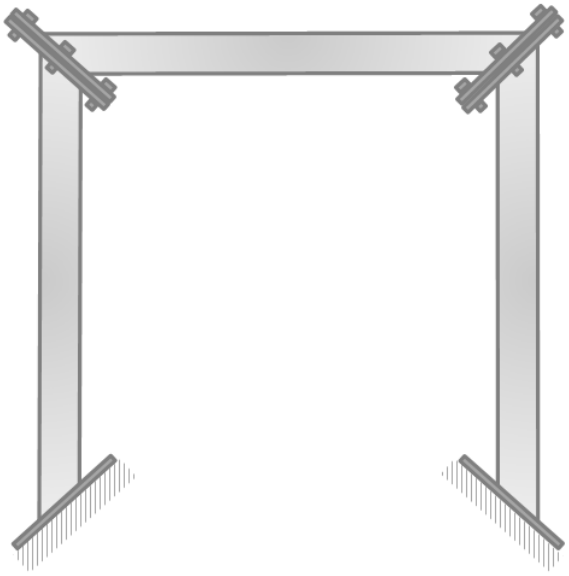

Figure 2.1: Schematic representation of the model of portal composed by three samples.

2.1 Selection of structure characteristics

The chosen structure is intentionally simple but it exhibits a wide range of frequency modes and is representative for the design of more complex components. In fact is a hyperstatic structure with simple mode shapes at low frequency (below 100 *Hz*), structural modes at mid-range frequency (100-800 *Hz*) and membrane modes at higher ones (greater than 1000 *Hz*). The main dimensions and shape of the structure were defined by means of FEM analysis in order to meet some constraints:

- Impact test was chosen as a measurement technique for the determination of the dynamic stiffness of the structure. Therefore the first eigenfrequency of the frame has to be higher than 20 *Hz*;
- The structure has to show a wide range of eigenfrequencies from low frequency (involving whole structure) to mid-range frequencies (complex shape modes) and to higher ones (involving only the membranes of the tubes) in order to obtain a complete overview of the fillings effects;
- Ground constraints compliance has to be negligible;
- The portal has to be easily filled using different fillings techniques.

The ABAQUS FEM model was built using S4R shell elements for the thin walls of the tubes and C3D8 brick elements for the connection plates and for the washers, with an average mesh size of less than 5 mm. Lastly the constraints were modeled using the ABAQUS tie constraint to reproduce the bolt coupling. As a result the structure elements are made up of three identical tubular elements, structure span is about 500 *mm* × 500 *mm*, and the tube section is 50 *mm* × 50 *mm*, with 2 *mm* of wall thickness. [18]

2.2 Filling of the tubes

As already said different types of foam fillings have been used and compared to the original empty structure and then to each other, in order to evaluate their dynamic performances. In particular the three different fillings are:

- Hybrid APM low density foam (ρ ~ 490 kg/m^3), composed by aluminum and polymer (used to fill 3 empty structures);
- Hybrid APM high density foam (ρ ~ 590 kg/m^3), composed as the previous one by aluminum and polymer (used to fill 3 empty structures);
- Alulight Foaminal aluminum foam (ρ ~ 550 kg/m^3, used to fill 3 empty structures);

For filling the portal structures with hybrid APM foam, each single tube element was cleaned with alcohol and then dried. The tube was then filled with foam spheres produced by foaming a granulated precursor material and subsequently coated with a thermally activated adhesive which contains a chemical foaming agent. The filled tubes, with two endplates mounted to maintain the spheres inside the hollow tube, were put horizontally into a furnace which was preheated to 160 $°C$ and were kept at this temperature for three hours, to effect the foaming and curing of the adhesive. Then the tubes were removed from the furnace and allowed to cool in air.

For filling with aluminum foam the steel tubes were left untreated. Alulight Foaminal AlSi10 commercial precursor was weighted in order to obtain a foam density of about 550 kg/m^3 and placed horizontally inside the tube. Two bolted steel endplates were used in order to limit foam expansion. The tubes were foamed horizontally in an air convection furnace preheated at 700 $°C$ for about 11.5 minutes and then cooled in a compressed air flux. Figures 2.2a and 2.2b

show respectively the cross sections of a Hybrid APM filled tube and an aluminum foam filled tube. [18]

a)

b)

Figure 2.2: a) Hybrid APM foam filled tube cross sections, b) Aluminum foam filled tube cross sections.

2.3 First dynamic analysis: setup and results

As previously said the aim of this first dynamic analysis (Baumeister et al. [18]), is to evaluate the effect of the different fillings on the dynamic behaviour of the structures, by establishing how the filling influences it. The results obtained for the empty structures will be compared with the results obtained for the three different foam fillings.

2.3.1 Experimental Setup

The setup shown in Figure 2.3 has been used for the determination of low frequency modes as a soft tip is mounted on the instrumented hammer. The middle and high (membrane) frequency modes were measured with a lighter hammer with harder tip to excite higher frequencies. The modal analysis performed was carried out with PCB® instrumented hammers and accelerometers (086C04, 086D05, 352C23, 352A24) and National Instruments®

Data Acquisition Device (2×9234 with cDAQ 9178). The frequency response functions (FRF) were computed with the commonly used *H1* estimator.

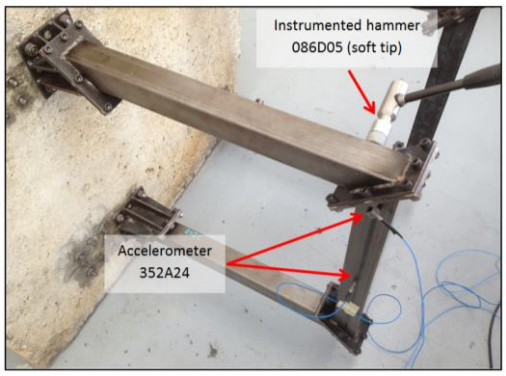

Figure 2.3: Experimental setup for the frequency response functions (FRF) estimation along with accelerometer and impact point positions.

The modal parameter identification was carried out by means of the manual selection of the peaks of interest. For each peak one of the three parameter identification algorithms was selected (peak-amplitude has been used in most of cases). In order to perform the analysis of the dynamic behavior, only two modes were selected, one in the low-frequency range (labeled 90 *Hz*) and the second in the mid-frequency range (labeled 700 *Hz*). As will be seen later, the high-frequency modes (membrane modes) disappear as the structures are filled so a quantitative comparison is not needed. Every structure was measured using the modal analysis technique before and after the filling process with estimation of the modal parameters for the two modes. The performance indicators are the percentage variations of the modal parameters for the filled structure with respect to the corresponding empty one:

- mode frequency;
- dynamic stiffness;
- modal mass;
- damping ratio (defined as the ratio between the damping factor and the critical damping factor).

2.3.2 Results

As can be seen in Figure 2.4, the three fillings have the same influence on the modal parameters of the low frequency mode. The damping ratio increases of 60 to 65%, whereas the dynamic stiffness is slightly reduced. It is obvious that the modal mass increases as the filling is introduced. As a result, the eigenfrequency decreases. In the mid-frequency mode it is possible to see that Alulight foam filling strongly increases the damping ratio, while hybrid APM (both low and high densities) reduces the ratio. It is possible to justify a reduction in the *damping ratio* considering that it is defined as the ratio between the damping coefficient c over the critical damping coefficient: $c_c = 2\sqrt{k \cdot m}$. If the damping coefficient is unchanged and the mass increases, the damping ratio decreases.

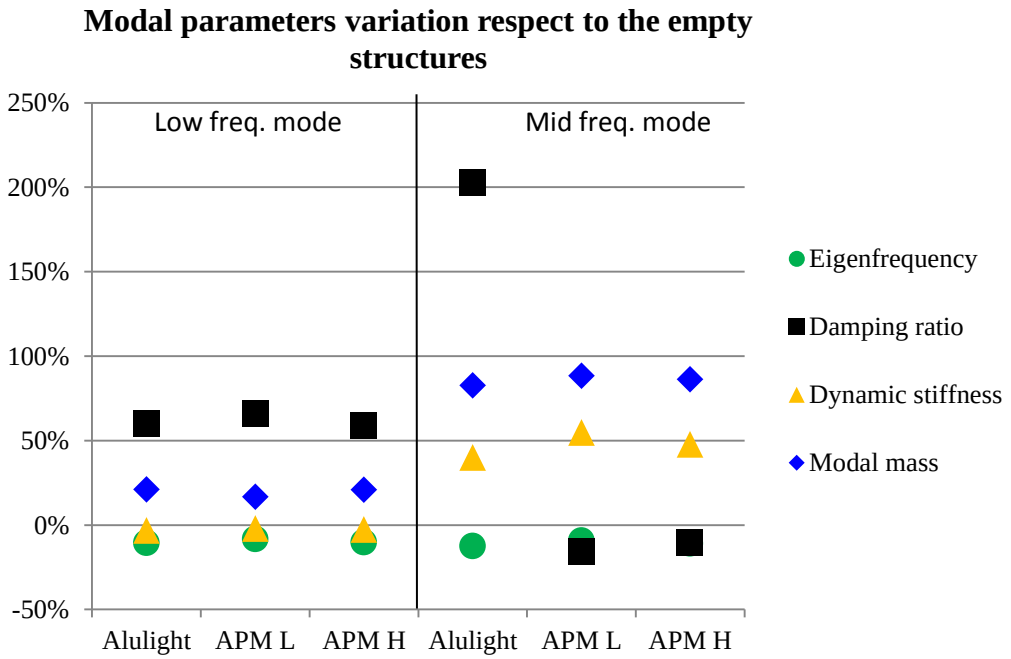

Figure 2.4: Average results for the different fillings.

Furthermore, it is important to note that the dynamic stiffness increases for the mid-frequency mode, whereas it is nearly unchanged at low frequency. Lastly, modal mass is nearly twice the corresponding empty structures for the mid-frequency mode. The behavior of the damping ratio, modal mass and dynamic stiffness for the two modes can be explained by their shape (Figure 2.5). The low frequency one is a straight line from the constraint to the free end (horizontal tubes in Figure 2.3) whereas the second is a parabola starting and ending at near-zero deformation. The hybrid APM filling types are bonded (glued) to the skin whereas the aluminum foam is not bonded. If such a bonding is not present, a 700 *Hz* parabolic shape mode enables a great energy dissipation (friction) while mass and stiffness exhibit the same behavior. This is the most promising hypothesis for the explanation of +200% of damping ratio shown in Figure 2.4.

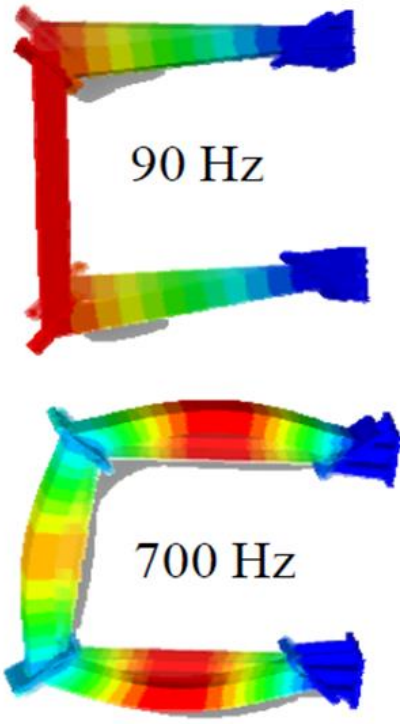

Figure 2.5: Low and mid-frequency modes considered.

Another important result is that both foam fillings (Alulight or hybrid APM) were able to suppress the membrane modes. This expected phenomenon results in a reduction of environmental noise and an increase in performance of the component.

Finally, the *foaming temperature* must be considered. In certain applications, the mechanical component has tolerances that must be respected after the foaming process. In this way hybrid APM has a great advantage as the foaming temperature is 120-180 °*C*, whereas Alulight precursor must be heated to up to the melting point of the precursor material, usually about 650 °*C*. A heat treatment involving a fast heating ramp up to 650 °*C* and a subsequent cooling phase can produce severe thermal deformations unacceptable in applications characterized by narrow tolerances. In these types of applications, hybrid APM fillings can be so considered an attractive alternative, because the low temperature foaming phase is easily controllable and nearly deformation free.

2.4 Cyclic three-points bending tests

While all the dynamic analysis have been executed at MUSP (the R&D consortium of public and private entities which represents the laboratory of the satellite campus of Politecnico di Milano located in Piacenza), this part of the work has been entirely carried out at university ÉTS (*École de technologie supérieure*) de Montréal.

As previously said the cyclic three-points bending tests have been executed on the foam filled steel samples, in order to simulate a certain number of work cycles, after which we will see through a new dynamic analysis if the dynamical behaviour of the foam fillings changes. In particular only three structures, one for each type of filling, have been subjected to bending tests.

2.4.1 Experimental setup: fixtures and devices

The machine used to execute the tests is the MTS (Material Test System) 810 represented in Figure 2.6, a versatile, multipurpose servohydraulic testing system for static and dynamic tests, characterized by an excellent accuracy, flexibility, high performance, and innovative standard features. [49]
It can be controlled through the displacement of the lower cylinder or through the force measured by the force transducers (chosen method for the experimental tests performed), and presents the following limitations:

- Minimum controlled displacement of the lower cylinder about 0.1 *mm*;
- Maximum load 100 *kN*.

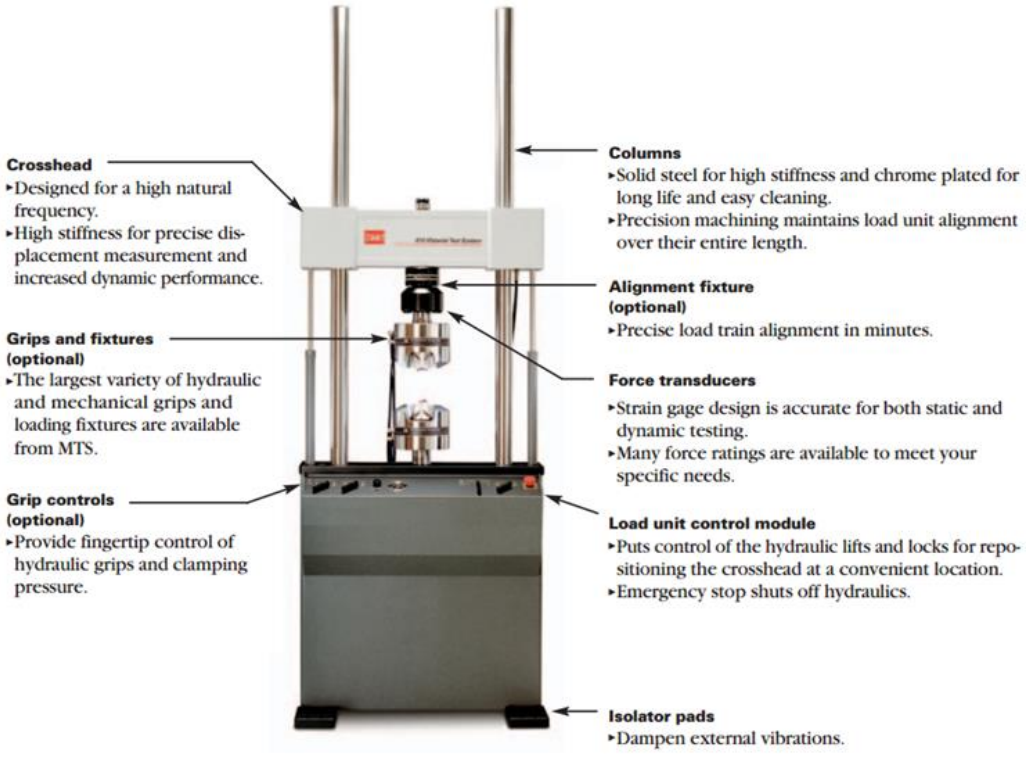

Figure 2.6: MTS 810 used for the three-points bending tests. [49]

Design and manufacture of the fixtures

The first steps have been the design and manufacture of the fixtures compatible with the MTS machine in order to execute the tests according to the standard *ISO 7438* (Metallic material - bend test), approximating the steel square tubes filled with metal foam with empty steel square tubes with the following characteristics:

- Square cross-section $b \times h = 50 \times 50$ *mm*;
- Thickness of the walls of the tubes $t = 2$ *mm*;
- Length 580 *mm*.

Design the fixtures for a three-points bending test consists in find out the dimension of the former, the dimensions of the two lower supports and the distance l between them (Figure 2.7):

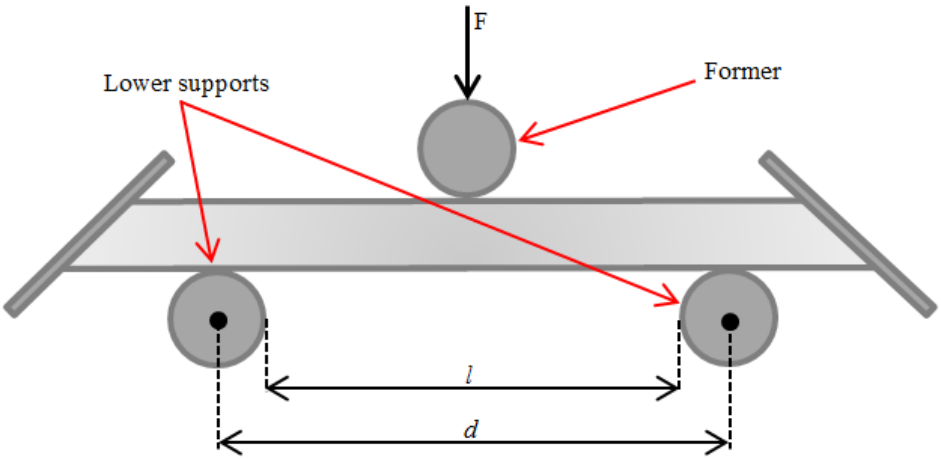

Figure 2.7: Schematic representation of the three-points bending test.

According with the standard ISO 7438, the distance between the lower supports (l) is given by:

$$l = (D + 3 \cdot a) \pm a/2$$

Where a is the diameter of the circle inscribed inside the cross-section of the square tube and D is the diameter of the former and the lower supports, who has to be simply greater then a. Therefore we have obtained the following results:

$$a = b - 2 \cdot t = 50\,mm - 2 \cdot 2\,mm = 46\,mm$$

$$D = 55\,mm$$

$$l = (D + 3 \cdot a) \pm a/2 = (55\,mm + 3 \cdot 46\,mm) \pm 46/2\ mm = 193 \pm 23\,mm$$

We have chosen the specific value of 55 *mm* for the diameter of the former, simply for manufacturing reasons and l equal to 216 *mm* because the samples were 580 mm long, so we could choose the maximum distance between the lower supports, respecting the reference standard. Finally the distance d between the axes of the lower supports is easily calculable:

$$d = l + D/2 + D/2 = 216\,mm + 55\,mm = 271\,mm$$

Obviously the former is centered on the length of the tube as shown in Figure 2.7. Table 2.2 summarizes all the values of interests for the manufacturing of the fixtures.

Parameter	***Value***
D[mm]	55
D [mm]	271
Maximum Load [kN]	100

Table 2.2: Summary of the values of interest for the manufacture of the fixtures for the bending tests on steel samples.

Note how the same fixtures have been used for the tests on cylindrical samples that will be described in *Chapter 3*.

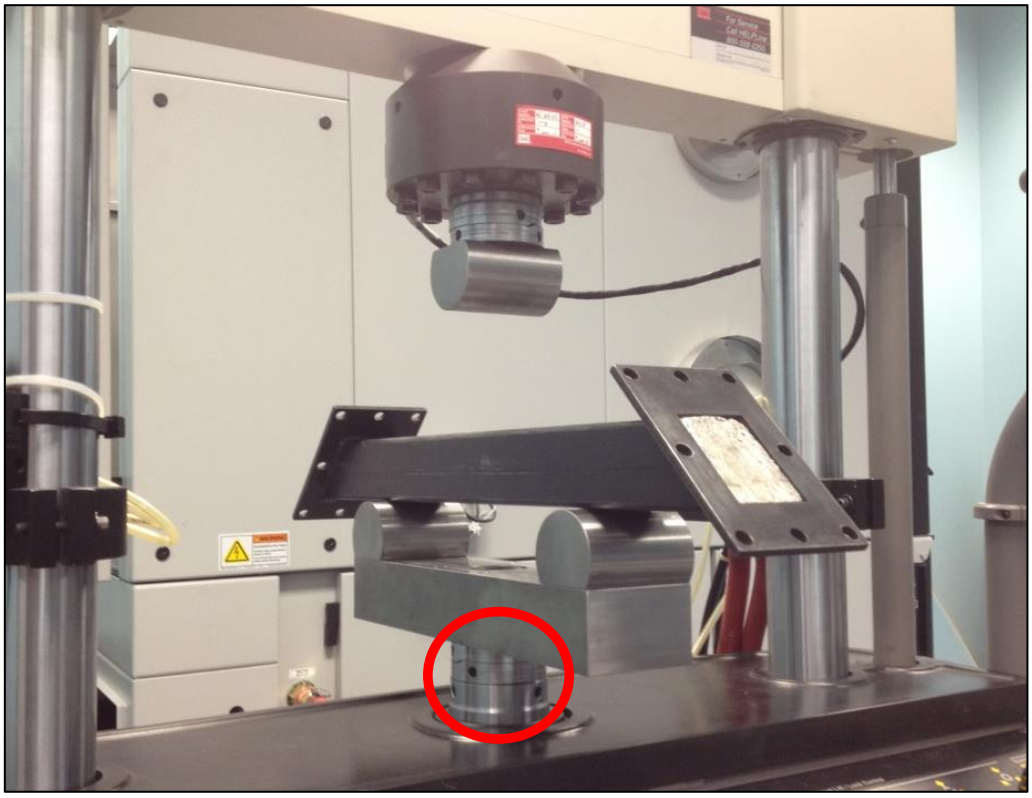

Figure 2.8: MTS machine ready for the three-points bending tests.

Devices used for the monitoring of the tests

Considering that the information given by the MTS machine are only the number of cycles, the displacement of the lower cylinder (circled in red in Figure 2.8) and the force applied in the middle of the upper part of the tube, measured by the force transducers indicated in Figure 2.6, other devices have been used for the monitoring of the tests. In particular:

- A dial indicator to measure the effective displacement of the middle point of the lower surface of each sample;
- An uniaxial accelerometer to monitor the vibrations inside the samples during the tests;

- An uniaxial ultrasonic detector whose functioning will be described below.

Dial indicator

As already said the dial indicator has been used to measure the effective displacement of the middle point of the lower surface of each sample during the tests. It has been installed as shown in Figure 2.9, fixing it to the lower part of the fixture through a magnetic base.

a) b)

Figure 2.9: a) Dial indicator fixed to the lower support through the magnetic base, b) Detail of the point of contact between the dial indicator and a sample.

In particular depending on the availability during the development of the tests, two different dial indicators have been used, whose main characteristics are listed in Table 2.3. However the measuring range hasn't been always binding because if the displacement between a measurement and the following one didn't exceed it, it was possible to reset the system on the zero conditions. So the term "exceed the measurement range" (*e.m.r.*) used in the following paragraphs, means that the displacement increases respect to the previous one of a quantity major than the measuring range.

	Resolution	***Measuring range***
Dial indicator 1	0.0100 *mm*	0.7500 *mm*
Dial indicator 2	0.0005 *in* = 0.0127 *mm*	0.03 *in* = 0.7620 *mm*

Table 2.3: Main characteristics of the dial indicators used.

Uniaxial accelerometer

To monitor the vibrations inside the samples during the tests, an uniaxial accelerometer PCB® 352C34 has been used, thinking that vibrations could be strictly connected with damages or cracks that could develop inside the sample during the cyclic three-points bending tests.

In particular the accelerometer has been installed as shown in Figure 2.10 because that direction is the presumable one for the development of a crack in this kind of tests.

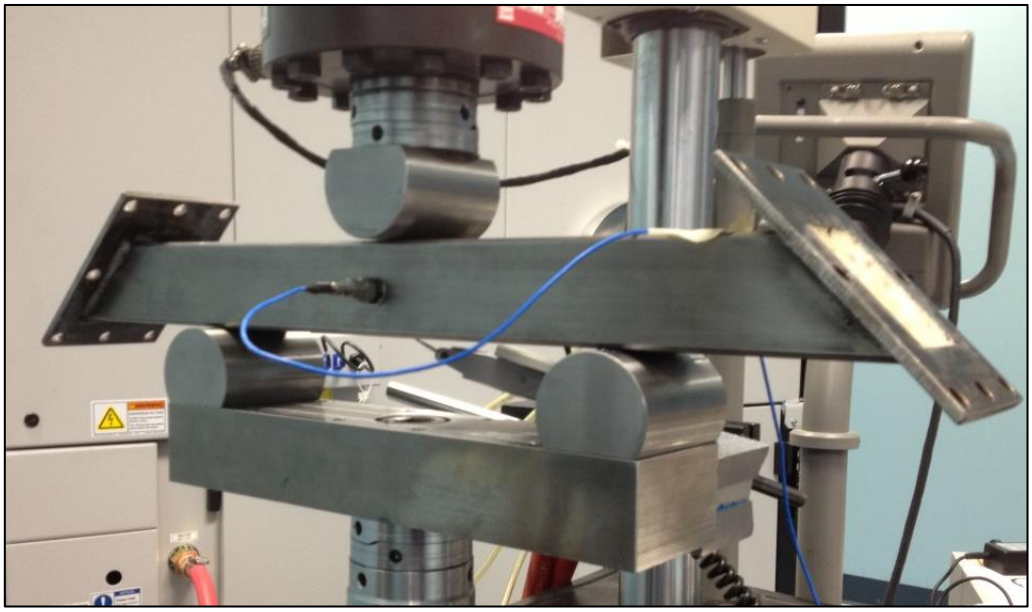

Figure 2.10: Position of the uniaxial accelerometer used.

Uniaxial ultrasonic detector

The last device used for the monitoring of the samples during the cyclic three-points bending tests is the ultrasonic detector UE Systems *UltraProbe 10000*. There are ultrasonic components in practically all forms of friction, for that reason we have chosen this technique thinking that acoustic emission could be strictly connected with any damages or cracks that can develop inside the samples during the tests.

Although the average threshold of human perception is 16.5 *kHz*, the highest sounds some humans are capable of hearing is 21 *kHz*. Anyhow ultrasound technology is usually concerned with frequencies from 20 *kHz* and up. In particular through *UltraProbe 10000*, is possible to acquire signals in a range of 5 *kHz* choosing the central frequency of this range between 20 and 100 *kHz*. [43]

This ultrasonic detection system functions through a heterodyne circuit which converts the high frequency acoustic emission signal as detected by the transducer, around a central frequency into an audible signal. In particular in these tests the signals have been acquired in a range between 27.5 and 32.5 *kHz*, and converted in the field of audible frequencies as schematically shown in Figure 2.11. This value have been chosen because we have no experience in ultrasound inspection for metal foams and this is the most common value used with this kind of instrument. [36] [37]

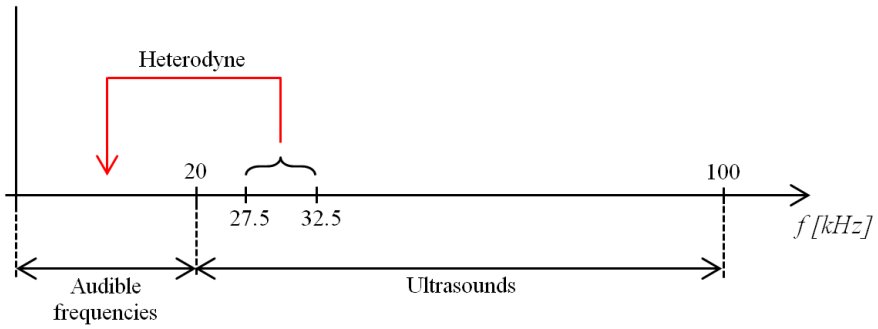

Figure 2.11: Conversion of ultrasounds into audible frequencies field executed by the heterodyne circuit.

The system has been installed as represented in Figure 2.12 using a magnetic attachment that permits to have consistent results by eliminating variables such as angle of approach and contact probe pressure.

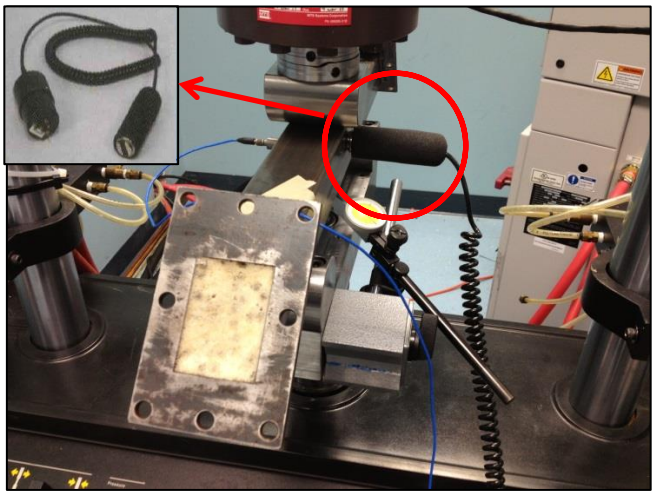

Figure 2.12: Detail of the ultrasonic detector installation.

Acquisition system

The accelerometer and the ultrasound detector are both connected with an analogue digital converter (THOR Analyzer PRO: DT9837-13310) characterized by a sampling frequency of 48 *kHz*, which is itself connected with a collector-analyzer system (BETAVIB) as shown in Figure 2.13 and 2.14. [50]

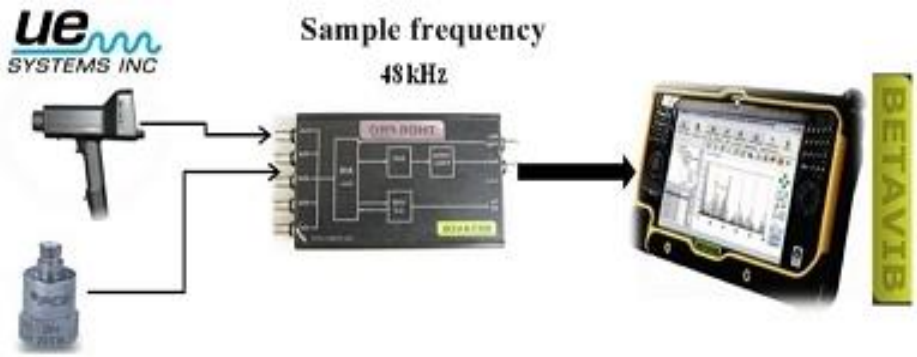

Figure 2.13: Schematic representation of the acquisition system used.

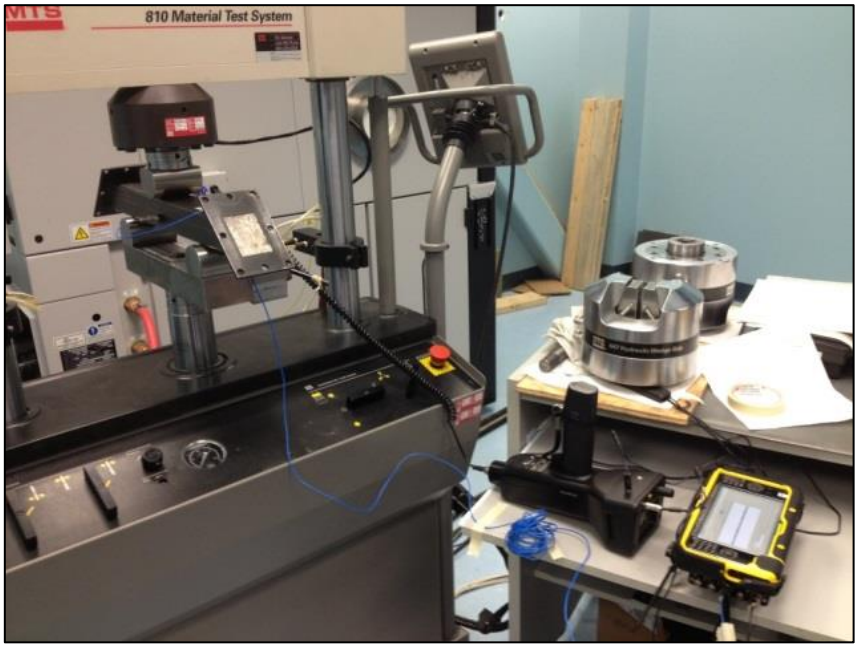

Figure 2.14: Definitive configuration of the acquisition system.

Note how the ultrasound detector used is capable to do acquisition in continuous of maximum 5 minutes, for that reason both the signals have been acquired during all the tests every 220-250 cycles for about 30 seconds.

2.4.2 Procedure and results

This part of the analysis of the steel samples filled with metal foam (listed in Table 2.4) splits into two steps:

1. Preliminary tests executed on all the samples that are not part of the models of machine tool portals (called “preliminary samples” in Table 2.4) executed in order to find the definitive parameters characterizing the tests of the following step;
2. Three-points bending tests executed on all the samples constituting the models of portal in order to simulate the work conditions without damage them.

ID number	***Filling***	***Type***	***Foam approximate density [kg/m^3]***
118_A	Alulight Foaminal aluminum foam	Portal	550
119_A	Alulight Foaminal aluminum foam	Portal	550
120_A	Alulight Foaminal aluminum foam	Portal	550
122_A	Alulight Foaminal aluminum foam	Preliminary sample	550
123_A	Alulight Foaminal aluminum foam	Preliminary sample	550
100_APMH	Hybrid APM high density foam	Portal	590
101_APMH	Hybrid APM high density foam	Portal	590
102_APMH	Hybrid APM high density foam	Portal	590
103_APMH	Hybrid APM high density foam	Preliminary sample	590
105_APMH	Hybrid APM high density foam	Preliminary sample	590
106_APML	Hybrid APM low density foam	Portal	490
107_APML	Hybrid APM low density foam	Portal	490
108_APML	Hybrid APM low density foam	Portal	490
110_APML	Hybrid APM low density foam	Preliminary sample	490
111_APML	Hybrid APM low density foam	Preliminary sample	490

Table 2.4: List of the steel samples filled with metal foam, subjected to three-points bending tests.

Preliminary tests

As previously said, the first part of the tests has been executed on the "preliminary samples" listed in Table 3.6 (122_A, 123_A, 103_APMH, 105_APMH, 110_APML, 111_APML) in order to define the parameters of the bending tests to which the samples, constituting the models of portal, have been subsequently subjected simulating the work conditions.

First of all few standard steps have been done in order to be sure to work in safety conditions: warm-up cycles without samples have been performed to tune in displacement the *MTS* machine and subsequently sample 122_A has been installed on the fixtures described in *paragraph 2.4.1 - Design and manufacture of the fixtures*, to execute the auto-tuning in load. Moreover before starting with the effective "preliminary tests" sample 122_A has been submitted to few bending cycles in which the frequency and the force applied have been changed manually in order to establish the security parameters then used for all the cyclic three-points bending tests performed on steel samples. In particular, the following values have allowed to work in safety conditions, keeping the samples in touch with the two supports and the former during each bending cycle:

- Preload $= 2\ kN$;
- Frequency $= 1\ Hz$.

The first cyclic three-points bending step loading test (Figure 2.15), carried out on sample 122_A, has the following characteristics:

- Preload $= 2\ kN$;
- Starting value of the maximum load, which increases of $4\ kN$ every 100 cycles, equal to $4\ kN$;
- Sinusoidal pattern;
- Frequency $= 1\ Hz$.

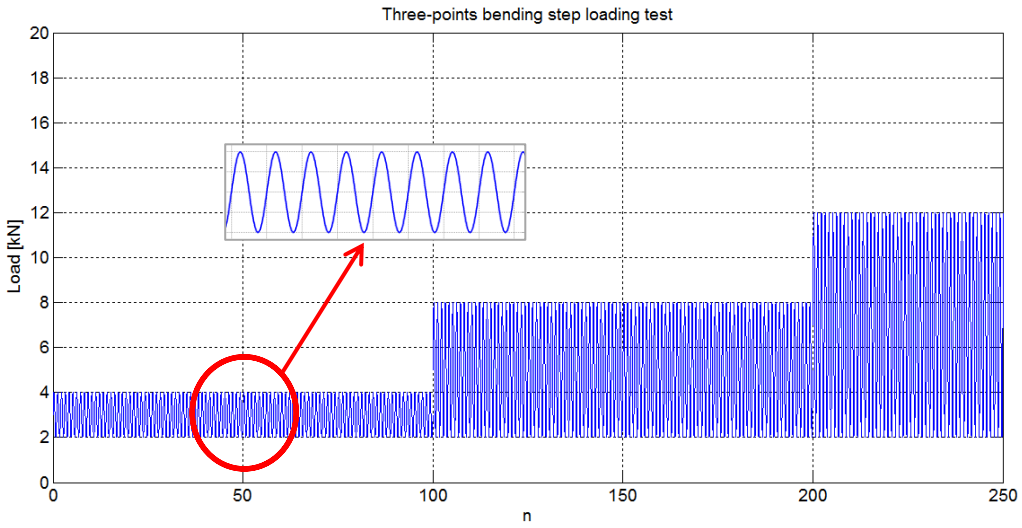

Figure 2.15: Representation of the first 250 cycles of the three-points bending step loading test with a zoom which points out the sinusoidal pattern.

During this first test the sample has been monitored only through the dial indicator 1 (installed as described in *paragraph 2.4.1 - Dial indicator*) measuring the displacement of the middle point of the sample (Figure 2.9) when the maximum value of force was applied. In particular, have been executed three measurements for each step of load, after the 1st, the 50th and the 100th cycle obtaining the results shown in Table 2.5 and Figure 2.16.

Sample 122_A (Alulight)					
Maximum Load [kN]	***Displacement [mm]***			***n***	***Cumulative n***
	1st	***2nd***	***3rd***		
4	0.26	0.26	0.26	100	1 - 100
8	0.39	0.39	0.39	100	101 - 200
12	0.51	0.51	0.51	100	201 - 300
16	0.69	0.70	0.71	100	301 - 400
20	0.90	0.90	0.90	100	401 - 500
24	1.17	1.21	1.23	100	501 - 600
28	1.70	*e.m.r.*	*e.m.r.*	100	601 - 700

Table 2.5: Displacement measured through the *dial indicator 1* at the 1st, the 50th and the 100th cycle of each step of load.

Note how *n* represents the number of cycles, the term *e.m.r.* means that the value exceeds the measurement range as previously described in *paragraph 2.4.1 - Dial indicator.* This is the reason why the last part of the graphic in Figure 2.16 is dashed.

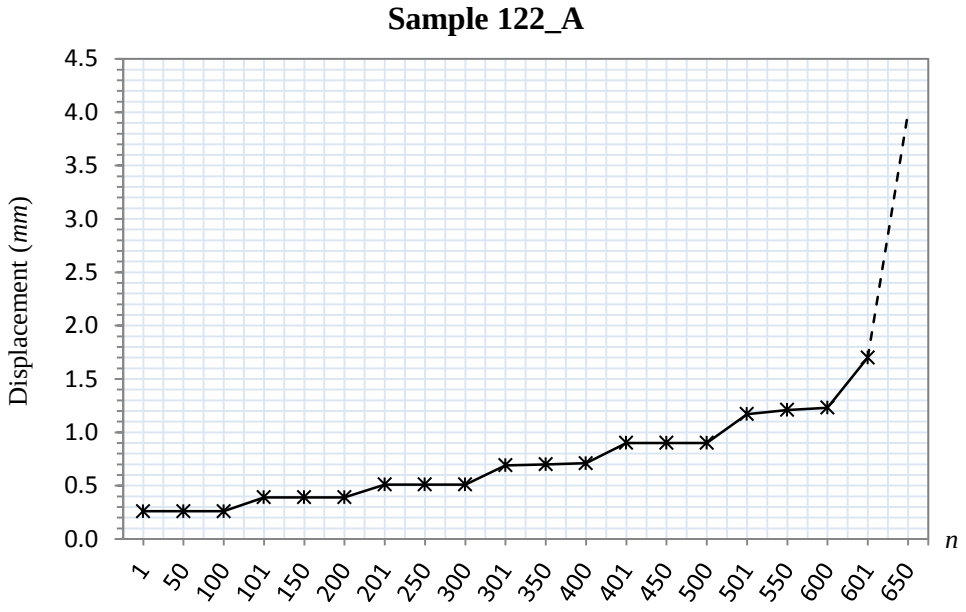

Figure 2.16: Displacements measured during the three-points bending step loading test on sample 122_A.

From the results obtained, it is possible to observe that:

- After the 4 - 12 *kN* loading step, passing from a step to the subsequent one the increasing of displacement rise from ~ 0.1 *mm* to ~ 0.2 (*or more*) *mm*;
- Till 20 *kN* (cycles from 601 to 700) there is no significant difference between the displacement of the middle point of the sample measured after the 1st, the 50th and the 100th cycle of each loading step. In other words the limited number of cycles for each step has no influence on the mechanical behaviour of the sample.

- The sample at the end of the test shows a clear residual plastic deformation (Figure 2.17) in correspondence of the point of contact with the former.

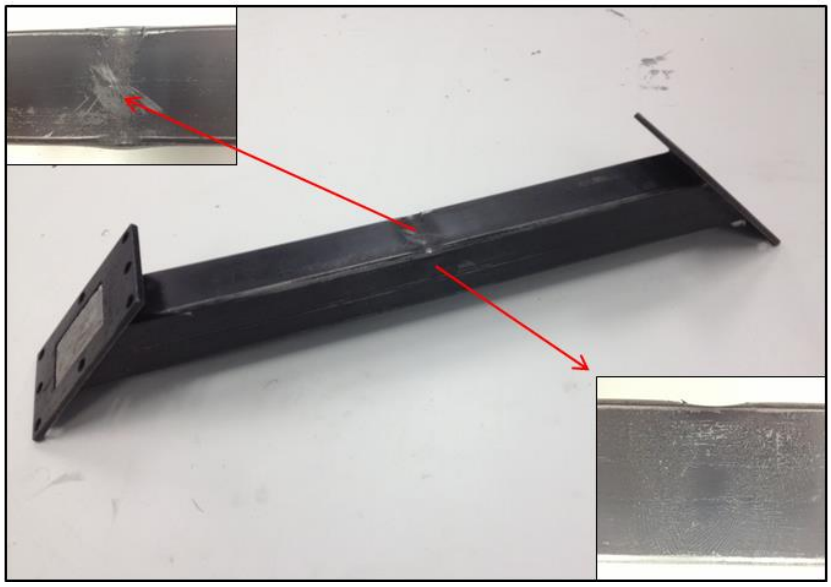

Figure 2.17: Details of the plastic deformation on sample 122_A.

As previously said, the main objective of this part of the experimental tests is to find the definitive parameters characterizing the bending tests that will be executed on all the samples constituting the models of portal, in order to simulate the work conditions without damage them. For that reason looking at the results has been chosen to focus the attention on the lower values of force applied (up to about 12 *kN*), increasing the number of cycles for each loading step in the subsequent tests.

In particular samples 123_A, 110_APML and 103_APMH (one for each type of metal foam filling) have been subjected to three-points bending step loading tests, which have been stopped when the displacement (measured through the dial indicator after the 1^{st}, the 500^{th} and the 1000^{th} cycle with the maximum

value of force applied) increased constantly during the same loading step. These tests (Figure 2.18), during which the samples have been monitored through all the devices described in *paragraph 2.4.1 - Devices used for the monitoring of the tests*, are characterized by the parameters listed below:

- Preload $= 2\ kN$;
- Starting value of the maximum load, which increases of $2\ kN$ every 1000 cycles, equal to $4\ kN$;
- Sinusoidal pattern;
- Frequency $= 1\ Hz$.

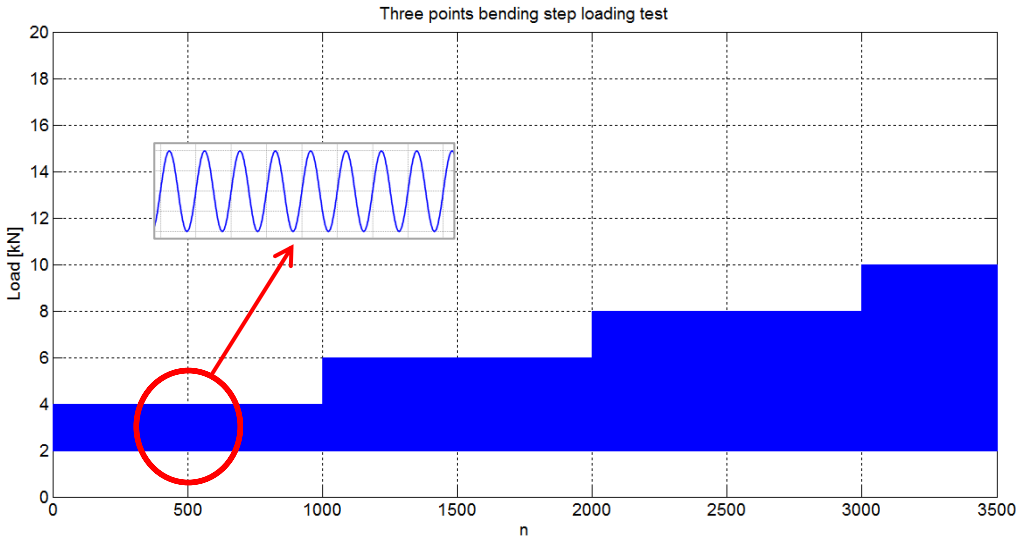

Figure 2.18: Representation of the first 3500 cycles of the three-points bending step loading test with a zoom which points out the sinusoidal pattern.

Considering the displacements measured through the dial indicator, summarized and represented respectively in Table 2.6 and Figure 2.19, it is possible to observe how in the same load conditions the maximum values have been obtained for sample 123_A for which the test has been interrupted earlier, due to the fact that the halting condition previously defined was already verified for a maximum load of 16 *kN*.

Maximum Load [kN]	*Displacement [mm]*			*n*	*Cumulative n*
	1st	*2nd*	*3rd*		
Sample 123_A (Alulight)					
4	0.15	0.15	0.15	1000	1000
6	0.21	0.22	0.22	1000	2000
8	0.28	0.29	0.29	1000	3000
10	0.34	0.35	0.35	1000	4000
12	0.41	0.41	0.41	1000	5000
14	0.47	0.48	0.49	1000	6000
16	0.57	0.58	0.60	1000	7000
Sample 103_APMH					
4	0.12	0.12	0.12	1000	1000
6	0.19	0.19	0.19	1000	2000
8	0.26	0.26	0.26	1000	3000
10	0.31	0.32	0.32	1000	4000
12	0.38	0.38	0.38	1000	5000
14	0.43	0.43	0.43	1000	6000
16	0.49	0.50	0.50	1000	7000
18	0.54	0.54	0.54	1000	8000
20	0.60	0.61	0.61	1000	9000
22	0.68	0.69	0.69	1000	10000
24	0.75	0.77	0.78	1000	11000
Sample 110_APML					
4	0.11	0.11	0.11	1000	1000
6	0.17	0.17	0.17	1000	2000
8	0.24	0.24	0.24	1000	3000
10	0.30	0.30	0.30	1000	4000
12	0.36	0.36	0.36	1000	5000
14	0.42	0.42	0.42	1000	6000
16	0.47	0.47	0.47	1000	7000
18	0.51	0.51	0.51	1000	8000
20	0.57	0.57	0.57	1000	9000
22	0.64	0.64	0.64	1000	10000
24	0.70	0.71	0.72	1000	11000

Table 2.6: Displacement of the middle point of samples measured through the *dial indicator* at the 1st, the 500th and the 1000th cycle of each step of load.

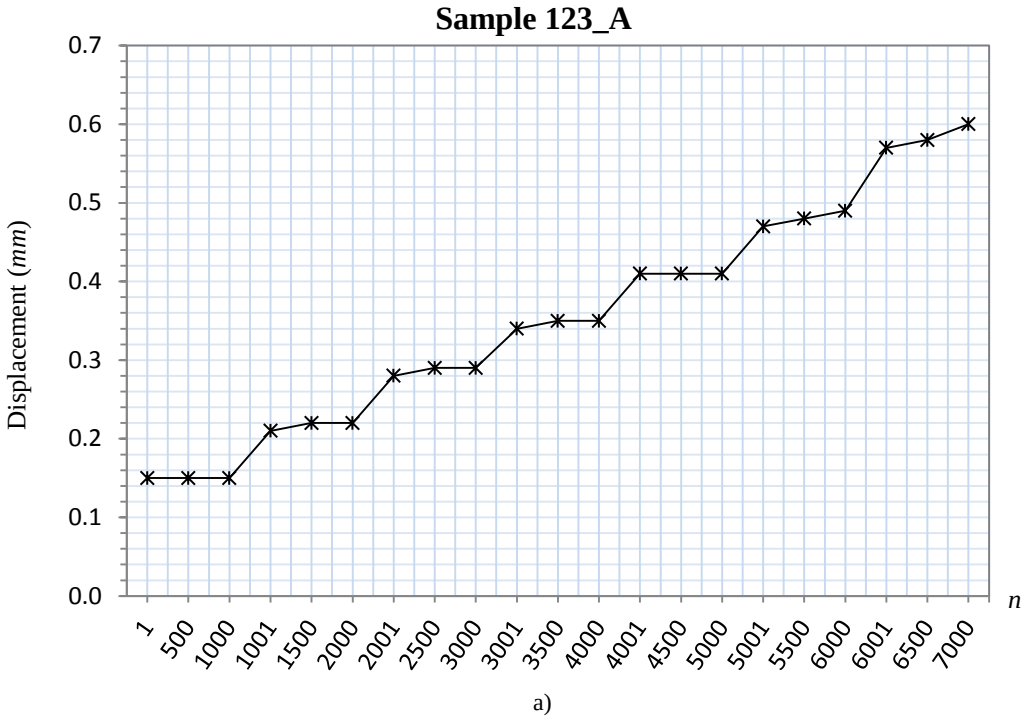
Sample 123_A
Displacement (mm)
0.0
0.1
0.2
0.3
0.4
0.5
0.6
0.7
n
1
500
1000
1001
1500
2000
2001
2500
3000
3001
3500
4000
4001
4500
5000
5001
5500
6000
6001
6500
7000

a)

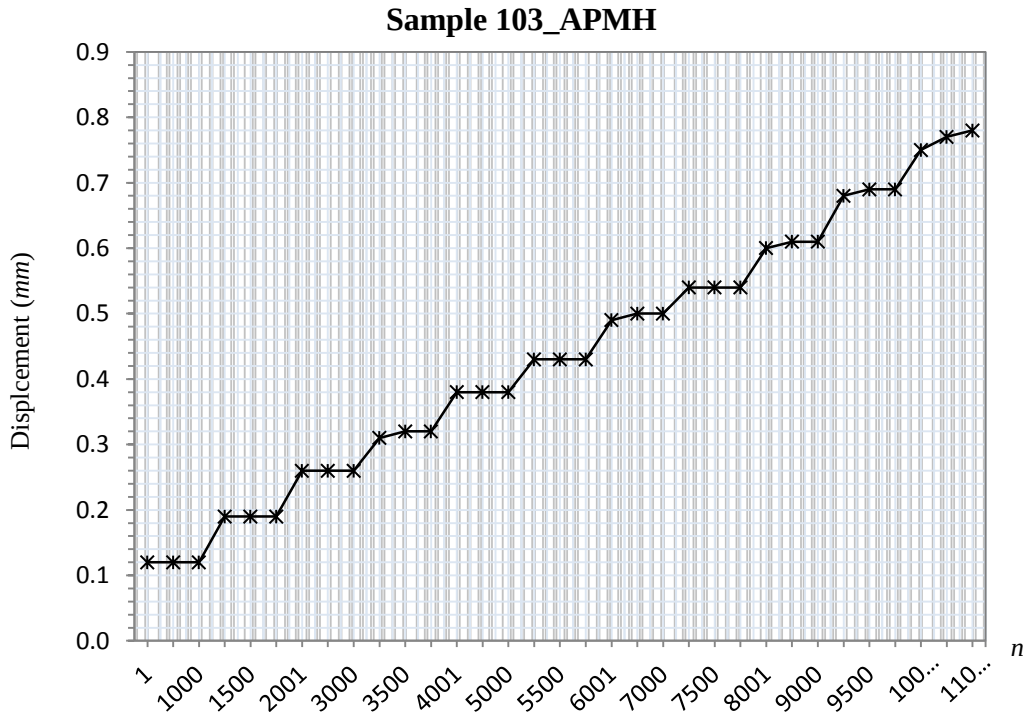
Sample 103_APMH
Displcement (mm)
0.0
0.1
0.2
0.3
0.4
0.5
0.6
0.7
0.8
0.9
n
1
1000
1500
2001
3000
3500
4001
5000
5500
6001
7000
7500
8001
9000
9500
100...
110...

b)

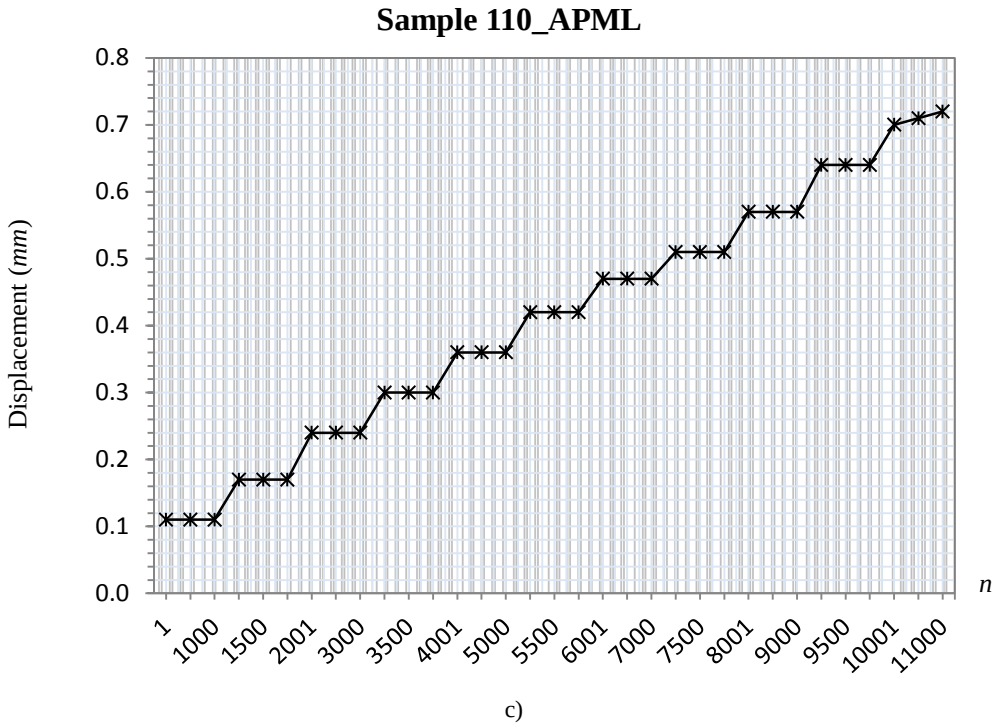

c)

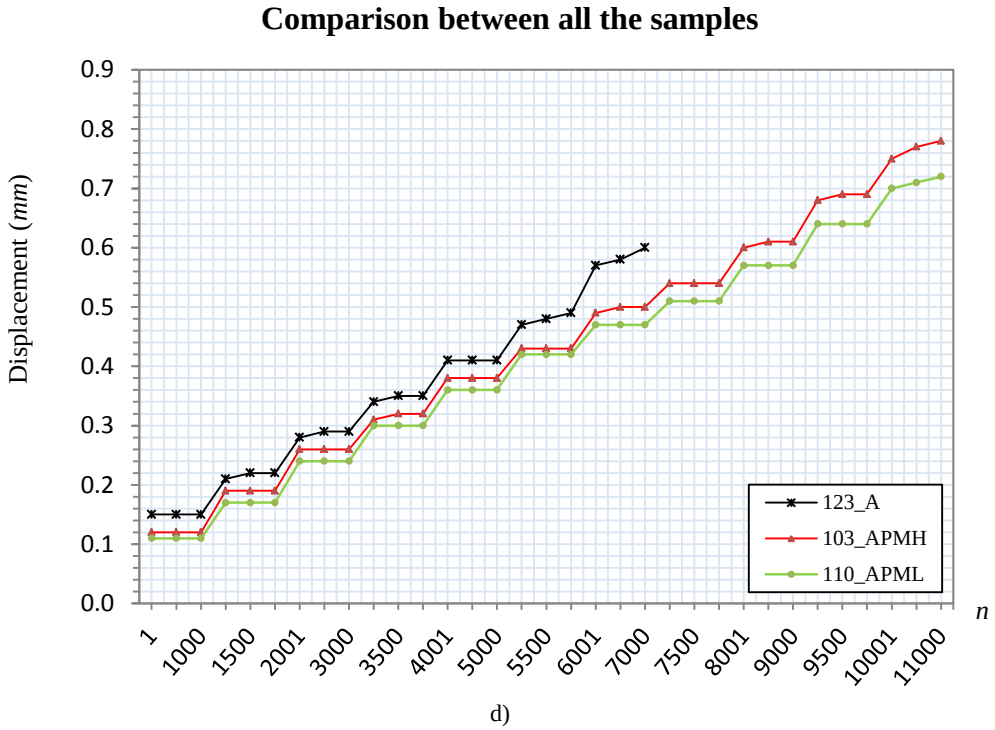

d)

Figure 2.19: Displacements measured during the three-points bending step loading tests, a) Sample 123_A, b) Sample 103_APMH, c) Sample 110_APML, d) Comparison between all the samples.

Moreover samples 122_A and 123_A, at the end of the tests, results to be the most superficially damaged as shown in Figure 2.20.

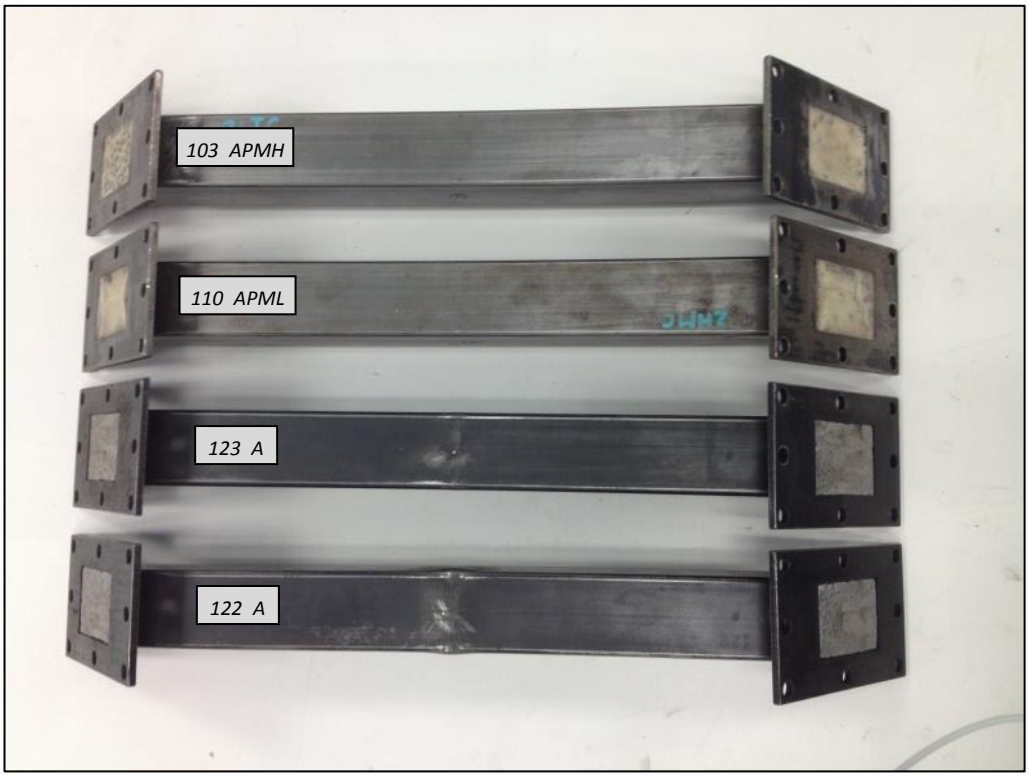

a)

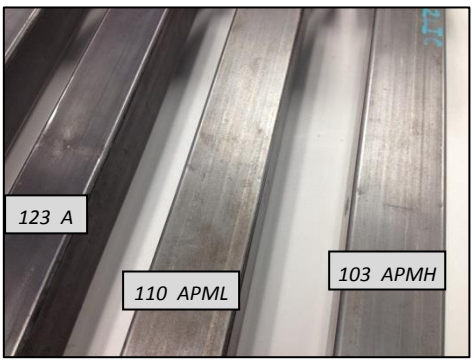

b)

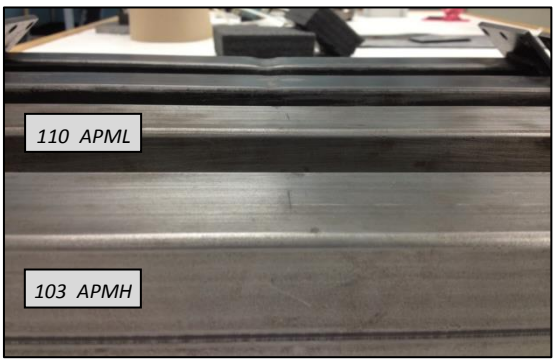

c)

Figure 2.20: Comparison between the surfaces of the samples after the tests.

This can be related with the different thermal treatment to which the steel has been submitted during the foaming process. In particular, as described in *paragraph 2.2*, filling tubes with aluminum foam the temperature reached is significantly higher respect to the one necessary for the hybrid (aluminum and polymer) foam (700 °*C* vs. 160 °*C*). Furthermore there is difference also between the results relative to the two samples filled with aluminum foam: sample 122_A shows more significant damages on the surface and higher values of displacements respect to sample 123_A when submitted to the same condition of load. These differences can be related to the fact that sample 122_A before the three-points bending step loading test, has been used for the tuning of the *MTS* machine and for the cycles executed to find the parameters, which would have allowed to proceed with the tests in safety conditions.

Moreover for each sample tested, has been calculated the *RMS* of the signals of vibration and acoustic emission, acquired respectively through the accelerometer and the ultrasounds detector whose characteristics and utilization have been described in *paragraph 2.4.1* (*Uniaxial accelerometer, Uniaxial ultrasonic detector*). In particular the *RMS* (*Appendix 2*) has been calculated for the band of frequency 1-5000 *Hz* due to the fact that for both the signals, the most of the energy was distributed in this frequency range.

Considering the vibration signals, for each sample the value of the *RMS* remains low and almost constant for all the 30 seconds acquisitions executed every 220-250 cycles during the three-points bending step loading test performed (*paragraph 2.4.1 - Acquisition system*). For that reason, considering this parameter, nothing seems to happen in term of damages inside the foam filled tubes. As shown in Figure 2.21 for sample 123_A the amplitude is higher respect to sample110_APML and sample 103_APMH, both filled with hybrid foam, probably due to the different structure of the foam itself. This result can be also explained through the values of the displacements of the middle point of

the samples previously listed and represented in Figure 2.19d. In fact such as for the displacements, the highest amplitude of the *RMS* has been obtained for sample 123_A.

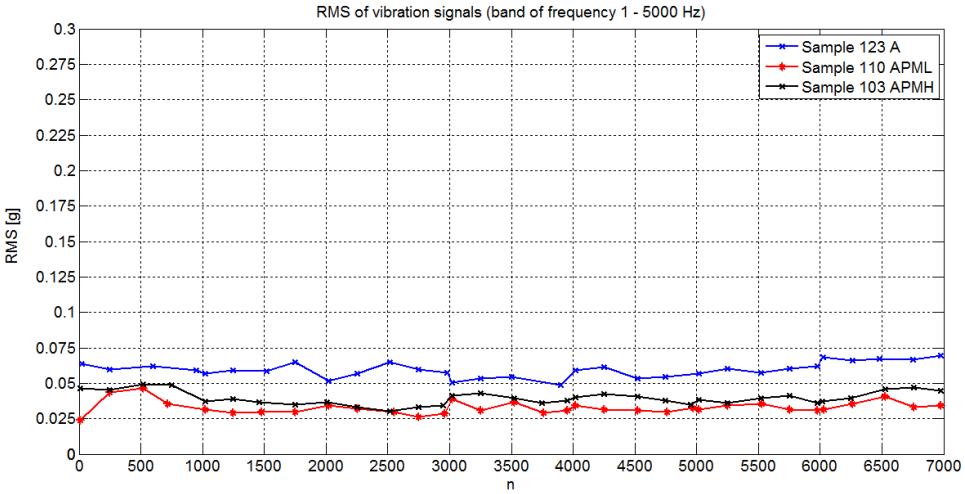

Figure 2.21: Trend of the RMS calculated for the vibration signals acquired during the three-points bending step loading tests.

As already said also for the acoustic emission data, acquired during the tests through the ultrasonic detector UE Systems *UltraProbe 10000*, the *RMS* has been calculated for the band of frequency 1-5000 *Hz* considering that the most of the energy was distributed in this frequency range as shown in Figure 2.22. In reality, as explained in detail in *paragraph 2.4.1 - Uniaxial ultrasonic detector*, this ultrasonic detection system functions converting the high frequency acoustic emission signal as detected by the transducer, around a central frequency into an audible signal. In particular in the tests performed, we have acquired signals in a range between 27.5 and 32.5 *kHz* converted as shown in Table 2.7:

Ultrasonic frequency acquired	***Audible frequency converted***
27.5 - 28.5 *kHz*	1 - 5000 *Hz*
28.5 - 32.5 *kHz*	5001 - 20000 *Hz*

Table 2.7: Frequencies conversion executed by the ultrasonic detection system.

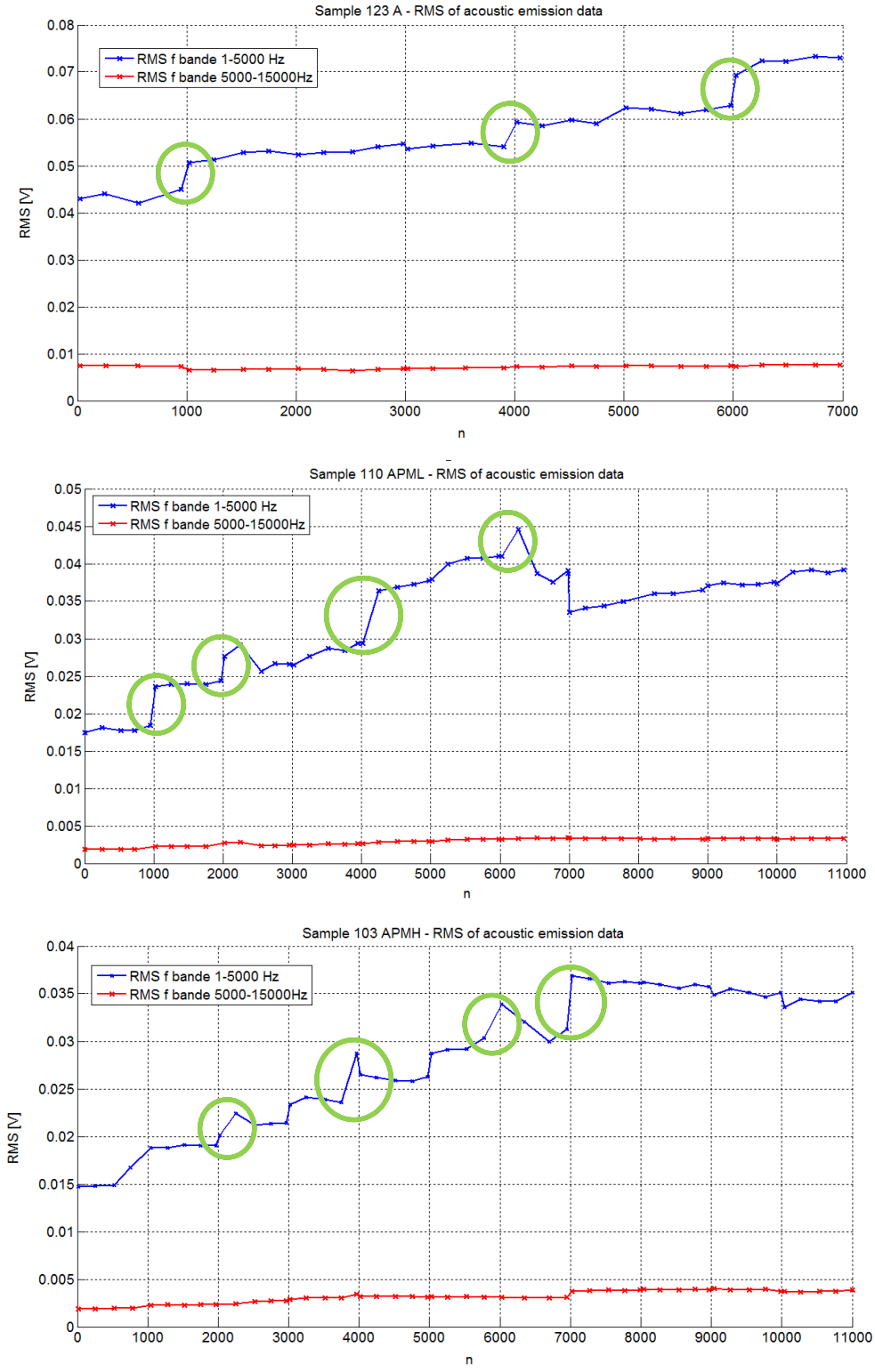

Figure 2.22: Trend of the RMS calculated for the acoustic emission signals acquired for each sample.

The low values and the trend of the *RMS* of acoustic emission signals confirm that nothing seems to happen in term of significant damages inside the foam filled tubes (*Appendix* 2). Moreover from Figure 2.23 it is possible to observe how sample 123_A shows the maximum value of *RMS* for all the duration of the test, coherently with the results previously obtained through the analysis of displacements and vibrations. Furthermore the *RMS* shows a general increasing trend according with the increment of the load during the bending test, differently from what happens considering vibration signals. In fact, the values obtained at the end of the tests are significantly higher respect to the starting ones. In Figure 2.22 it is possible also to observe how in many cases the changing of load leads to a jump of the *RMS* value (points circled in green).

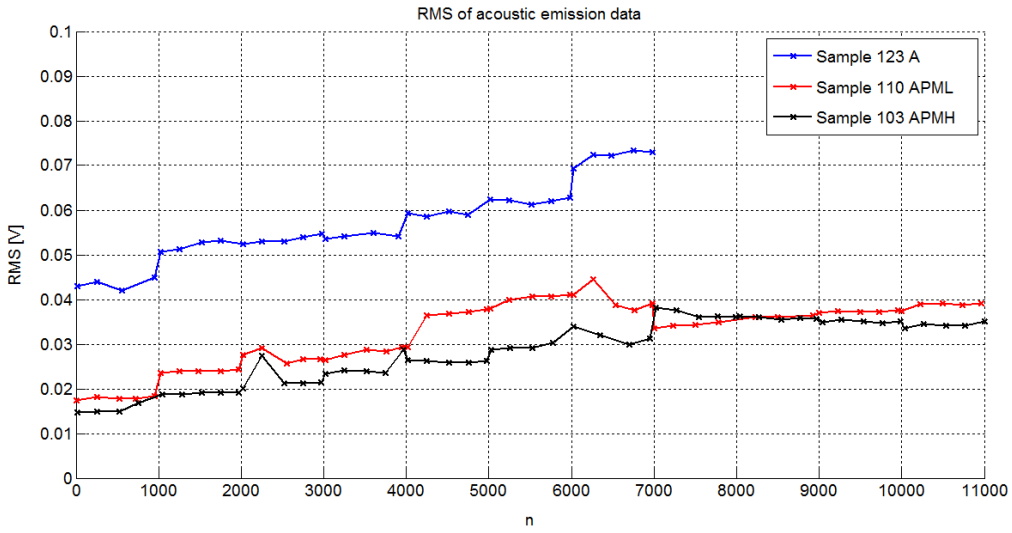

Figure 2.23: Comparison between the *RMS* values of acoustic emission signals for all the samples.

So considering the results obtained through vibrations and acoustic emission analysis it is clear how the samples have not been damaged during the tests, even if the measured displacements increase significantly and the surfaces show a plastic residual deformation (Figure 2.20). For that reason, due to the fact that the cyclic three-points bending tests which have to be performed on all the

samples constituting the models of portal in order to simulate the work conditions, do not have to damage them, the definitive values chosen for the parameters are:

- Preload $= 2\ kN$;
- Maximum load $= 10\ kN$;
- Sinusoidal pattern;
- 10000 cycles;
- Frequency $= 1\ Hz$.

The values of preload and frequency are always the ones which allow to work in safety conditions, find at the beginning of the "preliminary tests". The maximum load of 10 *kN* has been chosen for different reasons:

- The displacements measured for each sample remain almost constant during the loading step of 1000 *kN* (Table 2.5);
- Till 10 *kN* the difference between the displacements measured for the samples are still not to significant while, increasing the load, the gap rises (Figure 2.19d);
- In term of *RMS* it is clear how the samples have not been significantly damaged during the tests, but considering the acoustic emission signals there is a jump (particularly for samples 123_A and 110 APM_L - Figure 2.22) at the end of the 4000 cycles coincident, as shown in Table 2.5, to the end of the 10 *kN* - loading step.

A machine tool work obviously for more than 10000 cycles, but due to a lack of time, it was not possible to perform tests of millions cycles at 1 *Hz* of frequency. For that reason has been accepted a displacement higher respect to the one allowed to a real machine tool, simulating the work conditions through bending tests, characterized by a "limited" number of cycles.

Finally in order to conclude the "preliminary tests" samples 111_APML and 105_APMH have been subjected to the cyclic three-points bending test just described. The samples have been monitored through the dial indicator (measurement done every 1000 cycles) and the ultrasonic detection system in order to verify that, with these test parameters, the samples would not have been damaged. The results obtained, showed in Table 2.8 and Figure 2.24, confirm that the parameters chosen permit to simulate a certain number of work cycles, not causing damages at the samples.

Sample ID	***Displacement [mm]***	***n***
111_APML	0.34	0
	0.34	1000
	0.34	2000
	0.34	3000
	0.34	4000
	0.34	5000
	0.34	6000
	0.34	7000
	0.34	8000
	0.34	9000
	0.34	10000
105_APMH	0.33	0
	0.33	1000
	0.33	2000
	0.33	3000
	0.33	4000
	0.33	5000
	0.33	6000
	0.33	7000
	0.33	8000
	0.33	9000
	0.33	10000

Table 2.8: Displacement of the middle point of samples 111_APML and 105_APMH.

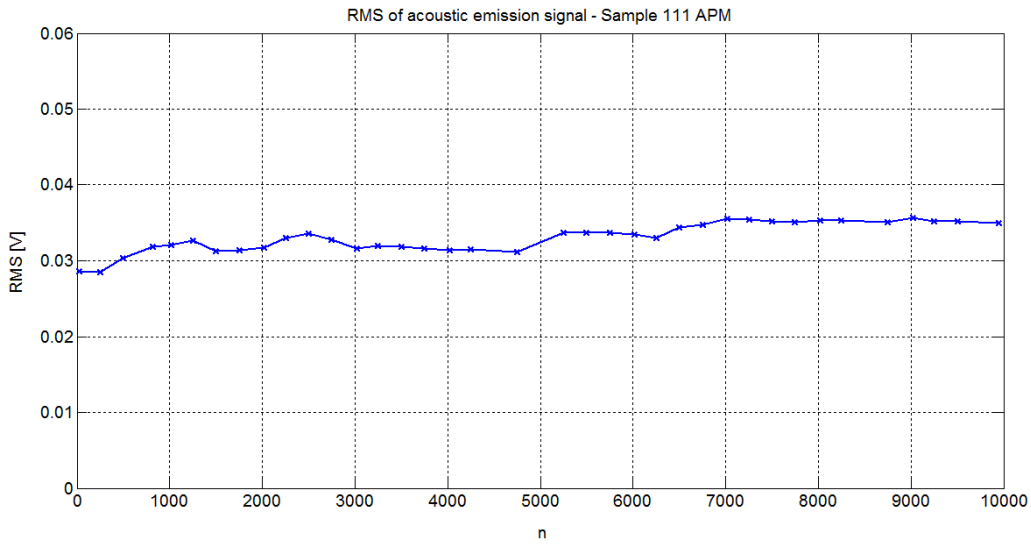

Figure 2.24: *RMS* of the acoustic emission signal of sample 111_APM.

In fact for both the samples, the value of the displacement of the middle point remain constant and the *RMS* (represented for sample 111_APM) increases but not significantly.

Simulation of work cycles

All the samples constituting the models of machine tool portal (Table 2.3) have finally been subjected to the cyclic three-points bending test previously defined, (simulating 10000 cycles of work) whose characteristics are here reported:

- Preload $= 2\ kN$;
- Maximum load $= 10\ kN$;
- Sinusoidal pattern;
- 10000 cycles;
- Frequency $= 1\ Hz$.

After all the verifications executed during the "preliminary tests", in these 10000 cycles the samples have been monitored simply measuring the

displacement, in order to control if the sample would have behaved as supposed, obtaining the positive results listed in Table 2.9 where only the first and the last measurement have been reported.

Sample ID	*Initial displacement [mm]*	*Final displacement [mm]*
118_A	0.41	0.41
119_A	0.42	0.42
120_A	0.41	0.41
106_APML	0.32	0.32
107_APML	0.34	0.34
108_APML	0.34	0.34
100_APMH	0.34	0.34
101_APMH	0.33	0.33
102_APMH	0.33	0.33

Table 2.9: Displacements of the middle point of the samples constituting the models of machine tool portal.

2.5 Dynamic analysis after 10000 bending cycles

After the bending tests, executed on each sample constituting a part of the models of machine tool portal, a new dynamic analysis of the whole structures have been performed in order to evaluate if the influence of the foam on the dynamic behaviour, changes after a certain number of work cycles.

The setup of the tests obviously doesn't change respect to the modal analysis previously described in *paragraph 2.3.1*, in particular the configuration shown in Figure 2.25 has been used for the determination of low frequency modes as a soft tip is mounted on the instrumented hammer. The modal parameter identification was carried out by means of the manual selection of the peaks of

interest. For each peak one of the three parameter identification algorithms was selected (peak-amplitude has been used in most of cases).

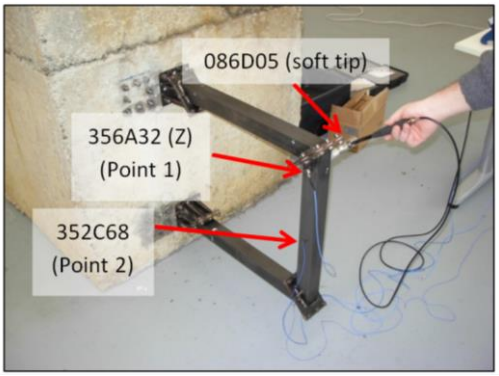

Figure 2.25: Experimental setup for the measurement of low frequency modes.

In order to compare the results obtained with the previous dynamical analysis, the same two modes were selected, one in the low-frequency range (labeled 90 *Hz*) and the second in the mid-frequency range (labeled 700 *Hz*). The modal mass obviously does not change because no more mass has been introduced in the tubes. Moreover as shown in Table 2.10 with respect to the 0 cycles structures the eigenfrequencies change abundantly of less than 10% and the dynamic stiffness shows some variations (increments except for Alulight filling and mid frequency mode) but not significant as the ones shown by the damping ratio (Table 2.11). In particular the attention has been focused on the damping ratio due to the fact it represents the most interesting parameter for the reference applications considered and the other parameters don't show significant changes after the 10000 bending cycles executed. In particular from the results of the analysis it is possible to observe how the value of the damping ratio increases for all the structures respect to the one measured before that the three-points bending tests have been performed. As shown in Table 2.11 the most significant change is the one relative to the 700 *Hz* mode for the Alulight structure whose

damping ratio increases of 1020% respect to the filled untested structure, corresponding to an increase of 3800% considering the initial empty portal.

[%] Variation of eigenfrequencies			
Type of foam filling	***Filled untested structure respect to empty structure***	***Filled structure after 10000 bending cycles respect to empty structure***	***Filled structure after 10000 bending cycles respect to filled untested structure***
90 *Hz* mode			
Alulight	-10.64	-8.68	+2.19
APM L	-7.46	-7.64	-0.19
APM H	-8.59	-9.06	-0.51
700 *Hz* Mode			
Alulight	-12.92	-6.90	+6.91
APM L	-8.40	-8.69	-0.32
APM H	-9.50	-10.34	-0.98
[%] Variation of dynamic stiffness			
90 *Hz* mode			
Alulight	-1.77	+17.70	+19.82
APM L	-8.89	+0	+9.76
APM H	-13.24	-2.94	+11.86
700 *Hz* Mode			
Alulight	+35.03	-31.08	-48.96
APM L	+19.75	+26.94	+6.02
APM H	+40.89	+56.52	+11.09

Table 2.10: Summary of the eigenfrequency and dynamic stiffness variations for the three structures submitted to bending tests.

These results, partially surprising (because of the really strong increment in damping ratio) but obviously positive, can be probably explained considering that the cyclic three-points bending tests, to which the samples have been

subjected, cause internal changes in correspondence of the foam cells and at the interface layer between foam and steel (*Appendix 3*).

[%] Variation of damping ratio			
Type of foam filling	***Filled untested structure respect to empty structure***	***Filled structure after 10000 bending cycles respect to empty structure***	***Filled structure after 10000 bending cycles respect to filled untested structure***
90 *Hz* mode			
Alulight	+65.96	+79.47	+8.14
APM L	+56.52	+86.17	+18.94
APM H	+53.85	+78.85	+16.25
700 *Hz* Mode			
Alulight	+248.28	+3800.97	+1020.08
APM L	-18.18	+15.79	+41.52
APM H	-30.56	-0.36	+43.48

Table 2.11: Summary of the damping ratio variations before and after the three-points bending tests.

The total effect is an increase of the internal friction and consequently of the energy dissipated that, as explained in detail in *paragraph 1.4*, is strictly connected with the damping capacity of the foam. The different effect of the bending tests performed, on the damping ratio for the two modes, can be explained by their shape (Figure 2.26). As already explained in *paragraph 2.3.2*, the low frequency one is a straight line from the constraint to the free end whereas the second is a parabola starting and ending at near-zero deformation. The hybrid APM filling types are bonded (glued) to the skin whereas the aluminum foam is not bonded. If such a bonding is not present, a 700 *Hz* parabolic shape mode enables a great energy dissipation (friction). This is the most promising hypothesis for the explanation of the high increase of damping ratio value for the 700 *Hz* mode, respect to the other increments.

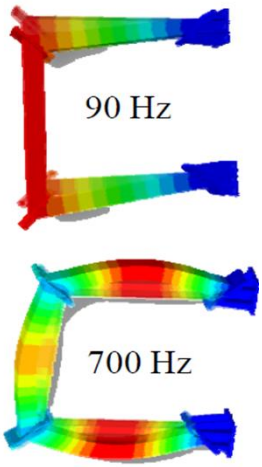

Figure 2.26: Shape of the low and the mid-frequency modes considered.

2.6 Discussion of results

At the end of the analysis executed on foam filled steel samples, it can be stated that, as expected, the filling has a significant positive influence on the dynamic behaviour of the structures considered (models of machine tool portal). The damping capacity of the overall structures in fact increases significantly (particularly for aluminum foam) considering the empty respect to the foam filled steel tubes whose membrane modes have been even suppressed by all the types of foam fillings (Alulight or hybrid APM). Anyway the main purpose of this analysis was to understand if the dynamical improvement would have been influenced by the simulation of a certain number of work cycles executed through three-points bending tests monitored in displacement and with an accelerometer and an ultrasound detector in order to be sure not to damage the samples. The final dynamic analysis shows how the damping capacity not only does not get worst but increases significantly after the simulated work cycles. This represents a surprising but obviously positive result and a starting point for future deep studies in which the interaction between the foam and the tube, presumably responsible of this effect, will be investigated in detail.

Chapter 3

Foam filled titanium tubes

This part of the work regards the analysis of the performance of titanium round tubes filled with Alulight aluminum foam, submitted to cyclic three-points bending tests and static axial compression tests. The general objective is to push the use of metal foam filled tubes in helicopters field, presenting all the results obtained (for both titanium filled samples and steel filled samples whose analysis has been previously described), to the *Bell Helicopter Textron Canada*.

3.1 Preparation of the samples

The set of samples produced for the tests is composed by different types of samples depending on the test in which they have to be used. In particular as previously said, the distinction is between the samples used for the cyclic three-points bending tests and the samples subjected to quasi- static axial compression tests.The tubes are in titanium grade 2 (characterized by a limited cost and more easily available respect to titanium grade 5) whose usual characteristics are listed in Table 3.1. This material presents the high strength, low weight ratio and outstanding corrosion resistance typical of titanium and its alloys, and is typically used for the following applications:

- Orthopaedic applications, such as implants and prosthesis;
- Airframe and aircraft engine parts;

– Marine chemical parts;
– Condenser tubing;
– Heat exchangers. [51]

Parameter	***Value***
ρ [kg/m^3]	4510
E [MPa]	105000
Yield point [MPa]	275 - 410

Table 3.1: Mechanical properties of titanium grade 2. [55]

3.1.1 Samples for the cyclic three-points bending tests

This set of round samples (Table 3.2), whose dimensions are reported in Table 3.3, is composed by 7 Ti tubes filled with aluminum foam of nominal density 560 *kg/m^3*, 1 Ti tubes filled with aluminum foam of nominal density 815 *kg/m^3*, 2 samples of only foam of nominal density 560 kg/m^3 and one empty Ti tube subjected to the same thermal treatment of the process of foaming. In particular:

ID number	***Type***	***Foam nominal density*** *[kg/m^3]*	***Foam approximate density*** *[kg/m^3]*
FF_560_1	Foamed filled Ti tube	560	574
FF_560_2	Foamed filled Ti tube	560	548
FF_560_3	Foamed filled Ti tube	560	562
FF_560_4	Foamed filled Ti tube	560	561
FF_560_5	Foamed filled Ti tube	560	562
FF_560_6	Foamed filled Ti tube	560	559
FF_560_7	Foamed filled Ti tube	560	560
FF_815_1	Foamed filled Ti tube	815	813
F_560_1	Foam only	560	542

F_560_2	Foam only	560	546
E_1	Empty Ti tube	-	-

Table 3.2: List of the samples used for the three-points bending tests.

Parameter	***Value***
Nominal length [mm]	215
Diameter of the tube [mm]	40
Thickness of the tube [mm]	2
Diameter of the foam [mm]	36

Table 3.3: Dimensions of the samples used for the three-points bending tests.

In order to fill the titanium tubes with aluminum foam, Alulight Foaminal commercial precursors were placed horizontally inside the tubes whose end parts have been then closed through the use of two stoppers as shown in Figure 3.1b. In particular have been used three precursors for the lower nominal density (560 kg/m^3) and four precursors for the higher one (815 kg/m^3). The samples have then been foamed horizontally in an air convection furnace preheated at 750 $°C$ for about 13 minutes and finally cooled in a compressed air flux (making them turn as shown in Figure 3.1c in order to obtain a density as uniform as possible), after which the stoppers have been removed and the end parts of the samples cut because usually inhomogeneous, obtaining the final nominal length of 215 *mm*.

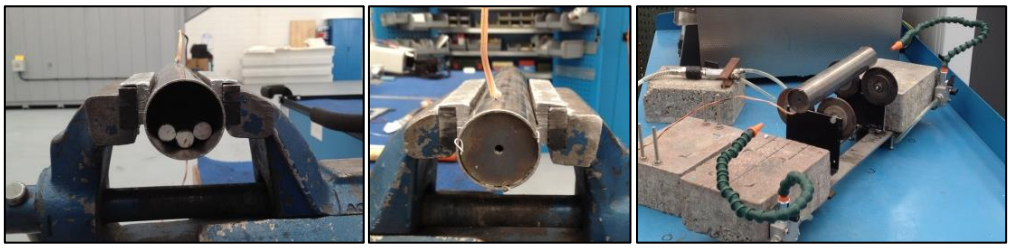

a) b) c)

Figure 3.1: a) Precursor placed horizontally inside a tube, b) Detail of a stopper used for the foaming process, c) Final cooling of the sample.

Note how there is no adhesion between the aluminum foam and the tube. In fact as explained by Yan et al. [9] the low solubility suppresses the growth of the intermediate layer at the interface of solid titanium and molten aluminum. In particular they have found a only 3 μm thick layer at the solid titanium - liquid aluminum interface, while under the same conditions the intermediate zone of stainless steel is about 30 μm thick. However, this fact has no negative influence on the performance of the foam. [Appendix 3: adhesion of the foam]
Regarding the samples of only foam, the only difference respect to the process previously described is that the tube is substituted with a mold (Figure 3.2a) and after the cooling the sample is extracted from it using the extractor shown in Figure 3.2b.

a) b)

Figure 3.2: a) Mold used to manufacture the sample of only foam, b) Extractor used after the cooling.

3.1.2 Samples for the quasi-static axial compression tests

This set of round samples (Table 3.4), whose dimensions are reported in Table 3.5, is composed 3 empty Ti tubes termically untreated, 3 empty Ti tubes subjected to the same thermal treatment of the process of foaming, 6 foam filled Ti tubes with nominal density of 560 kg/m^3, 3 foam filled Ti tubes with nominal density of 815 kg/m^3, 3 samples of only foam with nominal density of 560 kg/m^3 and 3 samples of only foam with a nominal density of 815 kg/m^3.

ID number	***Type***	***Foam nominal density*** *[kg/m^3]*	***Foam approximate density*** *[kg/m^3]*
E_1	Empty Ti tube untreated	-	-
E_2	Empty Ti tube untreated	-	-
E_3	Empty Ti tube untreated	-	-
ET_2	Empty Ti tube th. treated	-	-
ET_3	Empty Ti tube th. treated	-	-
ET_4	Empty Ti tube th. treated	-	-
FF_560_1a	Foamed filled Ti tube	560	712
FF_560_1b	Foamed filled Ti tube	560	567
FF_560_1c	Foamed filled Ti tube	560	400
FF_560_2a	Foamed filled Ti tube	560	577
FF_560_2b	Foamed filled Ti tube	560	602
FF_560_2c	Foamed filled Ti tube	560	468
FF_815_1a	Foamed filled Ti tube	815	827
FF_815_1b	Foamed filled Ti tube	815	838
FF_815_1c	Foamed filled Ti tube	815	760
F_560_1a	Foam only	560	615
F_560_1b	Foam only	560	484
F_560_1c	Foam only	560	544
F_815_1a	Foam only	815	1030
F_815_1b	Foam only	815	746
F_815_1c	Foam only	815	679

Table 3.4: List of the samples used for the quasi-static axial compression tests.

Parameter	*Value*
Nominal length [mm]	70
Diameter of the tube [mm]	40
Thickness of the tube [mm]	2
Diameter of the foam [mm]	36

Table 3.5: Dimensions of the samples used for the static axial compression tests.

The procedure used to fill the titanium tubes is exactly the same previously described for the samples subjected to the three-points bending tests. In fact the samples are obtained simply cutting samples of 210 *mm* of length.

3.2 Cyclic three-points bending tests

As the bending tests on the steel tubes described in *Chapter 2* this part of the work, whose aim is to study the performances of foam filled titanium samples subjected to cyclic three-points bending tests, has been entirely carried out at university ÉTS (*École de technologie supérieure*) de Montréal.

3.2.1 Experimental setup: fixtures and devices

The machine used to execute these tests is the same described in C*hapter 2*, used for the tests on foam filled steel samples (Figure 2.6). As previously said it can be controlled through the displacement of the lower cylinder or through the force measured by the force transducers which represent, with the number of cycles, the only information given by the MTS machine during the tests.

Design and manufacture of the fixtures

The first steps have been the design and manufacture of the fixtures compatible with the MTS machine available in order to execute the tests according to the

standard *ISO 7438* (Metallic material - bend test), approximating the titanium round samples filled with metal foam, with empty titanium round samples with the following characteristics:

- Diameter = 40 *mm*;
- Thickness of the walls of the tubes t = 2 *mm*;
- Length 215 *mm*.

As already said in *Chapter 2*, design the fixtures for a three-points bending test consists in find out the dimension of the former, the dimensions of the two lower supports and the distance l between them (Figure 3.3):

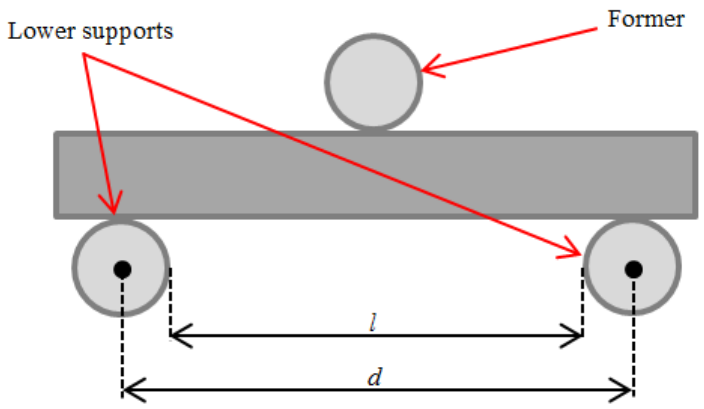

Figure 3.3: Schematic representation of the three-points bending test.

According with the standard ISO 7438, the distance between the lower supports (l) is given by:

$$l = (D + 3 \cdot a) \pm a/2$$

Where a is the diameter of the test piece and D is the diameter of the former and the lower supports, who has to be simply greater then a. Therefore we have obtained the following results:

$a = 40\ mm$

$D = 55\ mm$

$l = (D + 3 \cdot a) \pm a/2 = (55\ mm + 3 \cdot 40\ mm) \pm 40/2\ mm = 175 \pm 20\ mm$

The specific value of 55 *mm* for *D* has been chosen in order to use the same former and lower supports manufactured for the tests on steel square foam filled samples (*Chapter 2*). The chosen value for *l* is instead 155 *mm* because this represents the only solution to obtain a value of *d* (distance between the axes of the lower supports) lower than the length of the samples:

$d = l + D/2 + D/2 = 155\ mm + 55\ mm = 210\ mm < 215\ mm$

Obviously the former is centered on the length of the tube as shown in Figure 3.3. The following table summarizes all the values of interests for the manufacturing of the fixtures:

Parameter	***Value***
D [mm]	55
D [mm]	210
Maximum Load [kN]	100

Table 3.6: Summary of the values of interest for the manufacture of the fixtures for the bending tests on titanium tubes.

As already said for all the bending tests regarding *Chapter 2* and *Chapter 3* we have used the same fixtures because the former and the lower supports have been designed with the same dimensions for both the kind of samples. The only difference is represented by the distance between the lower supports which for that reason can be shifted (Figure 3.4).

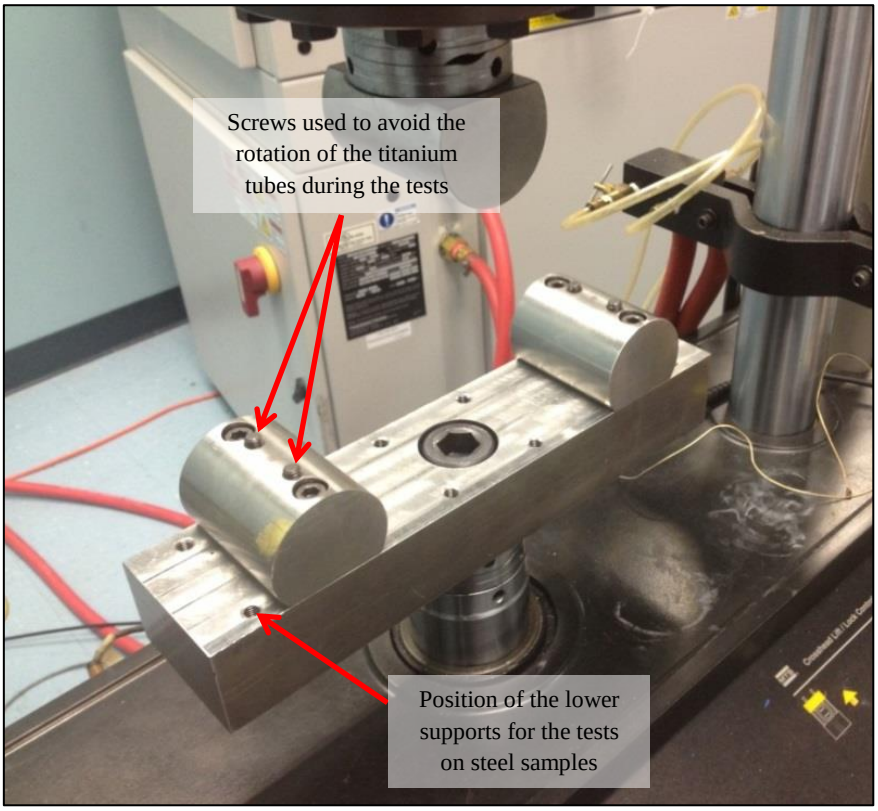

Figure 3.4: Fixtures installed for the cyclic three-points bending tests on titanium samples.

Devices used for the monitoring of the tests

Considering that the information given by the MTS machine are only the displacement of the lower cylinder and the force applied in the middle point of the upper part of the tube measured by the force transducers (Figure 2.6), other devices have been used for the monitoring of the tests. In particular:

- A dial indicator for measuring the effective displacement of the middle point of each sample;
- The Pocket AE-1 Acoustic Emission (AE) system whose functioning will be described below.

Dial indicator

As already said the dial indicator has been used to measure the effective displacement of the middle point of each sample during the tests. It has been installed as shown in Figure 3.5, fixing it to the lower part of the fixture through a magnetic base.

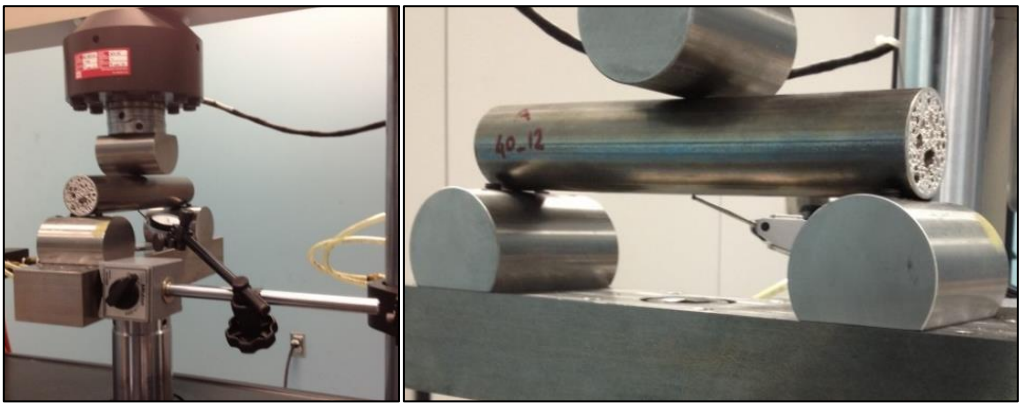

a) b)

Figure 3.5: a) Dial indicator fixed to the lower support through the magnetic base, b) Detail of the point of contact between the dial indicator and a sample.

The dial indicator used presents the following characteristics:

- Resolution 0.0005 *in* = 0.0127 *mm*;
- Measuring range 0.03 *in* = 0.7620 *mm*.

However the measuring range hasn't been always binding because if the displacement between a measurement and the following one didn't exceed it, it was possible to reset the system on the zero conditions. So the term "exceed the measurement range" used in the following paragraphs, means that the displacement increases respect to the previous one of a quantity major than the measuring range.

Pocket AE-1 Acoustic Emission (AE) system

As previously said for the tests on the square steel samples, there are ultrasonic components in practically all forms of friction, so it makes sense to suppose that acoustic emission could be strictly connected with any damages or cracks that can develop inside the samples during the tests.

For that reason the last device used for the monitoring of the samples during the cyclic three-points bending tests executed is the Pocket AE-1 Acoustic Emission system (Figure 3.6) which uses an architecture much like that used in hand-held PDA (Portable Data Assistant) and utilizes Microsoft Windows-CE™ operating system (compact version of Microsoft Windows™). The unit, which permits to do acquisition in continuous differently from the ultrasound detector *UltraProbe 10000* used for the bending tests on steel square samples, can be configured by the end-user according with the needs of the tests and presents a screen with 200 × 200 pixel resolution for the viewing of clear and sharp graphs. [41]

In particular the main settings chosen for the monitoring of the three-points bending tests executed are:

- 1 channel of acquisition;
- Variable threshold established by the software through the calculation of the moving average of the signal (choice recommended by the manual in case of inexperience in acoustic signals acquisition);
- Sample rate of 1 *MSPS* (Mega Samples Per Second) which means that one waveform sample is taken every *μsec* (standard value recommended by the manual in case of inexperience in acoustic signals acquisition);
- High pass analog filter 1 *MHz*;
- Low pass analog filter 1 *kHz*;
- Parameters of interest, typically used in detection of crack propagation: Hit, Counts and RMS. [Appendix 2]

Figure 3.6: Pocket AE-1 System composed by an hand-held AE unit, R15α AE sensor and 1 meter sensor cable. [41]

The sensor has been installed as represented in Figure 3.7, fixing it to the sample through a tape after have put a conductor gel between them, to favor a better transmission of the signal and to avoid friction which could damage the sensor and influence the results. [41] [42]

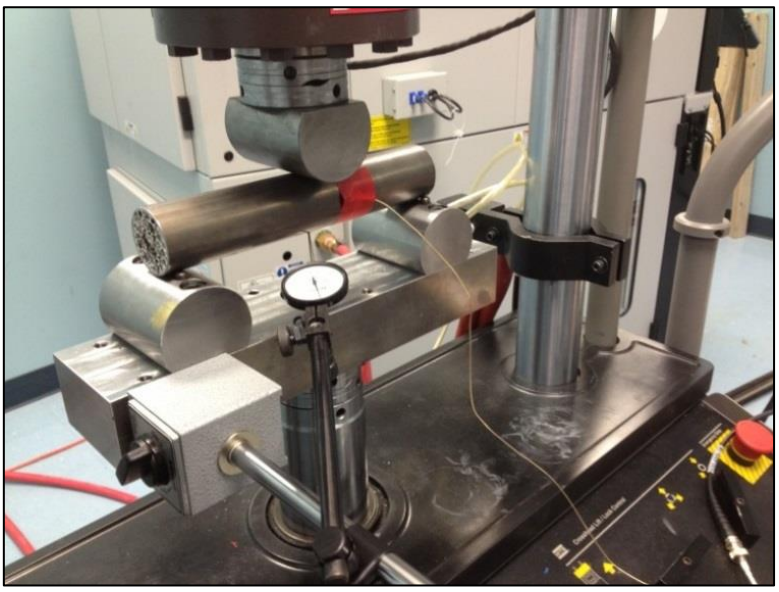

Figure 3.7: Dial indicator and acoustic sensor installed on a titanium sample.

3.2.2 Procedure and results

As previously said, the objective of this part of the work is to study the performances of foam filled titanium samples subjected to cyclic three-points bending tests (listed in Table 3.1), paying attention to the possible development of internal damages through the use of the AE system described in *paragraph 3.2.1* (*Experimental setup: fixtures and devices - Pocket AE-1 Acoustic Emission (AE) system*).

First of all, as for the steel samples, few standard steps have been done in order to be sure to work in safety conditions: warm-up cycles without samples have been performed to tune in displacement the *MTS* machine and subsequently sample FF_560_1 has been installed on the fixtures described in *paragraph 3.2.1 - Design and manufacture of the fixtures*, in order to execute the auto-tuning in load. Moreover before starting with the tests, sample FF_560_1 has been submitted to few bending cycles in which the frequency and the force applied have been changed manually in order to establish the security parameters then used for all the cyclic three-points bending tests performed on titanium samples. In particular, the following values have allowed to work in safety conditions, keeping the samples in touch with the two supports and the former during each bending cycle:

- Preload $= 0.5\ kN$;
- Frequency $= 1\ Hz$.

After this preliminary phase, a cyclic three-points bending step loading test (Figure 2.15) whose characteristics are here summarized, has been carried out on four samples (one of each type) listed in Table 3.7:

- Preload $= 0.5\ kN$;

- Starting value of the maximum load, which increases of $0.5\,kN$ every 100 cycles, equal to $1\,kN$;
- Sinusoidal pattern;
- Frequency $= 1\,Hz$.

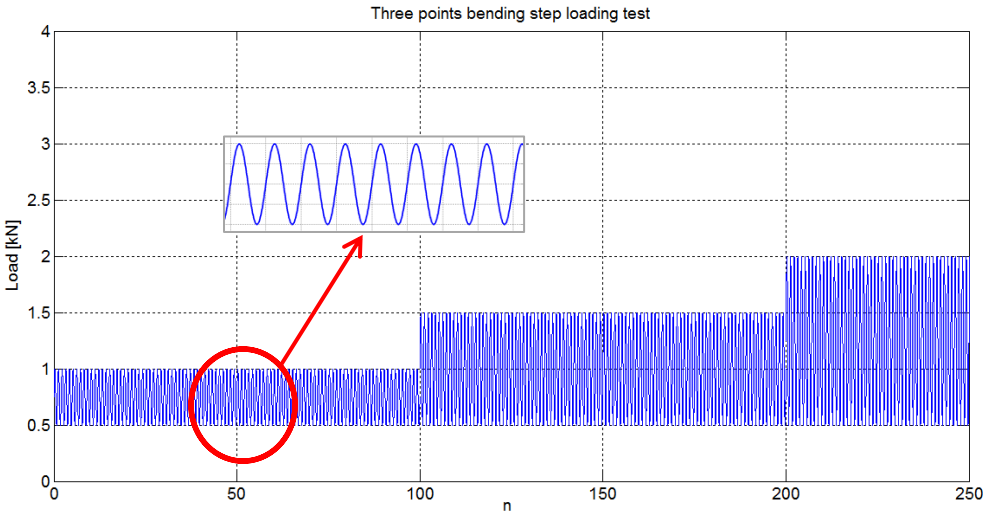

Figure 3.8: Representation of the first 250 cycles of the three-points bending step loading test with a zoom which points out the sinusoidal pattern.

ID number	***Type***	***Foam nominal density*** *[kg/m^3]*	***Foam approximate density*** *[kg/m^3]*
FF_560_2	Foamed filled Ti tube	560	548
FF_815_1	Foamed filled Ti tube	815	813
E_1	Empty Ti tube	-	-
F_560_1	Foam only	560	542

Table 3.7: List of the samples used for the cyclic three-points bending step loading tests.

During these first tests the sample has been monitored only through the dial indicator installed as described in *paragraph 3.2.1* measuring the displacement of the middle point of the samples (Figure 3.5) when the maximum value of force was applied. In particular, have been executed three measurements for

each loading step, after the 1st, the 50th and the 100th cycle obtaining the results shown in Table 3.8 and Figure 3.9. Note how the halting condition is the same one used for the bending tests on the square samples, in fact each test has been stopped when the displacement increased significantly for the measurements executed during the same loading step.

***Maximum Load** [kN]*	***Displacement** [mm]*			***n***	***Cumulative n***
	1st	***2nd***	***3rd***		
Sample FF_560_1					
1	0.04	0.04	0.04	100	100
1.5	0.09	0.10	0.10	100	200
2	0.13	0.14	0.14	100	300
2.5	0.18	0.19	0.19	100	400
3	0.25	0.27	0.27	100	500
3.5	0.34	0.36	0.37	100	600
4	0.46	0.47	0.47	100	700
4.5	0.57	0.58	0.58	100	800
5	0.69	0.70	0.70	100	900
5.5	0.77	0.79	0.79	100	1000
6	0.86	0.88	0.89	100	1100
6.5	0.98	1.00	1.03	100	1200
7	1.12	1.17	1.19	100	1300
7.5	1.28	1.33	1.35	100	1400
8	1.44	*e.m.r.*	*e.m.r.*	100	1500
Sample FF_815_1					
1	0.05	0.06	0.06	100	100
1.5	0.14	0.15	0.15	100	200
2	0.25	0.25	0.25	100	300
2.5	0.32	0.32	0.32	100	400
3	0.37	0.38	0.38	100	500
3.5	0.42	0.43	0.43	100	600
4	0.48	0.50	0.50	100	700
4.5	0.55	0.55	0.56	100	800

5	0.61	0.62	0.62	100	900
5.5	0.69	0.70	0.70	100	1000
6	0.76	0.77	0.77	100	1100
6.5	0.85	0.86	0.86	100	1200
7	0.94	0.95	0.95	100	1300
7.5	1.03	1.04	1.05	100	1400
8	1.12	1.13	1.14	100	1500
8.5	1.22	1.24	1.26	100	1600
9	1.33	1.35	1.35	100	1700
9.5	1.42	1.45	1.46	100	1800
10	1.51	1.52	1.54	100	1900
10.5	1.60	1.61	1.63	100	2000
11	1.68	1.70	1.70	100	2100
11.5	1.77	1.79	1.82	100	2200
12	1.88	1.91	1.93	100	2300
Sample ET_1					
1	0.13	0.13	0.13	100	100
1.5	0.28	0.29	0.29	100	200
2	0.51	0.52	0.53	100	300
2.5	0.76	0.77	0.77	100	400
3	0.89	0.90	0.91	100	500
3.5	1.00	1.03	1.03	100	600
4	1.13	*e.m.r.*	*e.m.r.*	100	700
Sample F_560_2					
1	0.24	0.24	0.24	100	100
1.5	0.76	0.76	0.76	100	200
2	*e.m.r.*	*e.m.r.*	*e.m.r.*	100	300
2.5	*break after the 1st cycle*			1	301

Table 3.8: Displacement measured after the 1st, the 50th and the 100th cycle of each step of load.

Note how *n* represents the number of cycles and the term *e.m.r.* means that the value exceeds the measurement range as already explained in *paragraph 3.2.1*.

This is the reason why the last part of the graphic in Figure 3.9a, 3.9c and 3.9d is dashed.

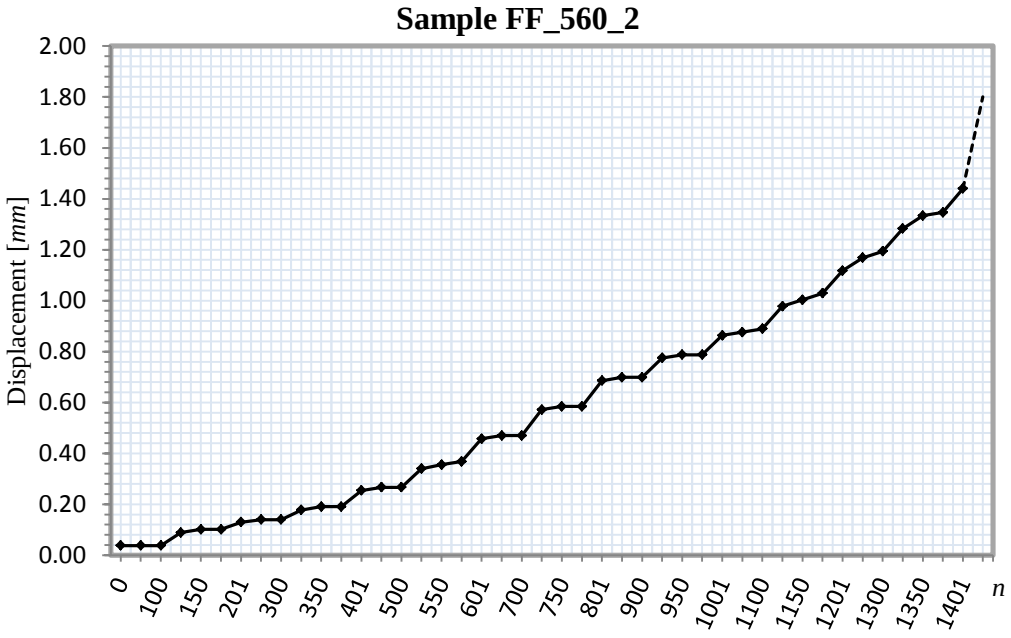

a)

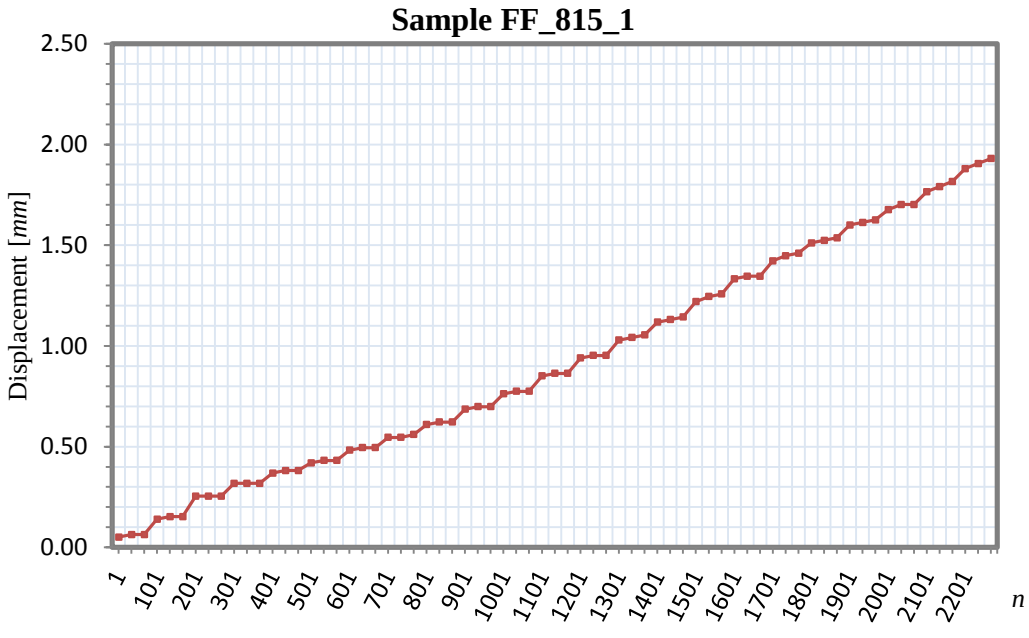

b)

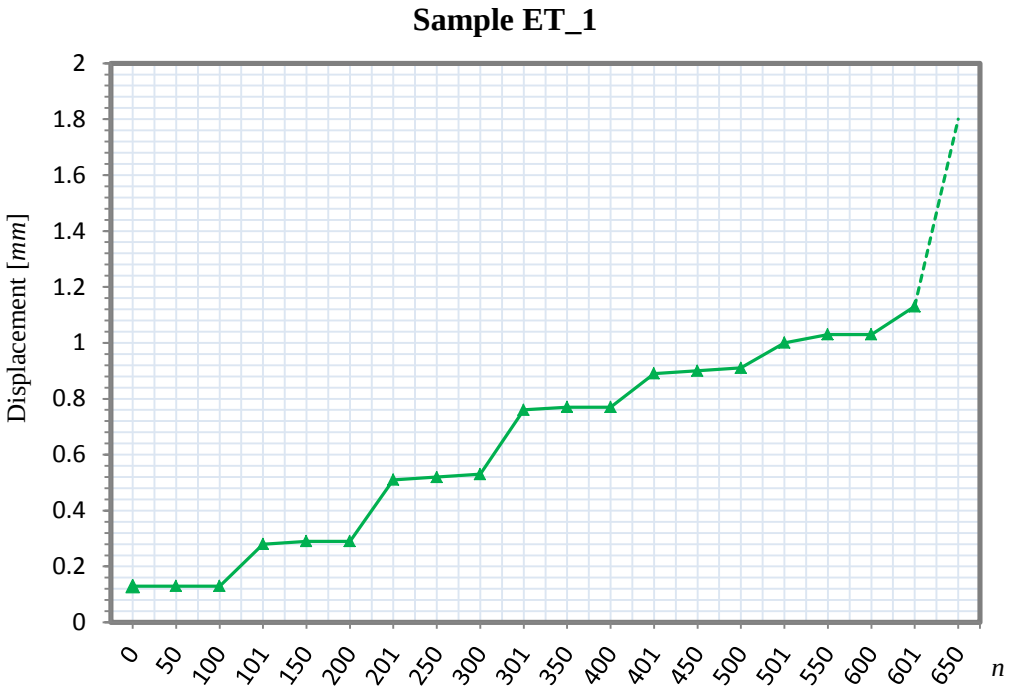
Sample ET_1
Displacement [mm]
2
1.8
1.6
1.4
1.2
1
0.8
0.6
0.4
0.2
0
0
50
100
101
150
200
201
250
300
301
350
400
401
450
500
501
550
600
601
650
n

c)

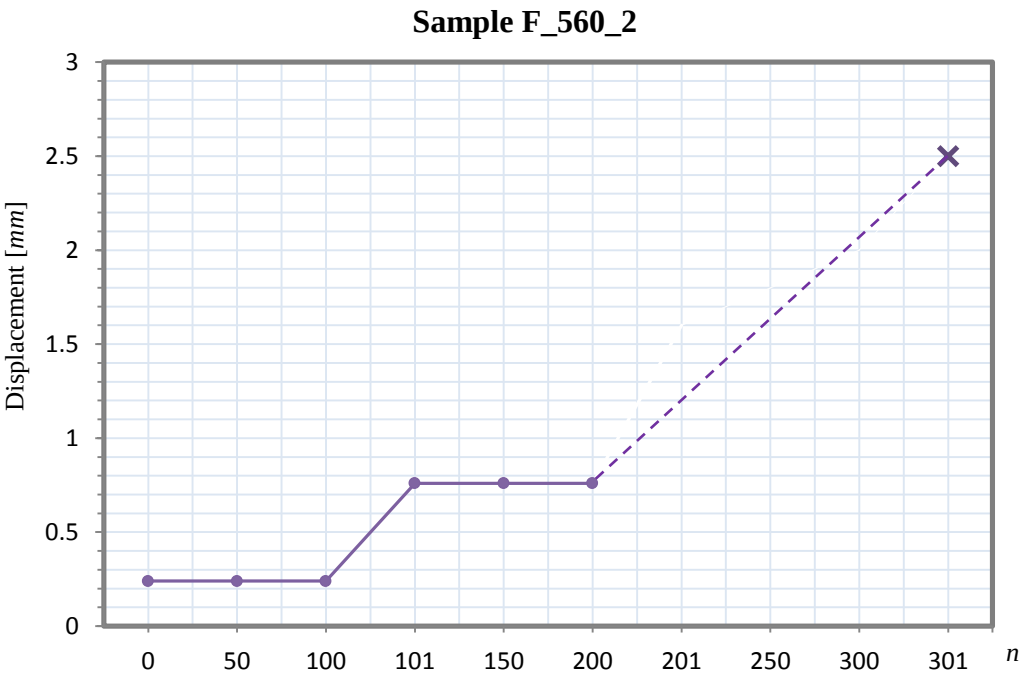
Sample F_560_2
Displacement [mm]
3
2.5
2
1.5
1
0.5
0
0
50
100
101
150
200
201
250
300
301
n

d)

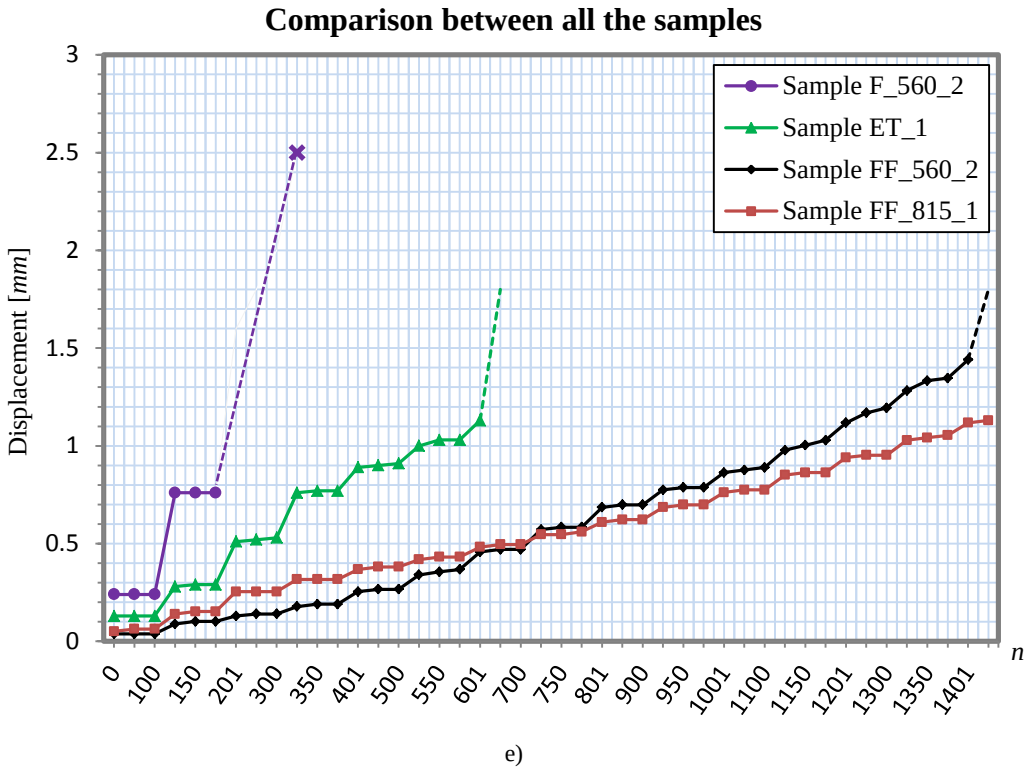

e)

Figure 3.9: Displacements measured during the three-points bending step loading test on all the samples. a) Sample FF_560_2, b) Sample FF_815_1, c) Sample ET_1, d) Sample F_560_2, e) Comparison between all the samples tested.

From the results it is possible to observe how the worst behaviour, as expected, is the one obtained for sample F_560_2 constituted of only foam (Figure 3.9e) for which the displacement is constantly higher respect to the one measured for the other samples. In particular the gap increases according to the growth of the maximum value of load, till the break in two parts of the sample which happens in correspondence of the 1st bending cycle at 2.5 *kN* (Figure 3.9d). Note how for testing this type of sample has been necessary to execute a new auto - tuning in load of the machine and some preliminary bending cycles (both executed on sample F_560_1, Figure 3.10) in order to be sure to work in safety condition using the parameters previously defined for titanium tubes (empty or filled).

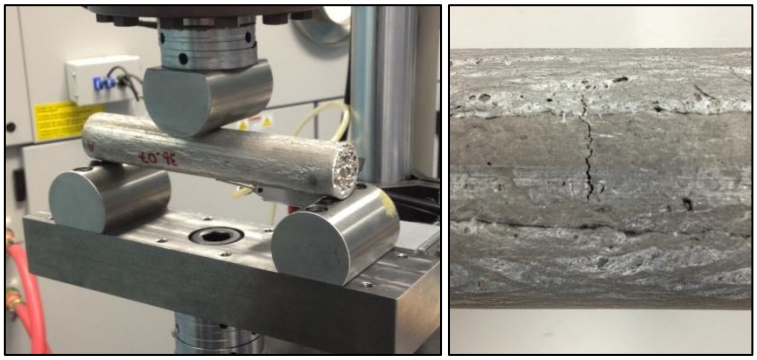

a) b)

Figure 3.10: a) Image of the test executed on sample F_560_2, b) Detail of the crack on sample F_560_1, used for the auto-tuning of the *MTS* machine.

Observing Figure 3.9e it is clear how, filling the titanium tubes, the mechanical behaviour improves significantly as indicated by the gap in displacement between the empty titanium sample (ET_1) and the filled ones (FF_560_2 and FF_815_1), which grows with the increase of the load and the number of cycles. Moreover sample ET_1, shows a strong plastic deformation on the surface which decreases significantly, till almost disappear, considering the two samples filled with different density of foam as shown in Figure 3.11, even if they have been subjected to higher values of load (Table 3.7).

a)

b)

Figure 3.11: Comparison between the plastic deformation in correspondence of the point of contact with the former of samples ET_1 (a) and sample FF_815_1 (b), after the cyclic bending step loading tests.

Focusing instead the attention on the two filled sample, it is possible to observe how, as expected, increasing the density the displacement decreases except for the first loading steps for which the lower density is more performing. Moreover, while as indicated in Table 3.8, with sample FF_560_2 the measuring range is exceeded (*e.m.r.*) in the loading step characterized by a maximum load of 8 *kN*, sample FF_815_1 doesn't show this problem, maintaining a linear behaviour till the end of the test (12 *kN*). However the most interesting result is represented by the fact that, increasing the density of the aluminum foam, the response of the material to the bending condition, changes (Figure 3.9a and 3.9b). In fact, as shown in Figure 3.12, sample FF_560_2 shows a quadratic trend, while the response of sample FF_815_1 is, as already said, clearly linear from the beginning till the end of the test.

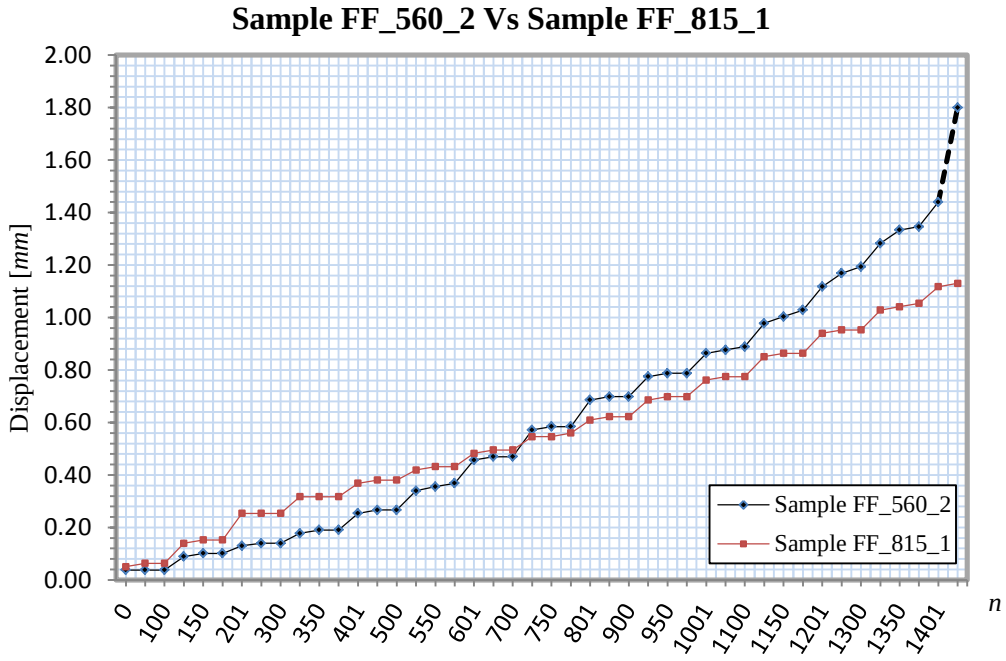

a)

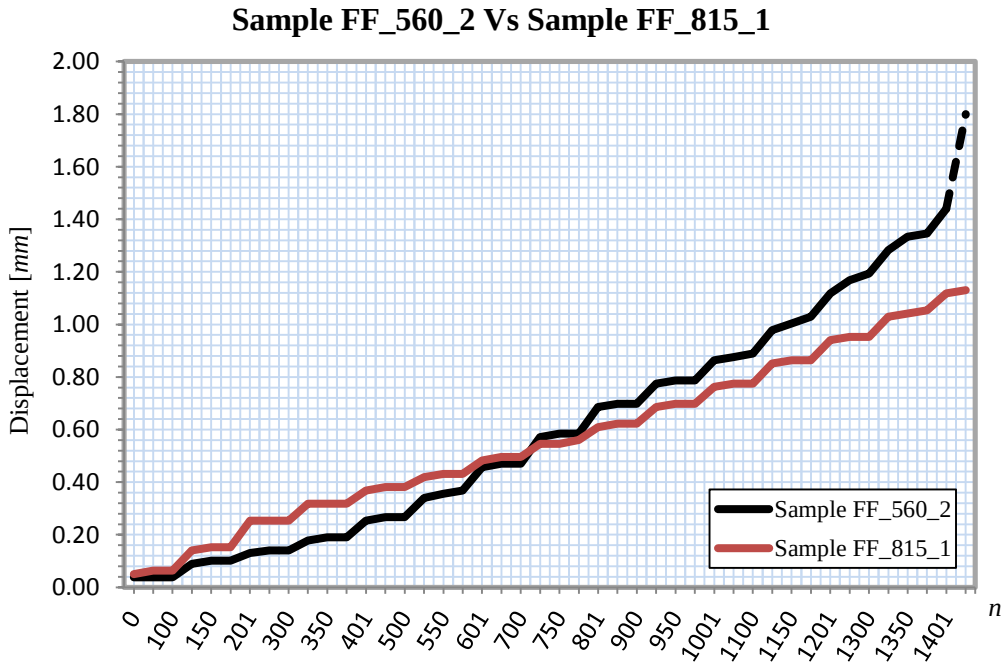

b)

Figure 3.12: a) Comparison between the results obtained for sample FF_560_2 and sample FF_815_1, b) Comparison between the quadratic and the linear trend of the displacements of the two samples.

After these comparisons between the different types of samples, the attention has been focused on sample FF_560_2 in order to establish the parameters for the subsequent tests to perform on the remaining samples (Table 3.1) filled with aluminum foam of low density (560 kg/m^3). In particular Figure 3.13 shows the displacements of the middle point of the sample, measured after the 1st and the 100th cycle of each loading step.

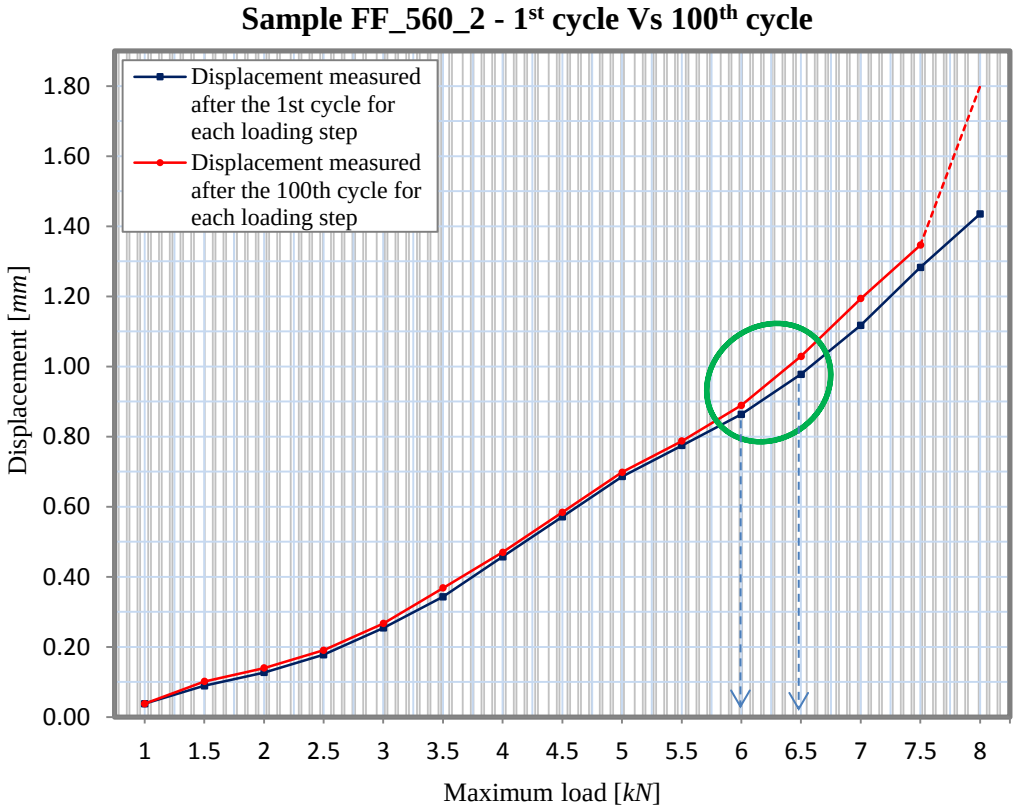

Figure 3.13: Comparison between the displacements of the middle point of sample FF_560_2, measured after the 1st and the 100th cycle of each loading step.

Looking at Figure 3.13, it is possible to observe how starting from the circled loading steps (corresponding to a maximum load of 6 and 6.5 *kN*) the difference between the values measured at the beginning and at the end of each step increases constantly till the end of the test, plausibly as consequence of an

irreversible dynamical effect. Considering that this behaviour is surely due also to the effect of the precedent loading steps and the number of cycles of the next test is significantly higher, a lower value respect to 6 *kN* has been chosen for the maximum load of the subsequent cyclic bending test (Figure 3.14), whose characteristics are here listed:

- Preload $= 0.5\ kN$;
- Maximum load $= 5\ kN$;
- Sinusoidal pattern;
- Frequency $= 1\ Hz$;
- Number of cycles $= 10000$.

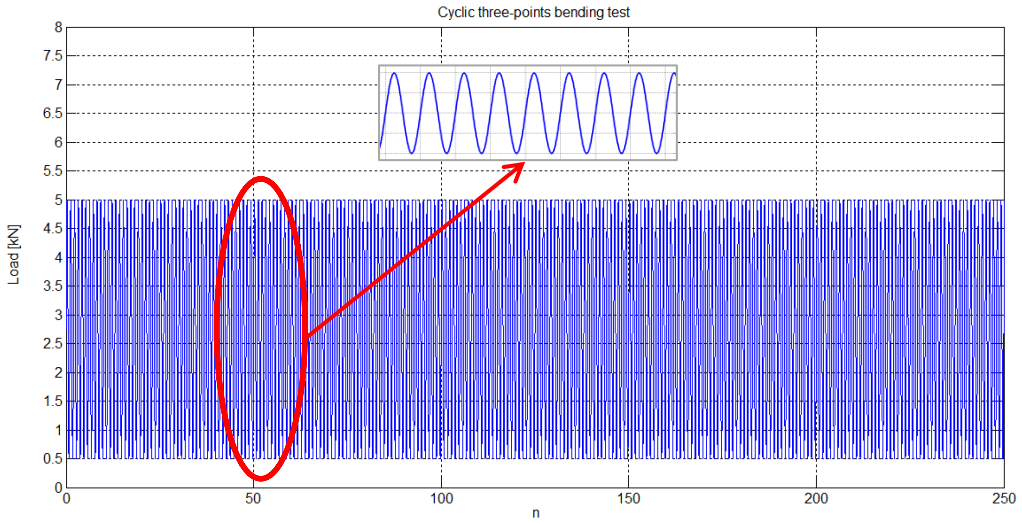

Figure 3.14: Cyclic three-points bending test performed on sample FF_560_3.

Note how from this moment, all the tests described, have been monitored not only in displacement using the dial indicator, but also through the AE system as represented in Figure 3.15 and described in *paragraph 3.2.1* (*Experimental setup: fixtures and devices*) in order to control if internal damages develop during the test, knowing that this type of technique, whose parameters are

described in detail in *Appendix 2 - Acoustic emission*, is currently used for traditional materials but there is no experience with metal foams.

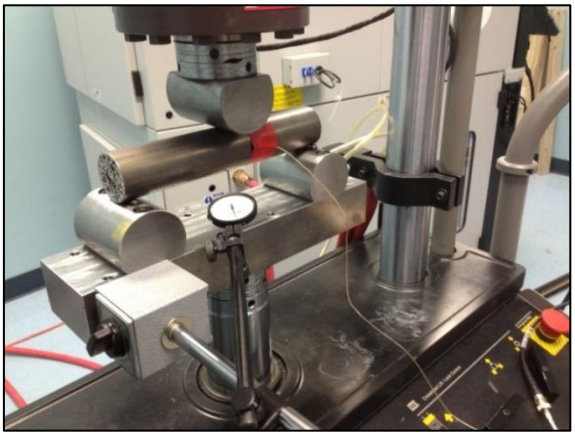

Figure 3.15: Dial indicator and acoustic sensor installed on sample FF_560_3.

At the end of the test it is possible to observe that, even if the displacement of the middle point of sample FF_560_3 increases gradually and significantly from the first to the last cycle, as reported in Table 3.9, the AE parameters do not show the exponential trend typical of crack propagation. This can be explained supposing that the increase of the displacement is due to an elasto-plastic deformation of the sample (relaxing the sample it shows a residual deflection) and not to the development of a crack inside it.

	Value
Displacement after 1 cycle *[mm]*	0.46
Displacement after 10000 cycles *[mm]*	0.56

Table 3.9: Initial and final displacement of sample FF_560_3.

In particular there is no increment of the parameters values which remain almost constant during all the 10000 cycles. Unfortunately the graphs relative to the trend of RMS, hits and counts are not available due to a problem with the AE acquisition system. In fact the sample rate chosen for the tests has been too high (the default one, as clearly suggested in the system manual for new users) for the

AE software through which hasn't been possible to open the data acquired because of their too big dimensions. For this reason has been decided to proceed performing other bending tests of 10000 cycles, reducing the maximum load, until was not found a value for which the displacement did not increase significantly between the first and the last cycle. The idea has been to use that value, for which nothing significant in terms of damages seemed to happen (coherent results between displacement ad acoustic emission), as maximum load of a 50000 cycles test in order to see if the values of the acoustic parameters would have increased, with the increase of number of cycles and displacement measured. The following tests have been executed:

- FF_560_4 → 10000 cycles, sinusoidal pattern $0.5 - 4\ kN$, $f = 1\ Hz$;
- FF_560_5 → 10000 cycles, sinusoidal pattern $0.5 - 3\ kN$, $f = 1\ Hz$;
- FF_560_6 → 10000 cycles, sinusoidal pattern $0.5 - 2\ kN$, $f = 1\ Hz$.

Obviously reducing the value of the maximum load, the acoustic parameters remain almost constant during all the test (there are no graphs due to the problem with the acquisition system previously described). From the values of all the displacements measured (listed in Table 3.10) it is possible instead to observe how, reducing the maximum load, the benefit in term of difference of displacement between the first and the last cycle, increases till we pass from 3 to 2 *kN*.

Sample ID	***Displacement after 1 cycle*** *[mm]*	***Displacement around 2000 cycles [mm]***	***Displacement after 10000 cycles*** *[mm]*
FF_560_4	0.35	0.38	0.38
FF_560_5	0.18	0.20	0.20
FF_560_6	0.13	0.15	0.15

Table 3.10: Displacements measured during the 10000 cycles tests.

In fact, even if the displacement is correctly lower for a maximum load of 2 *kN* the total increment of displacement is 0.02 *mm* for both the samples. Moreover this low difference of 0.02 *mm* is due to a sort of initial settling of the samples which after the first 2000 cycles stabilize and show the same value of displacement till the end of the tests (Table 3.10). For that reason the 10000 cycles tests have been stopped, and the value of 2 kN has been chosen as maximum load for the three-points bending test of 50000 cycles, whose characteristics are here summarized:

- FF_560_7 → 50000 cycles, sinusoidal pattern $0.5 - 2\ kN$, $f = 1\ Hz$.

The displacement increases from the first cycle (0.13 *mm*) to the last one (0.17 *mm*) of only 0.04 *mm* but the most interesting results have been obtained considering one of the AE parameters. In fact from the *Hits vs Time* graph (Figure 3.16) it is possible to observe the typical exponential trend of a crack propagation between 15000 and 20000 cycles (*Appendix 2 - Acoustic emission*).

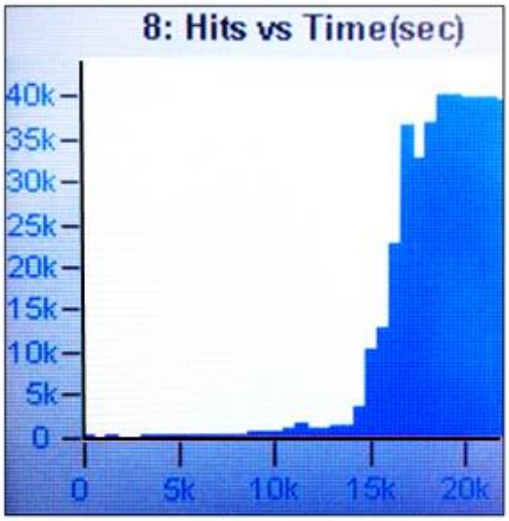

Figure 3.16: Exponential trend of the *Hits vs Time* graph for the test executed on sample FF_560_7.

The same indication is given by the *Counts vs Time* graph (Figure 3.17), even if with a less marked trend, probably due to fact that a variable threshold

established by the software through the calculation of the moving average of the signal (choice recommended by the manual in case of inexperience in acoustic signals acquisition) has been used, limiting the increase of this parameter.

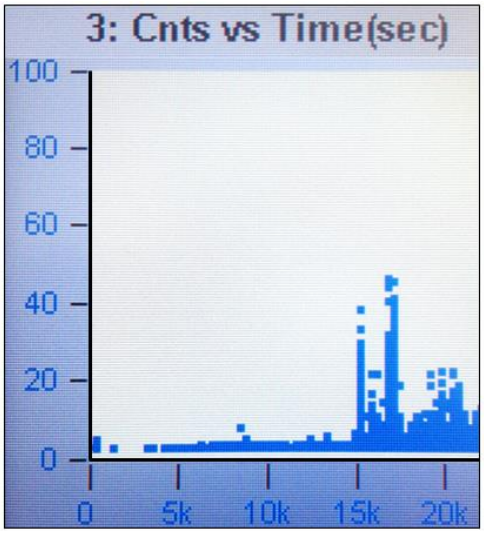

Figure 3.17: Trend of the *Counts vs Time* graph for the test executed on sample FF_560_7.

In correspondence of 15000-20000 cycles it is possible also to observe an increase of the RMS and the amplitude of the signal (Figure 3.18). However in this case they are not clear indexes of an internal damage compared with the parameters previously considered.

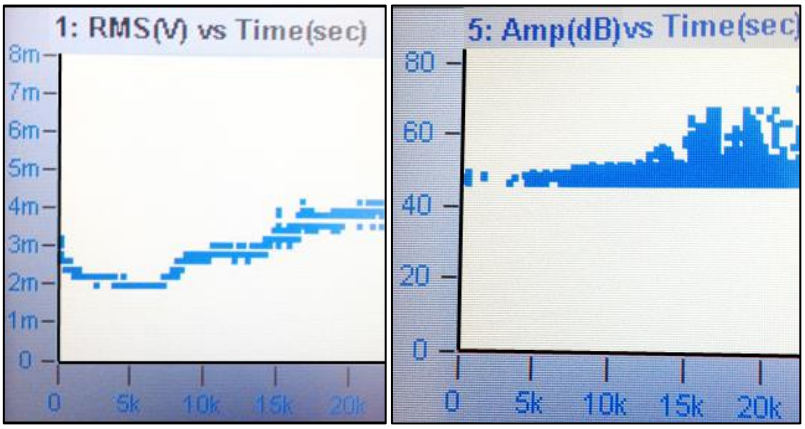

Figure 3.18: Trend of the *RMS vs Time and Amplitude vs Time* graphs for the test executed on sample FF_560_7.

Considering all the results, it can be stated that, the AE analysis suggests an internal damage which develops between 15000 and 20000 cycles but, considering the values of the displacement obtained, with a limited difference between the first and the last measurement executed (only 0.04 mm), it seems that whatever is the cause of the exponential increment of the hits, it does not influence significantly in a negative way, the mechanical behaviour of the sample.

3.2.3 Microscopic inspection of the samples

The next step of the analysis, has been the microscopic inspection of the samples tested, in order to verify, if the indications of the AE parameters were correct. In particular this part of the analysis has been carried out on samples FF_560_6 and FF_560_7 which had been previously subjected to the cyclic bending tests here summarized, which differed only for the number of cycles:

- FF_560_6 → 10000 cycles, sinusoidal pattern $0.5 - 2\ kN,\ f = 1\ Hz$.
- FF_560_7 → 50000 cycles, sinusoidal pattern $0.5 - 2\ kN,\ f = 1\ Hz$.

First of all the foam fillings have been removed from the tubes simply eliminating, through a metallographic honing machine, the metallic burr created in correspondence of the end parts of the samples (*paragraph 3.1.1* and *Appendix 3- Adhesion of the foam*). Therefore it was possible to proceed with the microscopic analysis comparing the two samples subjected to 10000 and 50000 cycles for which the AE parameters gave different indications. The most interesting results, obtained from the accurate analysis of all the lateral surface of the samples, are shown in Figure 3.19.

a)

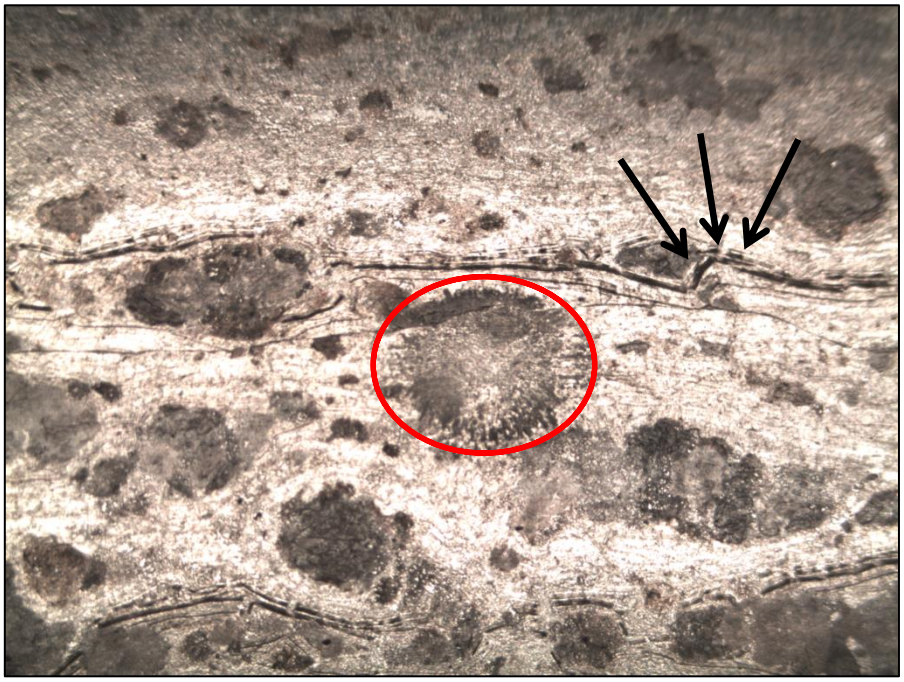

b)

Figure 3.19: a) Sample FF_560_6, detail of the zone around the point of contact with the former, b) Sample FF_560_7, detail of the zone around the point of contact with the former.

In fact comparing the two images it is possible to observe how the point of contact (circled in red for both the samples) is, as expected, more marked for sample FF_560_7 which has been subjected to a higher number of bending cycles (50000 Vs 10000). Moreover sample FF_560_7 shows clearly two canals in correspondence of the zones of conjunction between the precursors used for the foaming process. In particular one of them is strongly marked in the zone around the point of contact (it seems even open, as indicated by the black arrows) and both are extended for all the length of the sample. Figure 3.19a shows instead how sample FF_560_6 presents only one canal and it is significantly less marked respect to the ones shown in Figure 3.19b. Furthermore it is not developed along all the length of the sample. Obviously it is not possible to know if these surface irregularities were already present before the tests but it is possible to suppose that the differences between the samples are due to the increment of the bending cycles number and that this canals are so related with AE parameters trend.

Figure 3.20 shows finally another irregularity on the surfaces of sample FF_560_7, located under the neutral axis, that however seems negligible because of its limited dimensions and particularly for its rounded shape.

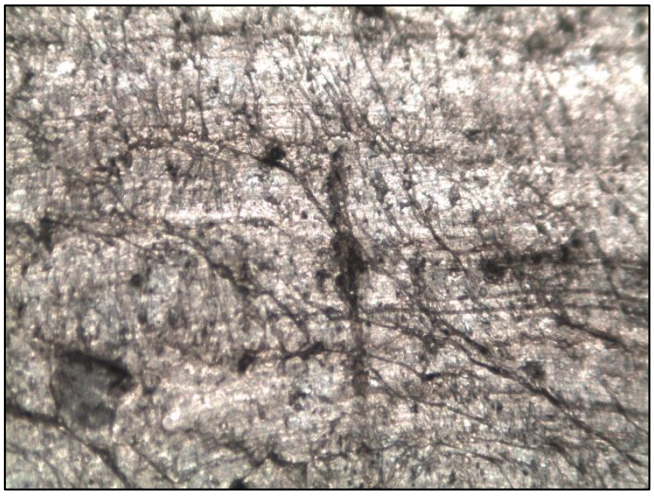

Figure 3.20: Irregularity under the neutral axes of sample FF_560_7.

In conclusion through the microscopic analysis (Figure 3.21) no cracks have been found and it can be supposed that the AE parameters trend is connected with the development of the canals shown in Figure 3.19b.

Figure 3.21: Image of sample FF_560_7 ready to be analyzed.

The final step executed to complete the study on these samples, has been the cut of sample FF_560_7, executed in order to:

- Evaluate the depth of the canal indicated by the black arrows in Figure 3.19b;

- Find out if sample FF_560 _7 had some internal damages through which the significant increment of the AE parameters between 15000 and 20000 cycles could have been explained in an alternative way.

Cutting transversely and longitudinally the sample using a saw, it has been possible to observe how the canal in correspondence of the zone of conjunction of the precursors has not a significant depth and in particular it stops almost on the surface. Moreover no internal damages have been found so it can be supposed that the superficial canal previously described is responsible of the AE parameters trend and its limited depth explains why there is no influence on the mechanical performances as explained at the end of *paragraph 3.2.2*.

3.2.4 Discussion of results

In conclusion referring to Figure 3.9 it can be stated that, as expected, if subjected to bending, metal foam alone does not give high performances but, if used as filling, its contribution permits to the tube to reduce significantly the deflection and the superficial plastic deformation. Moreover, increasing the density of the foam, the material response to bending changes. In particular the tube filled with the lower density of aluminum foam (FF_560_2) shows a quadratic trend, while the response of sample FF_815_1 (high density of metal foam) is clearly linear from the beginning till the end of the test. This implies that increasing the density of the foam, the deflection decreases particularly for the higher values of load.

Furthermore the AE analysis indicates that with the dimensions of samples and the configurations of the tests considered, under 10000 cycles nothing happens in terms of internal damages of the material. In fact the displacement it is totally due to an initial settling of the samples that after the first 2000 cycles stabilizes and shows the same value of deflection till the end of the test.

For an higher number of cycles (around 15000 and 20000) the trend of the AE parameters (particularly hits) suggests instead an internal damage of the sample. In particular it can be supposed that this is related with the opening of a canal, not so marked for samples subjected to 10000 cycles tests, observed through the microscopic inspection of the foam, in correspondence of the zone of conjunction between the precursors used for the foaming process. Cutting the sample it is possible to observe how this canal has a very limited depth but other internal cracks were not found so it can be considered responsible of the AE parameters growth and its limited depth can explain why there is no influence on the mechanical performances of the sample, whose displacement does not increase significantly.

3.3 Compression tests

The last part of the work, regards the quasi-static axial compression tests (Figure 3.22) executed on all the cylindrical samples previously listed in Table 3.4.

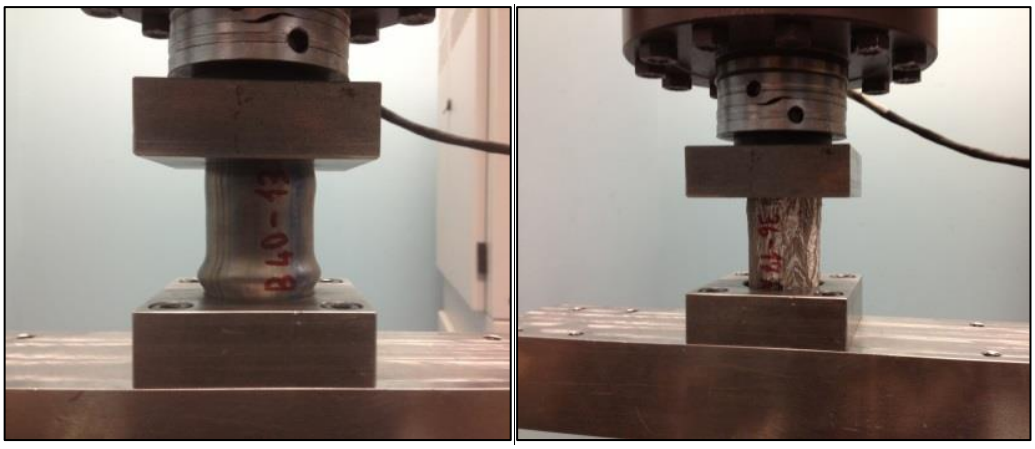

Figure 3.22: Examples of quasi-static compression tests executed on a: a) Foam filled titanium sample, b) Sample of only foam.

These tests have carried out in order to have some data about the mechanical behaviour of titanium foam filled tubes, in these condition of load, because it was the first time in which we were filling titanium tubes in our laboratory and no literature has been found about the interaction between these two materials.

3.3.1 Setup, design and manufacture of the fixtures

First of all, considering the dimensions of the samples available, a verification against buckling has been done in order to verify to work in safety conditions, as explained in *Appendix 4 - Verification against buckling*. After that the attention has been focused on the design and manufacture of the fixtures compatible with the MTS machine considering that the samples tested had the following characteristics:

- Round cross-section *diameter* = 40 *mm*;
- Thickness of the walls of the tubes t = 2 *mm*;
- Length 70 *mm*.

Differently from what have been done for the bending tests, no particular standards have been followed obtaining the fixtures shown in Figure 3.23.

a) b)

Figure 3.23: a) Image of the fixture used for the compression tests, b) Detail of the hole on the lower plate.

Therefore in order to test the samples in compression two plates, which present on their surface of contact with the samples a hole of 41 *mm* of diameter and 10 *mm* of depth in order to lock the sample and work in safety conditions, have been designed and manufactured. Note how the lower plate has been fixed to the same base on which the lower supports used for the bending tests have been installed. The tests have been monitored through the values of force and displacements given by the MTS machine (as already explained in detail for the bending tests), from which it has been possible to calculate the stress-strain curves subsequently described. Moreover a strain rate of 10^{-3} s^{-1} of percentage deformation (corresponding to 0.07 *mm/s* considering the length of the samples used) has been used during all the tests. This value has been chosen arbitrarily considering the absence of marked strain rate sensitivity for metal foam (*paragraph 1.3.2 - Influence of strain rate*) and the fact that this is the typical strain rate value used at ÉTS for quasi-static compression tests.

3.3.2 Results

First of all few tests on samples of only foam have been executed and the results obtained have been, as expected, coherent with what already stated in *paragraph 1.3.1 - Influence of density*. In fact as shown in Figure 3.24 the flow stress values and the energy absorption (represented by the area under the stress - strain curve) are strong function of relative density. In particular we can observe how increasing the density the mechanical behaviour of the samples improves significantly and the dependence of the energy absorption from the density it is not linear.

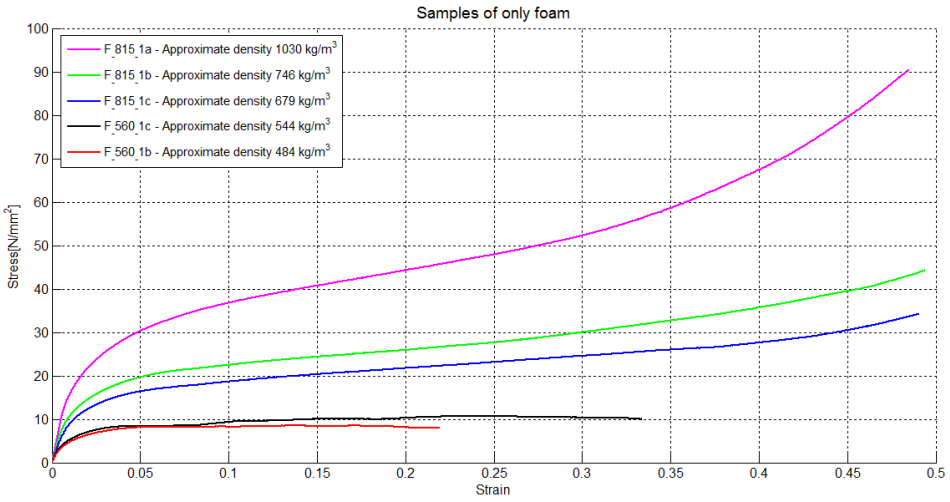

Figure 3.24: *Stress-strain* curves of samples of only foam with different approximate densities.

Obviously of more interest are the subsequently results obtained considering foam filled titanium tubes.

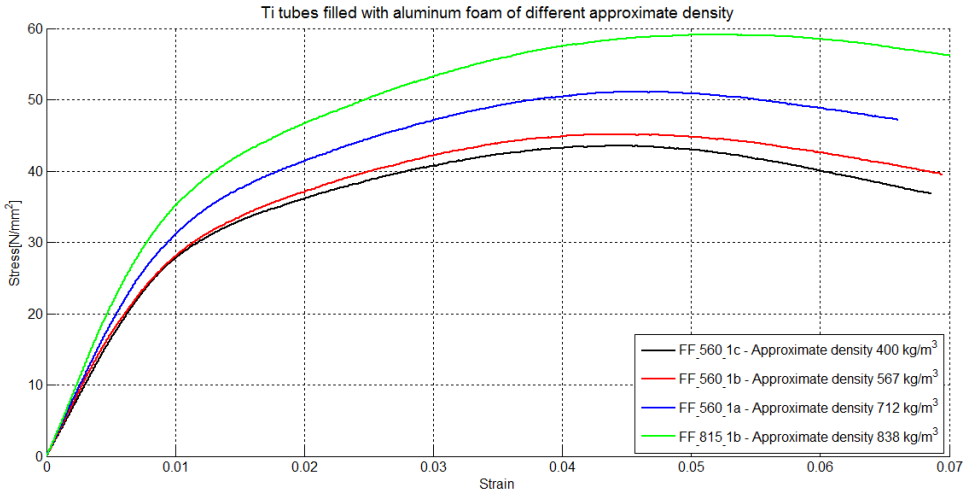

Figure 3.25: S*tress-strain* curves of titanium samples filled with different densities of metal foam.

In particular, in Figure 3.25, titanium samples filled with aluminum foam of different approximate density are compared. It is possible to observe how increasing the density of the foam the mechanical behaviour improves and the dependence is not linear, analogously with what happens for samples of only

foam. The most interesting and positive results have been obtained comparing the foam filled titanium samples with the empty one.

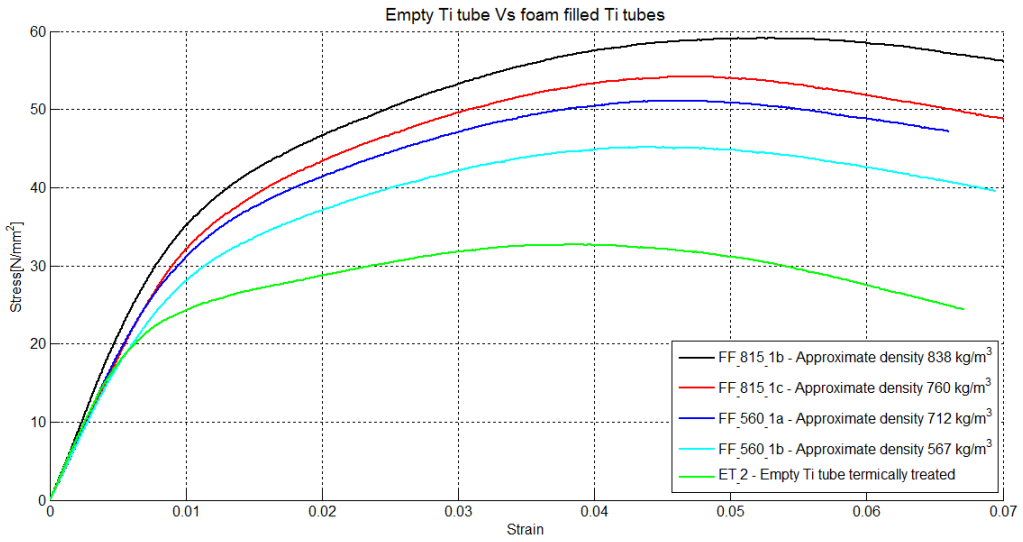

Figure 3.26: S*tress-strain* curves of titanium samples filled with different densities of metal foam.

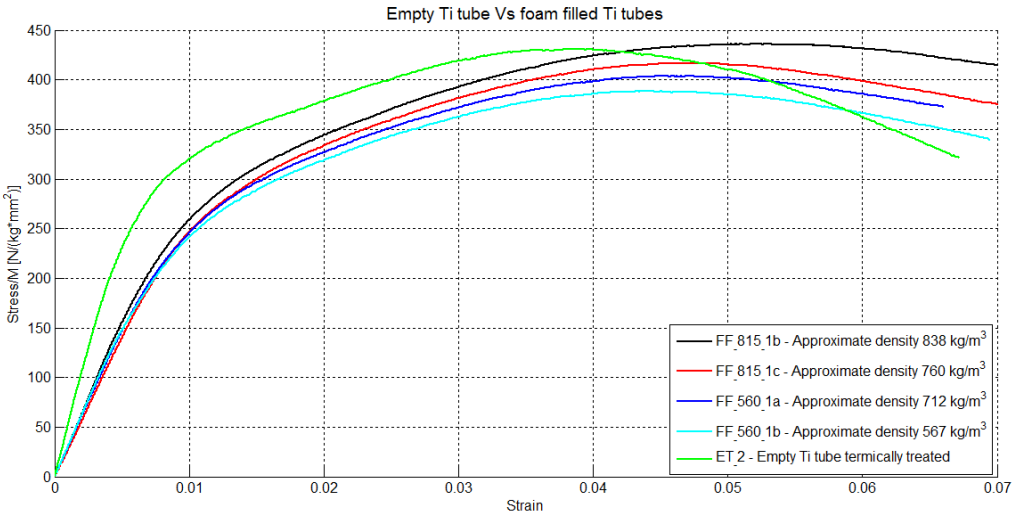

Figure 3.27: S*tress/M-strain* curves of titanium samples filled with different densities of metal foam.

In fact as shown in Figure 3.26 the foam filling has a clear positive influence on the mechanical behaviour of the tube whose curve rises significantly even considering the lower density of metal foam (567 kg/m^3). A last observation can

be done considering not only the stress-strain curve but dividing the stress axis by the mass as shown in Figure 3.27. In fact considering the mass, the behaviour of the empty titanium tube is comparable with the one of foam filled samples. More precisely, in this specific configuration of testing, for low deformations the curve representing the empty titanium tube remains above the ones relative to foam filled samples, but even considering the mass, passing the 4% of deformation, the situation returns the one previously described for the stress-strain curve.

Finally it is important to underline how in all the type of tests executed, the results are obviously strongly influenced by the dimension of the samples used (particularly for the compression tests) and it wasn't a purpose of this work, to optimize the effect of the foam filling, changing the dimension of the samples. The only objective was to prove the excellent properties of metal foam which effectively if used as filling, permits to improve the performances of steel and titanium empty tubes in all the condition of load analyzed.

Chapter 4

Implications for industrial applications

As already explained in detail, the work has been developed in two separated parts in order to focus the attention on different aspects and analyze different types of materials. In particular the main objective of the study has been to prove the high performances of metal foam if used as filling in order to push its use in the reference industrial fields considered:

- Machine tools field;
- Helicopter (more generally aeronautic) field.

4.1 Machine tools field

Because of their interesting damping properties, described in detail in *Chapter 1 - Metal foam: production, properties and applications* and abundantly demonstrated in previous studies, aluminum foams are widely considered a promising material for applications in which the dynamic behaviour of a mechanical structure needs to be improved. [57] In the machine tools field different studies have already been executed regarding the use of metal foams for different applications such as energy absorbing lining for the protective covers of high-speed grinding machines (*Paragraph 1.6.1 Energy absorbers*) [15] or filling of milling centers steel structures in order to improve the overall dynamic performance [57], obtaining excellent results. This work, in which the improvement of the dynamic behaviour of empty structures obtained through

foam fillings is clearly confirmed, shows further surprising results. In fact the main objective of the analysis of the steel foam filled structures was to understand if the improvement in damping would have reduced after the simulation of 10000 work cycles executed through three-points bending tests. The fact that the damping capacity not only does not get worst but increases significantly after the work cycles represents a surprising but obviously positive result. This is the starting point for future deep studies in which the interaction between the foam and the tube, presumably responsible of this effect, will be investigated in detail.

4.2 Helicopters field

All the results obtained for titanium filled samples and steel filled samples, have been finally presented to the *Bell Helicopter Textron Canada* company. Considering the mechanical and dynamical performances of the tested samples, some applications have been suggested by the engineers of Bell. Particular attention has been given to the damping capacity of metal foam which has been considered of potential interest for:

- Attenuate vibrations from the rotor towards the cabin (rotor mounting on the cabin);
- Attenuate vibrations from the engine towards the cabin (engine mounting on the cabin);
- Landing gears cross;
- Attenuate vibrations for the seats comfort.

Some examples of the mentioned components are shown in Figure 4.1. In conclusion the next step, if possible, will be to focus the future researches towards real applications, starting to produce more realistic prototypes of the components for which metal foams have been found potentially interesting. A

first indication has been given about the new test frequencies: it would be interesting to investigate the behaviour of the foam in a range of frequencies between 10 and 30 *Hz*, values suggested by *Bell*, being characteristic for the mentioned components.

Figure 4.1: a) Preassembled rotor head , b) Detail of an installed rotor and the structure containing the engine, c) Rotor head and flight commands, d) Example of landing gears cross.

Appendix 1

Preliminary simulations

Before starting with the design and the manufacturing of the fixtures (*Paragraphs 2.4.1 and 3.2.1*) installed on the *MTS* machine for the tests, preliminary calculations and FEM simulations (using the software *ABAQUS 6.12*) have been done in order to define an hypothetical value for the parameters of interest (force applied and displacement of the middle point of the samples) for the three-points bending tests executed on the steel samples constituting the models of machine tool portal (Figure A1.1), executed to simulate the working conditions.

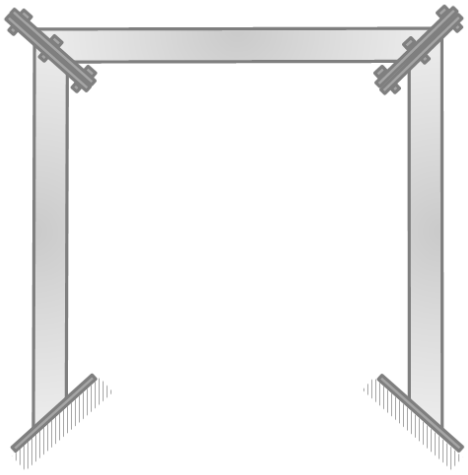

Figure A1.1: Representation of a model of tool machine portal.

The first step has been to find a plausible value for the cutting force through a stiffness comparison between the model of the portal and a real machine tool whose dimensions are summarized in Table A1.1.

Dimensions of the real machine tool *[mm]*		
Columns	Cross-section	450 × 450
	Thickness	5
	Length	3800
Crosspiece	Cross-section	450 × 450
	Thickness	5
	Length	5875

Table A1.1: Dimensions of the real tool machine, slightly adapted to obtain square cross-sections.

The dimensions of the columns and the crosspiece have been slightly adapted to obtain square cross-sections, analogous to the one of the samples tested, obtaining a simplification of the real machine tool considered which have been used for the comparison (Figure A1.2).

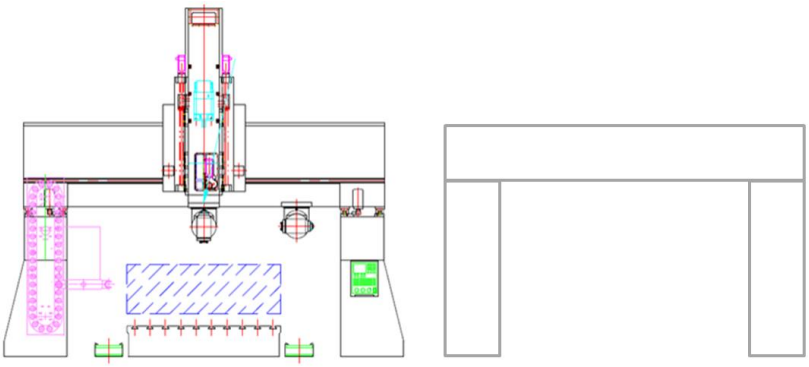

a) b)

Figure A1.2: a) Real machine tool considered as reference, b) Simplification of the real machine tool.

When the real machine tool considered as reference is working, plausible values of the cutting force components applied in correspondence of the spindle nose, positioned as represented in Figure A1.3, are:

- $F_x = 15000\ N$;

- $F_y = 15000\ N$;
- $F_z = 15000\ N$.

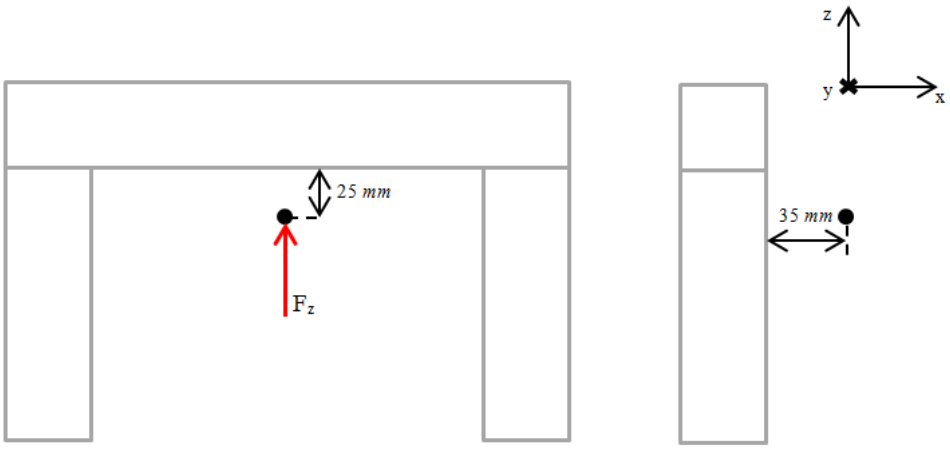

Figure A1.3: Position of the spindle nose considering the cross slide in the middle of the crosspiece.

In particular, as shown in Figure A1.3, has been considered only the component of the force in direction z which represents the direction of interest, as it is the direction that identify the mid-frequency mode considered in the dynamical analysis of the portal (*paragraph 2.3* and *paragraph 2.5*) and so the direction of load in the cyclic three-points bending tests executed on the samples (*paragraph 2.4*).

First of all have been executed two simulations, modeling through beam elements both the structures considered. Two different values of load have been applied in direction z for the two models, in correspondence of the point representing the spindle nose (connected to the middle point of the crosspiece through a coupling), verifying to remain in the elastic field not obtaining plastic deformations in the results. In particular:

- $F_z = 15000\ N$ for the model representing the simplification of the real tool machine considered as reference;

- $F_z = 2145\ N$ for the model representing the machine tool portal composed by the empty steel samples (the foam hasn't been modeled).

Note how:

- These values have been chosen simply to obtain a displacement of the same order of magnitude for the two models but we could choose any values which would have permitted to remain in the elastic field;
- The presence of the foam has been ignored because its static effect is negligible respect to the dynamic one and it is not clear how to reproduce the real conditions at the interface (adhesion) between the foam and the samples.

In the elastic field the stiffness *k* can be defined as:

$$k = \frac{force}{displacement}$$

Considering that:

- The subscript *mp* indicates the model of the portal composed by the three steel samples;
- The subscript *s* indicates the simplification of the real tool machine considered as reference;
- The displacement considered is the one of the middle point of the crosspiece.

It is possible to calculate the stiffness for both the structures as:

$$k_{mp} = \frac{force}{displacement} = \frac{2145\ N}{0.183\ mm} = 11721.311\ \ N/mm$$

$$k_s = \frac{force}{displacement} = \frac{15000\ N}{0.575\ mm} = 26086.957\ \ N/mm$$

The correspondent ratio is:

$$\frac{k_{mp}}{k_s} = \frac{11721.311\ N/mm}{26086.957\ N/mm} = 0.45$$

Considering this result and the typical value of the component of the force in direction z for the real machine tool considered, it is possible to calculate a plausible value for the component of the force in direction z in work conditions for the model of the portal analyzed:

$$F_{z,mp} = 0.45 \cdot F_{z,s} = 0.45 \cdot 15000\ N = 6750\ N$$

The next step has been to execute a simulation in which the structure, composed by the three steel samples, has been modeled through shell elements applying $F_{z,mp}$ in the point representing the spindle nose, in order to calculate the correspondent plausible displacement in direction *z*. The displacement obtained is about 0.800 *mm* obviously too high for this kind of application but accepted because the portal considered is only a model, not a real machine tool.

Finally a static three-points bending test has been simulated in order to calculate the load imposing the displacement of the middle point of the sample obtained in the previous step.

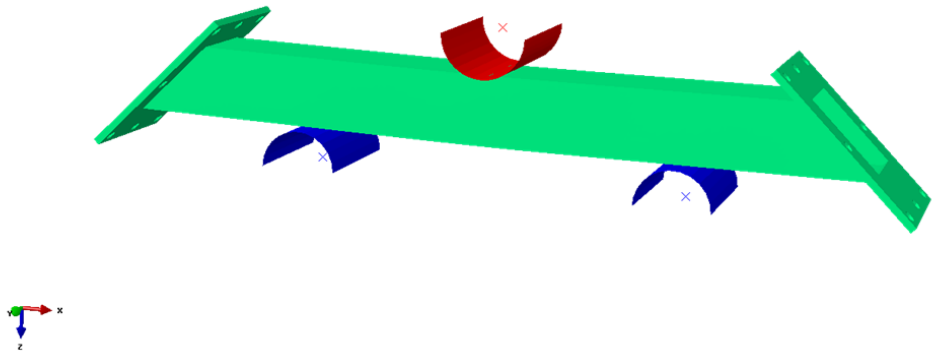

Figure A1.4: Simulation of a static three-points bending test.

Note how in this simulation (Figure A1.4) the supports and the former, have been modeled as rigid parts while the sample has been modeled through shell elements. The hypothetic parameters of interest obtained are summarized in Table A1.2.

	Value
Displacement simulating the work conditions *[mm]*	0.800
Correspondent load *[kN]*	64

Table A1.2: Hypothetical values of the parameters of interest of the three-points bending tests, obtained through preliminary simulation.

Obviously these values represent only a starting point and they have been strongly modified proceeding with the experimental tests.

Appendix 2

Acoustic emission

Acoustic Emission (AE) is a phenomenon of sound and ultrasound wave radiation in materials undergone to deformation and fracture processes. [44]
A typical AE apparatus consists of the components represented in Figure A2.1.

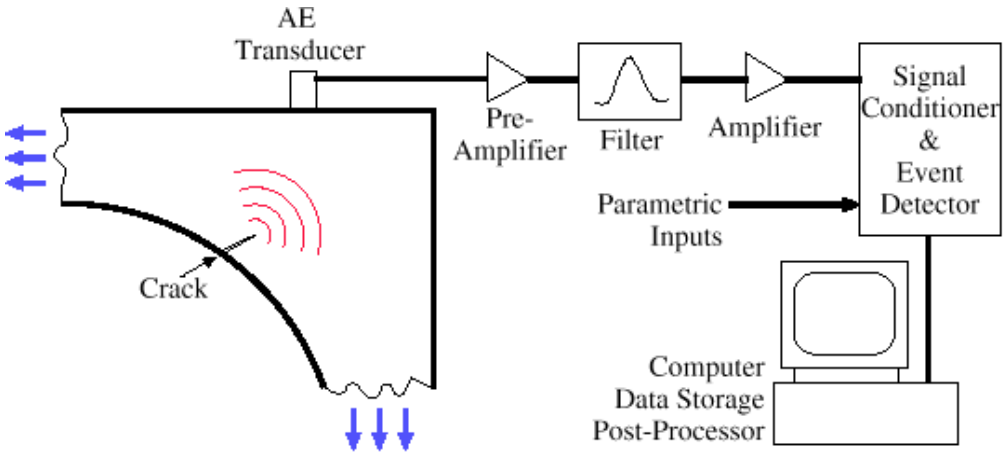

Figure A2.1: A typical AE system setup. [53]

The AE transducers are generally very sensitive piezoelectric sensors. The traditional AE technique only uses AE features for that reason the actual waveforms are not critical to this method. The AE sensors used are usually resonance sensors, which are only very sensitive to a certain frequency. Since the AE signals are very weak, a preamplifier is connected right after the AE transducer to minimize the noise interference and prevent the signal loss (a typical amplification gain is 40 or 60 *dB* [44]). Note how sometimes, the transducer and the preamplifier are built as a unit. Then the signals pass through

a filter (to remove the noise) after which they are amplified by the main amplifier before being sent, usually through coaxial cables, to the signal conditioner. After that, the AE features are subtracted and stored in a computer for further analysis. [53] In particular the main acoustic emission parameters typically used for the detection of propagation of cracks in traditional materials are:

- RMS;
- Hits;
- Counts. [38] [40]

For that reason we have considered these parameters during the tests previously described.

Root mean square (RMS)

The RMS value of a set of values (or a continuous-time waveform) is the square root of the arithmetic mean (average) of the squares of the original values (or the square of the function that defines the continuous waveform).

In the case of a set of *N* values $\{x_1, x_2, \dots, x_N\}$, the RMS value is given by the following formula:

$$RMS = \sqrt{\frac{1}{N} \cdot \sum_{i=1}^{N} x_i^2}$$

The corresponding formula for a continuous function/signal, which expresses the RMS for a period *T*, is:

$$RMS = \sqrt{\frac{1}{T} \cdot \int_0^T x^2(t)dt}$$

Finally for the complete signal the expression changes as follows:

$$RMS = \lim_{T\to\infty} \sqrt{\frac{1}{T} \cdot \int_0^T x^2(t)dt}$$

This parameter is of particular interest because strictly connected with the energy of the signal and so can be related with propagations of defects or deformations inside the samples during the tests. In fact as a crack propagates in a material, molecular bonds are broken, releasing small amounts of energy. The energy released spreads throughout the surrounding material in the form of strain waves. These waves are minute deformations in the material with wave frequencies in the ultrasonic range. Moreover generally all structural deformations transmit some form of energy into the material, resulting in waves similar to those of crack growth. [54]
In Particular the RMS presents a typical exponential trend in case of crack propagation inside traditional materials.

Hits and Counts

These two parameters (Figure A2.2), whose values increase exponentially in case of crack propagation inside traditional materials till the end of the propagation itself, are defined as follows:

- Hits: detection and measurement of an AE signal (wave) on a channel;
- Counts: number of times in which the signal amplitude exceeds the threshold (established in our tests through the moving average of the signal calculated by the acquisition system). [44]

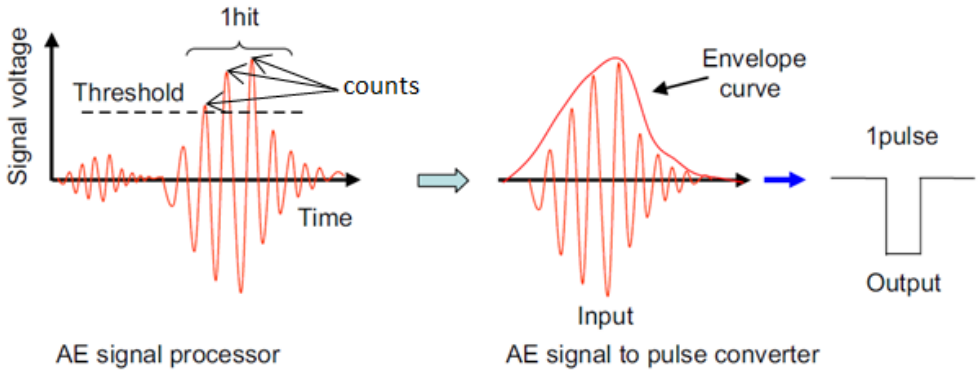

Figure A2.2: Definition of counts, AE hit signal and pulse signal. [39]

Appendix 3

Ahdesion of the foam

As previously said metal foams are characterized by a cellular structure which gives them high energy absorption and damping capacity. In order to improve the behaviour of hollow structures, a metallurgical bonding at the interface should allow the foam filling to be firmly fixed to the internal walls of the structure giving it bending and torsional strength higher than those of the starting component. [7]

In particular Monno et al. [7] [8] have studied the growth of the intermetallic layer considering empty **steel** tubes and Alulight aluminum foam. During the filling process, the molten aluminum foam comes in contact with the solid steel wall of the tube and the diffusion of Fe and Al atoms leads to the formation and growth of an intermetallic layer at the interface which should make the filling foam firmly fixed to the steel skin. They have concluded that the process parameters strongly influence the thickness and morphology of the formed interlayer, in fact foaming time, atmosphere and time-temperature interaction seem to drive the process.

As explained by Yun et al. [9] **titanium** differently from steel, is sparingly soluble in liquid aluminum. The low solubility makes the liquid layer surrounding the solid titanium more readily saturated with titanium solute and the saturation inhibits the further diffusion of titanium. Although many intermetallic compounds exist in the binary Ti-Al phase diagram, it has been found that the typical compound formed between solid titanium and liquid

aluminum during foaming processes is $TiAl_3$. In particular Yun et al. have found a planar and rather thin layer (whose growth is controlled by the diffusion rate) of only 3 μm of thickness at the solid titanium - liquid aluminum interface while under the same conditions the intermediate zone of stainless steel is about 30 μm thick.

Considering our tests, as already said in *paragraph 3.1.1* there is no adhesion between the titanium tubes and the fillings of aluminum foam. The foam in fact is fixed inside the samples simply through the burr created in the end parts of the samples, cutting them with a saw to eliminate the inhomogeneous zones resulting from the foaming process. This fact as no negative influence on the performances of the titanium foam filled samples whose adhesion at the end parts after the tests doesn't change.

Moreover the absence of adhesion is not a problem, in fact considering for instance the axial compression tests, the fact that there is no adhesion can be considered even positive. The tube submitted to axial compression collapses as represented in Figure A3.1 and if the foam adhered perfectly with it, would follow the wall of the tube, working in tension instead of in compression as shown in Figure A3.2a with obviously worst performances (stress - strain curve in Figure A3.2).

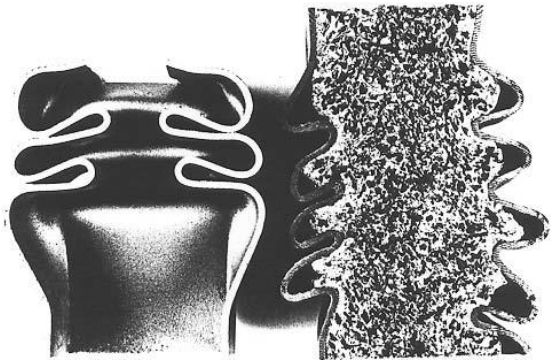

Figure A3.1: Collapse of an empty tube and a foam filled tube submitted to axial compression test. [2]

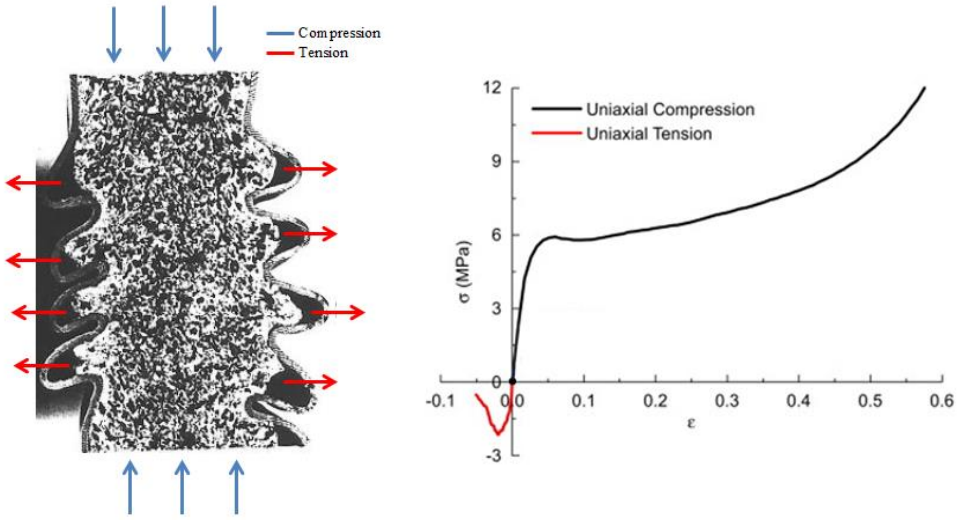

a) b)

Figure A3.2: a) Section of a foam filled tube collapsed due to axial compression, b) Generic behaviour of metal foam in tension and compression.

Appendix 4

Verification against buckling

Before the manufacture of the samples and the fixtures for the compression tests, it was necessary to verify analitically not to have problems of buckling due to the dimensions chosen for the samples (Table A4.1), in order to be sure that the MTS machine would have worked in safety conditions.
In particular the verification has been executed for the empty titanium tubes because if we are in safety conditions for them, obviously there won't be problems testing in the same way the foam filled titanium samples.

Parameter	***Value***
Nominal length [mm]	70
External diameter of the tube (D_e) *[mm]*	40
Internal diameter of the tube (D_i) *[mm]*	36

Table A4.1: Dimensions of the samples.

The generic eulerian expression of the critical load for a vertical beam is:

$$P_{cr} = \frac{\pi^2 \cdot E \cdot I}{(\mu L)^2} = \frac{\pi^2 \cdot E \cdot I}{L_c^2}$$

Where:

- E is the Young's modulus of titanium grade 2;
- I is the second moment of area;
- μ is a value depending on the kind of constraints (Figure A4.1);

- L is the length of the sample;
- L_c is the effective length. [52]

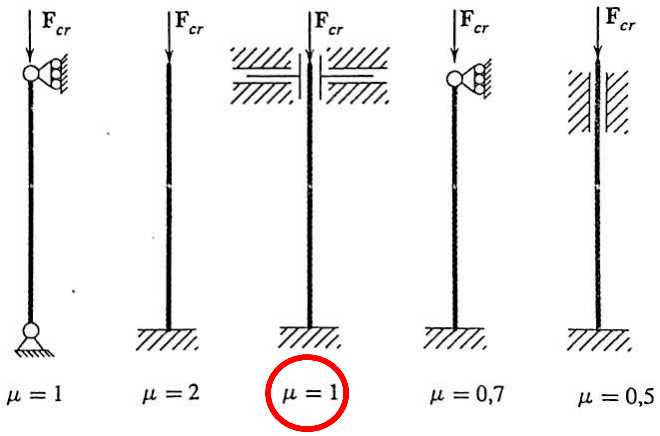

Figure A4.1: Effective length for beam with different kinds of constraints. The circled value is the one representing the condition of interest. [52]

Table A4.2 resumes the values of the parameters previously defined considering that:

$$I_{\,empty\ Ti\ tube} = \frac{\pi}{64} \cdot (D_e^4 - D_i^4)$$

Parameter	***Value***
E *[MPa]*	~ 102000
I *[mm^4]*	~ 43216
μ *[.]*	1
L *[mm]*	70
L_c *[mm]*	70

Table A4.2: Values of the parameters of interest.

Therefore the critical load obtained is:

$$P_{cr} = \frac{\pi^2 \cdot E \cdot I}{(\mu L)^2} = \frac{\pi^2 \cdot E \cdot I}{L_c^2} = 8878680\ N = 8878{,}68\ kN$$

So P_{cr} » 100 kN which represent the maximum load applicable using the MTS machine available. For that reason we can say that with these dimensions of the samples we won't have problems of buckling during the static compression tests and in particular, the machine will work abundantly in safety conditions.

Appendix 5

Matlab code

```
%% Representation of the sinusoidal pattern of tests executed on
steel samples filled with metal foam
clear all
close all
clc
% Three-points bending step loading test (100 cycles)
x1=[0:0.01:100];
y1=1*sin(2*pi*x1)+3;
x2=[100:0.01:200];
y2=3*sin(2*pi*x2)+5;
x3=[200:0.01:300];
y3=5*sin(2*pi*x3)+7;
x4=[300:0.01:400];
y4=7*sin(2*pi*x4)+9;
figure(1)
plot(x1,y1)
ylim([0 20])
hold on
grid on
plot(x2,y2)
plot(x3,y3)
plot(x4,y4)
xlim([0 350])
Title('Three points bending step loading test')
xlabel('Number of cycles')
ylabel('Load [kN]')
% Three-points bending step loading (1000 cycles)test
clear all
clc
x1=[0:0.01:1000];
y1=1*sin(2*pi*x1)+3;
x2=[1000:0.01:2000];
y2=2*sin(2*pi*x2)+4;
x3=[2000:0.01:3000];
y3=3*sin(2*pi*x3)+5;
```

```
x4=[3000:0.01:4000];
y4=4*sin(2*pi*x4)+6;
figure(2)
plot(x1,y1)
ylim([0 20])
hold on
grid on
plot(x2,y2)
plot(x3,y3)
plot(x4,y4)
xlim([0 3500])
Title('Three points bending step loading test')
xlabel('Number of cycles')
ylabel('Load [kN]')

%% RMS of acoustic emission signals of three-points bending
tests on steel samples
clear all
close all
clc
% 1)1000 cycles for each loading step
% sample 123 [Alulight]
load Alulight_123_bande_1_5000.txt;
cycles_123_bande_1_5000=Alulight_123_bande_1_5000(:,1);
RMS_123_bande_1_5000=Alulight_123_bande_1_5000(:,4);
figure(1)
title('Sample Alulight 123 - Increasing the load of 2 kN every
1000 cycles [4-16 kN] - bande 1 - 5000 Hz')
xlabel('n')
ylabel('RMS [V]')
grid on
plot(cycles_123_bande_1_5000,RMS_123_bande_1_5000)
ylim ([0.04 0.08])
load Alulight_123_bande_5000_15000.txt;
cycles_123_bande_5000_15000=Alulight_123_bande_5000_15000(:,1);
RMS_123_bande_5000_15000=Alulight_123_bande_5000_15000(:,4);
figure(2)
title('Sample Alulight 123 - Increasing the load of 2 kN every
1000 cycles [4-16 kN] - bande 5000 - 15000 Hz')
xlabel('n')
ylabel('RMS [V]')
grid on
plot(cycles_123_bande_5000_15000,RMS_123_bande_5000_15000)
ylim ([0.006 0.008])
% sample 110 [APM low density]
```

```
load APM_ld_110_bande_1_5000.txt;
cycles_110_bande_1_5000=APM_ld_110_bande_1_5000(:,1);
RMS_110_bande_1_5000=APM_ld_110_bande_1_5000(:,2);
figure(3)
title('Sample 110 [APM low density] - Increasing the load of 2
kN every 1000 cycles [4-24 kN] - bande 1 - 5000 Hz')
xlabel('n')
ylabel('RMS [V]')
grid on
plot(cycles_110_bande_1_5000,RMS_110_bande_1_5000)
ylim ([0.01 0.05])
load APM_ld_110_bande_5000_15000.txt
cycles_110_bande_5000_15000=APM_ld_110_bande_5000_15000(:,1);
RMS_110_bande_5000_15000=APM_ld_110_bande_5000_15000(:,2);
figure(4)
title('Sample 110 [APM low density] - Increasing the load of 2
kN every 1000 cycles [4-24 kN] - bande 5000 - 15000 Hz')
xlabel('n')
ylabel('RMS [V]')
grid on
plot(cycles_110_bande_5000_15000,RMS_110_bande_5000_15000)
ylim ([0.0015 0.0037])
% sample 103 [APM high density]
load APM_hd_103_bande_1_5000.txt;
cycles_103_bande_1_5000=APM_hd_103_bande_1_5000(:,1);
RMS_103_bande_1_5000=APM_hd_103_bande_1_5000(:,2);
figure(5)
title('Sample 103 [APM high density] - Increasing the load of 2
kN every 1000 cycles [4-24 kN] - bande 1 - 5000 Hz')
xlabel('n')
ylabel('RMS [V]')
grid on
plot(cycles_103_bande_1_5000,RMS_103_bande_1_5000)
ylim ([0.01 0.04])
load APM_hd_103_bande_5000_15000.txt
cycles_103_bande_5000_15000=APM_hd_103_bande_5000_15000(:,1);
RMS_103_bande_5000_15000=APM_hd_103_bande_5000_15000(:,2);
figure(6)
title('Sample 103 [APM high density] - Increasing the load of 2
kN every 1000 cycles [4-24 kN] - bande 5000 - 15000 Hz')
xlabel('n')
ylabel('RMS [V]')
grid on
plot(cycles_103_bande_5000_15000,RMS_103_bande_5000_15000)
ylim ([0.0015 0.0045])
```

```
% comparisons between the different frequency bands for each
sample
figure(7)
title('Sample 123 A - RMS of acoustic emission data')
xlabel('n')
ylabel('RMS [V]')
grid on
hold on
plot(cycles_123_bande_1_5000,RMS_123_bande_1_5000)
plot(cycles_123_bande_5000_15000,RMS_123_bande_5000_15000,'r')
legend('RMS f bande 1-5000 Hz','RMS f bande 5000-15000Hz')
ylim ([0 0.08])
figure(8)
title('Sample 110 APML - RMS of acoustic emission data')
xlabel('n')
ylabel('RMS [V]')
grid on
hold on
plot(cycles_110_bande_1_5000,RMS_110_bande_1_5000)
plot(cycles_110_bande_5000_15000,RMS_110_bande_5000_15000,'r')
legend('RMS f bande 1-5000 Hz','RMS f bande 5000-15000Hz')
ylim ([0 0.05])
figure(9)
title('Sample 103 APMH - RMS of acoustic emission data')
xlabel('n')
ylabel('RMS [V]')
grid on
hold on
plot(cycles_103_bande_1_5000,RMS_103_bande_1_5000)
plot(cycles_103_bande_5000_15000,RMS_103_bande_5000_15000,'r')
legend('RMS f bande 1-5000 Hz','RMS f bande 5000-15000Hz')
ylim ([0 0.04])
% comparison between the samples for the frequency band 1-5000
Hz
figure(10)
title('RMS of acoustic emission data')
xlabel('n')
ylabel('RMS [V]')
grid on
hold on
plot(cycles_123_bande_1_5000,RMS_123_bande_1_5000)
plot(cycles_110_bande_1_5000,RMS_110_bande_1_5000,'r')
plot(cycles_103_bande_1_5000,RMS_103_bande_1_5000,'k')
legend('Sample 123 A','Sample 110 APML','Sample 103 APMH')
ylim ([0 0.08])
```

```
% 2)10000 cycles with the same load
clc
clear all
close all
% sample 111 [APM low density]
load APM_ld_111_bande_1_5000.txt;
cycles_111_bande_1_5000=APM_ld_111_bande_1_5000(:,1);
RMS_111_bande_1_5000=APM_ld_111_bande_1_5000(:,2);
figure(11)
title('RMS of acoustic emission signal - Sample 111 APM')
xlabel('n')
ylabel('RMS [V]')
plot(cycles_111_bande_1_5000,RMS_111_bande_1_5000)
ylim ([0 0.06])
grid on

%% Representation of the sinusoidal pattern of tests executed on
aluminum samples filled with aluminum foam
% Three-points bending step loading test (10000 cycles)
clear all
close all
clc
x1=[0:0.01:100];
y1=0.25*sin(2*pi*x1)+0.75;
x2=[100:0.01:200];
y2=0.5*sin(2*pi*x2)+1;
x3=[200:0.01:300];
y3=0.75*sin(2*pi*x3)+1.25;
x4=[300:0.01:400];
y4=sin(2*pi*x4)+1.5;
x5=[400:0.01:500];
y5=1.25*sin(2*pi*x5)+1.75;
figure(3)
plot(x1,y1)
ylim([0 4])
hold on
grid on
plot(x2,y2)
plot(x3,y3)
plot(x4,y4)
plot(x5,y5)
xlim([0 450])
Title('Three points bending step loading test')
xlabel('Number of cycles')
ylabel('Load [kN]')
```

```
% Three-points bending test (10000 cycles)
clear all
close all
clc
x1=[0:0.01:10000];
y1=2.25*sin(2*pi*x1)+2.75;
figure(4)
plot(x1,y1)
ylim([0 8])
grid on
xlim([0 450])
Title('Cyclic three-points bending test')
xlabel('n')
ylabel('Load [kN]')

%% Calculation of the critic load for the compression tests
(samples 80 mm)
clear all
close all
clc
% DATA:
D_e=40;    %[mm]
D_i=36;    %[mm]
E=102000; %[N/mm^2]
l=70;      %[mm]
u=1;       %coefficient depending by the conditions of constraint
% CALCULATION:
l_0=u*l
J=pi/64*(D_e^4-D_i^4)
N_cr=pi^2*E*J/(l_0^2)

%% PLOT OF ALL THE COMPRESSION TESTS
clear all
close all
clc
% A)Simple plot of the data
% 1)Samples filled with aluminum foam (nominal density 560
kg/m^3)
% sample 40_01a
dati_40_01a=importdata('40_01a.txt');
time_40_01a=dati_40_01a.data(:,1);
time_40_01a=time_40_01a-time_40_01a(1);
force_40_01a=dati_40_01a.data(:,2);
disp_40_01a=dati_40_01a.data(:,2);
figure(1)
```

```
plot(time_40_01a,force_40_01a)
title('Sample 40__01a - Ti tube filled with aluminum foam
(approximative density 712 kg/m^3)')
xlabel('Time [s]')
ylabel('Force [kN]')
grid on
% sample 40_01b
dati_40_01b=importdata('40_01b.txt');
time_40_01b=dati_40_01b.data(:,1);
time_40_01b=time_40_01b-time_40_01b(1);
force_40_01b=dati_40_01b.data(:,2);
disp_40_01b=dati_40_01b.data(:,2);
figure(2)
plot(time_40_01b,force_40_01b)
title('Sample 40__01b - Ti tube filled with aluminum foam
(approximative density 567 kg/m^3)')
xlabel('Time [s]')
ylabel('Force [kN]')
grid on
% sample 40_01c
dati_40_01c=importdata('40_01c.txt');
time_40_01c=dati_40_01c.data(:,1);
time_40_01c=time_40_01c-time_40_01c(1);
force_40_01c=dati_40_01c.data(:,2);
disp_40_01c=dati_40_01c.data(:,2);
figure(3)
plot(time_40_01c,force_40_01c)
title('Sample 40__01c - Ti tube filled with aluminum foam
(approximative density 400 kg/m^3)')
xlabel('Time [s]')
ylabel('Force [kN]')
grid on
% sample 40_02a
dati_40_02a=importdata('40_02a.txt');
time_40_02a=dati_40_02a.data(:,1);
time_40_02a=time_40_02a-time_40_02a(1);
force_40_02a=dati_40_02a.data(:,2);
disp_40_02a=dati_40_02a.data(:,2);
figure(4)
plot(time_40_02a,force_40_02a)
title('Sample 40__02a - Ti tube filled with aluminum foam
(approximate density 577 kg/m^3)')
xlabel('Time [s]')
ylabel('Force [kN]')
grid on
```

```
% sample 40_02b
dati_40_02b=importdata('40_02b.txt');
time_40_02b=dati_40_02b.data(:,1);
time_40_02b=time_40_02b-time_40_02b(1);
force_40_02b=dati_40_02b.data(:,2);
disp_40_02b=dati_40_02b.data(:,2);
figure(5)
plot(time_40_02b,force_40_02b)
title('Sample 40__02b - Ti tube filled with aluminum foam
(approximate density 602 kg/m^3)')
xlabel('Time [s]')
ylabel('Force [kN]')
grid on
% sample 40_02c
dati_40_02c=importdata('40_02c.txt');
time_40_02c=dati_40_02c.data(:,1);
time_40_02c=time_40_02c-time_40_02c(1);
force_40_02c=dati_40_02c.data(:,2);
disp_40_02c=dati_40_02c.data(:,2);
figure(6)
plot(time_40_02c,force_40_02c)
title('Sample 40__02c - Ti tube filled with aluminum foam
(approximate density 468 kg/m^3)')
xlabel('Time [s]')
ylabel('Force [kN]')
grid on
% 2)Samples filled with aluminum foam (nominal density 815
kg/m^3)
% sample 40_13a
dati_40_13a=importdata('40_13a.txt');
time_40_13a=dati_40_13a.data(:,1);
time_40_13a=time_40_13a-time_40_13a(1);
force_40_13a=dati_40_13a.data(:,2);
disp_40_13a=dati_40_13a.data(:,2);
figure(8)
plot(time_40_13a,force_40_13a)
title('Sample 40__13a - Ti tube filled with aluminum foam
(approximate density 827 kg/m^3)')
xlabel('Time [s]')
ylabel('Force [kN]')
grid on
% sample 40_13b
dati_40_13b=importdata('40_13b.txt');
time_40_13b=dati_40_13b.data(:,1);
time_40_13b=time_40_13b-time_40_13b(1);
```

```
force_40_13b=dati_40_13b.data(:,2);
disp_40_13b=dati_40_13b.data(:,2);
figure(9)
plot(time_40_13b,force_40_13b)
title('Sample 40__13b - Ti tube filled with aluminum foam
(approximate density 838 kg/m^3)')
xlabel('Time [s]')
ylabel('Force [kN]')
grid on
% sample 40_13c
dati_40_13c=importdata('40_13c.txt');
time_40_13c=dati_40_13c.data(:,1);
time_40_13c=time_40_13c-time_40_13c(1);
force_40_13c=dati_40_13c.data(:,2);
disp_40_13c=dati_40_13c.data(:,2);
figure(10)
plot(time_40_13c,force_40_13c)
title('Sample 40__13c - Ti tube filled with aluminum foam
(approximate density 760 kg/m^3)')
xlabel('Time [s]')
ylabel('Force [kN]')
grid on
% 3)Empty titanium samples untreated
% sample E40_01
dati_E40_01=importdata('E40_01.txt');
time_E40_01=dati_E40_01.data(:,1);
time_E40_01=time_E40_01-time_E40_01(1);
force_E40_01=dati_E40_01.data(:,2);
disp_E40_01=dati_E40_01.data(:,2);
figure(12)
plot(time_E40_01,force_E40_01)
title('Sample E40__01 - Empty Ti tube untreated')
xlabel('Time [s]')
ylabel('Force [kN]')
grid on
% sample E40_02
dati_E40_02=importdata('E40_02.txt');
time_E40_02=dati_E40_02.data(:,1);
time_E40_02=time_E40_02-time_E40_02(1);
force_E40_02=dati_E40_02.data(:,2);
disp_E40_02=dati_E40_02.data(:,2);
figure(13)
plot(time_E40_02,force_E40_02)
title('Sample E40__02 - Empty Ti tube untreated')
xlabel('Time [s]')
```

```
ylabel('Force [kN]')
grid on
% sample E40_03
dati_E40_03=importdata('E40_03.txt');
time_E40_03=dati_E40_03.data(:,1);
time_E40_03=time_E40_03-time_E40_03(1);
force_E40_03=dati_E40_03.data(:,2);
disp_E40_03=dati_E40_03.data(:,2);
figure(14)
plot(time_E40_03,force_E40_03)
title('Sample E40__03 - Empty Ti tube untreated')
xlabel('Time [s]')
ylabel('Force [kN]')
grid on
%% 4)Empty titanium samples simulated foam
% sample ET40_01
dati_ET40_01=importdata('ET40_01.txt');
time_ET40_01=dati_ET40_01.data(:,1);
time_ET40_01=time_ET40_01-time_ET40_01(1);
force_ET40_01=dati_ET40_01.data(:,2);
disp_ET40_01=dati_ET40_01.data(:,2);
figure(16)
plot(time_ET40_01,force_ET40_01)
title('Sample ET40__01 - Empty Ti tube simulated foam')
xlabel('Time [s]')
ylabel('Force [kN]')
grid on
% sample ET40_02
dati_ET40_02=importdata('ET40_02.txt');
time_ET40_02=dati_ET40_02.data(:,1);
time_ET40_02=time_ET40_02-time_ET40_02(1);
force_ET40_02=dati_ET40_02.data(:,2);
disp_ET40_02=dati_ET40_02.data(:,2);
figure(17)
plot(time_ET40_02,force_ET40_02)
title('Sample ET40__02 - Empty Ti tube simulated foam')
xlabel('Time [s]')
ylabel('Force [kN]')
grid on
% sample ET40_03
dati_ET40_03=importdata('ET40_03.txt');
time_ET40_03=dati_ET40_03.data(:,1);
time_ET40_03=time_ET40_03-time_ET40_03(1);
force_ET40_03=dati_ET40_03.data(:,2);
disp_ET40_03=dati_ET40_03.data(:,2);
```

```
figure(18)
plot(time_ET40_03,force_ET40_03)
title('Sample ET40__03 - Empty Ti tube simulated foam')
xlabel('Time [s]')
ylabel('Force [kN]')
grid on
% sample 36_12b
dati_36_12b=importdata('36_12b.txt');
time_36_12b=dati_36_12b.data(:,1);
time_36_12b=time_36_12b-time_36_12b(1);
force_36_12b=dati_36_12b.data(:,2);
disp_36_12b=dati_36_12b.data(:,2);
figure(22)
plot(time_36_12b,force_36_12b)
title('Sample 36__12b - Sample of only foam(approximate density
484 kg/m^3)')
xlabel('Time [s]')
ylabel('Force [kN]')
grid on
% sample 36_12c
dati_36_12c=importdata('36_12c.txt');
time_36_12c=dati_36_12c.data(:,1);
time_36_12c=time_36_12c-time_36_12c(1);
force_36_12c=dati_36_12c.data(:,2);
disp_36_12c=dati_36_12c.data(:,2);
figure(23)
plot(time_36_12c,force_36_12c)
title('Sample 36__12c - Sample of only foam(approximate density
544 kg/m^3)')
xlabel('Time [s]')
ylabel('Force [kN]')
grid on
% sample 36_17a
dati_36_17a=importdata('36_17a.txt');
time_36_17a=dati_36_17a.data(:,1);
time_36_17a=time_36_17a-time_36_17a(1);
force_36_17a=dati_36_17a.data(:,2);
disp_36_17a=dati_36_17a.data(:,2);
figure(24)
plot(time_36_17a,force_36_17a)
title('Sample 36_17a - Sample of only foam(approximate density
1030 kg/m^3)')
xlabel('Time [s]')
ylabel('Force [kN]')
grid on
```

```
% sample 36_17b
dati_36_17b=importdata('36_17b.txt');
time_36_17b=dati_36_17b.data(:,1);
time_36_17b=time_36_17b-time_36_17b(1);
force_36_17b=dati_36_17b.data(:,2);
disp_36_17b=dati_36_17b.data(:,2);
figure(25)
plot(time_36_17b,force_36_17b)
title('Sample 36_17b - Sample of only foam(approximate density
746 kg/m^3)')
xlabel('Time [s]')
ylabel('Force [kN]')
grid on
% sample 36_17c
dati_36_17c=importdata('36_17c.txt');
time_36_17c=dati_36_17c.data(:,1);
time_36_17c=time_36_17c-time_36_17c(1);
force_36_17c=dati_36_17c.data(:,2);
disp_36_17c=dati_36_17c.data(:,2);
figure(26)
plot(time_36_17c,force_36_17c)
title('Sample 36_17c - Sample of only foam(approximate density
679 kg/m^3)')
xlabel('Time [s]')
ylabel('Force [kN]')
grid on
% B)Absolute value of the correspondent graph stress-strain with
calculation of the first derivative
close all
clc
% dati
initial_length=70;                          %[mm]
strain_rate=10^-3*initial_length;           %[mm/s]
dt=time_40_01a(2)-time_40_01a(1);           %[s]
r=20;                                       %[mm]
initial_surface=r*r*pi;                     %[mm^2]
r_f=18;                                     %[mm]
initial_surface_f=r_f*r_f*pi;               %[mm^2]
% 1)Samples filled with aluminum foam (nominal density 560
kg/m^3)
% sample 40_01a
force_pos_40_01a=abs(force_40_01a);
stress_40_01a=1000*force_pos_40_01a/initial_surface;
strain_40_01a=time_40_01a*strain_rate/initial_length;
figure(37)
```

```
plot(strain_40_01a,stress_40_01a)
title('Sample 40__01a - Ti tube filled with aluminum foam
(approximate density 712 kg/m^3)')
xlabel('Strain')
ylabel('Stress[N/mm^2]')
grid on
der_stress_40_01a=diff(stress_40_01a)/dt;
figure(38)
plot(der_stress_40_01a)
grid on
max_der_stress_40_01a=der_stress_40_01a(1);
% length(der_stress_40_01a)
for ii=2:783
    if der_stress_40_01a(ii)>max_der_stress_40_01a
        max_der_stress_40_01a=der_stress_40_01a(ii);
        pos_40_01a=ii;
    end
end
stress_40_01a=stress_40_01a(pos_40_01a:end);
stress_40_01a=stress_40_01a-stress_40_01a(1);
strain_40_01a=strain_40_01a(1:(end-pos_40_01a+1));
figure(39)
plot(strain_40_01a,stress_40_01a)
title('Sample 40__01a - Ti tube filled with aluminum foam
(approximate density 712 kg/m^3)')
xlabel('Strain')
ylabel('Stress[N/mm^2]')
grid on
% sample 40_01b
force_pos_40_01b=abs(force_40_01b);
stress_40_01b=1000*force_pos_40_01b/initial_surface;
strain_40_01b=time_40_01b*strain_rate/initial_length;
figure(40)
plot(strain_40_01b,stress_40_01b)
title('Sample 40__01b - Ti tube filled with aluminum foam
(approximate density 567 kg/m^3)')
xlabel('Strain')
ylabel('Stress[N/mm^2]')
grid on
der_stress_40_01b=diff(stress_40_01b)/dt;
figure(41)
plot(der_stress_40_01b)
grid on
max_der_stress_40_01b=der_stress_40_01b(1);
% length(der_stress_40_01b)
```

```
for ii=2:733
    if der_stress_40_01b(ii)>max_der_stress_40_01b
        max_der_stress_40_01b=der_stress_40_01b(ii);
        pos_40_01b=ii;
    end
end
stress_40_01b=stress_40_01b(pos_40_01b:end);
stress_40_01b=stress_40_01b-stress_40_01b(1);
strain_40_01b=strain_40_01b(1:(end-pos_40_01b+1));
figure(42)
plot(strain_40_01b,stress_40_01b)
title('Sample 40__01b - Ti tube filled with aluminum foam
(approximate density 567 kg/m^3)')
xlabel('Strain')
ylabel('Stress[N/mm^2]')
grid on
% sample 40_01c
force_pos_40_01c=abs(force_40_01c);
stress_40_01c=1000*force_pos_40_01c/initial_surface;
strain_40_01c=time_40_01c*strain_rate/initial_length;
figure(43)
plot(strain_40_01c,stress_40_01c)
title('Sample 40__01c - Ti tube filled with aluminum foam
(approximate density 400 kg/m^3)')
xlabel('Strain')
ylabel('Stress[N/mm^2]')
grid on
der_stress_40_01c=diff(stress_40_01c)/dt;
figure(44)
plot(der_stress_40_01c)
grid on
max_der_stress_40_01c=der_stress_40_01c(1);
for ii=2:length(der_stress_40_01c)
    if der_stress_40_01c(ii)>max_der_stress_40_01c
        max_der_stress_40_01c=der_stress_40_01c(ii);
        pos_40_01c=ii;
    end
end
stress_40_01c=stress_40_01c(pos_40_01c:end);
stress_40_01c=stress_40_01c-stress_40_01c(1);
strain_40_01c=strain_40_01c(1:(end-pos_40_01c+1));
figure(45)
plot(strain_40_01c,stress_40_01c)
title('Sample 40__01c - Ti tube filled with aluminum foam
(approximate density 400 kg/m^3)')
```

```
xlabel('Strain')
ylabel('Stress[N/mm^2]')
grid on
% sample 40_02a
force_pos_40_02a=abs(force_40_02a);
stress_40_02a=1000*force_pos_40_02a/initial_surface;
strain_40_02a=time_40_02a*strain_rate/initial_length;
figure(46)
plot(strain_40_02a,stress_40_02a)
title('Sample 40__02a - Ti tube filled with aluminum foam
(approximate density 577 kg/m^3)')
xlabel('Strain')
ylabel('Stress[N/mm^2]')
grid on
der_stress_40_02a=diff(stress_40_02a)/dt;
figure(47)
plot(der_stress_40_02a)
grid on
max_der_stress_40_02a=der_stress_40_02a(1);
% length(der_stress_40_02a)1059
for ii=2:1059
    if der_stress_40_02a(ii)>max_der_stress_40_02a
        max_der_stress_40_02a=der_stress_40_02a(ii);
        pos_40_02a=ii;
    end
end
stress_40_02a=stress_40_02a(pos_40_02a:end);
stress_40_02a=stress_40_02a-stress_40_02a(1);
strain_40_02a=strain_40_02a(1:(end-pos_40_02a+1));
figure(48)
plot(strain_40_02a,stress_40_02a)
title('Sample 40__02a - Ti tube filled with aluminum foam
(approximate density 577 kg/m^3)')
xlabel('Strain')
ylabel('Stress[N/mm^2]')
grid on
% sample 40_02b
force_pos_40_02b=abs(force_40_02b);
stress_40_02b=1000*force_pos_40_02b/initial_surface;
strain_40_02b=time_40_02b*strain_rate/initial_length;
figure(49)
plot(strain_40_02b,stress_40_02b)
title('Sample 40__02b - Ti tube filled with aluminum foam
(approximate density 602 kg/m^3)')
xlabel('Strain')
```

```
ylabel('Stress[N/mm^2]')
grid on
der_stress_40_02b=diff(stress_40_02b)/dt;
figure(50)
plot(der_stress_40_02b)
grid on
max_der_stress_40_02b=der_stress_40_02b(1);
for ii=2:length(der_stress_40_02b)
    if der_stress_40_02b(ii)>max_der_stress_40_02b
        max_der_stress_40_02b=der_stress_40_02b(ii);
        pos_40_02b=ii;
    end
end
stress_40_02b=stress_40_02b(pos_40_02b:end);
stress_40_02b=stress_40_02b-stress_40_02b(1);
strain_40_02b=strain_40_02b(1:(end-pos_40_02b+1));
figure(51)
plot(strain_40_02b,stress_40_02b)
title('Sample 40__02b - Ti tube filled with aluminum foam
(approximate density 602 kg/m^3)')
xlabel('Strain')
ylabel('Stress[N/mm^2]')
grid on
% sample 40_02c
force_pos_40_02c=abs(force_40_02c);
stress_40_02c=1000*force_pos_40_02c/initial_surface;
strain_40_02c=time_40_02c*strain_rate/initial_length;
figure(49)
plot(strain_40_02c,stress_40_02c)
title('Sample 40__02c - Ti tube filled with aluminum foam
(approximate density 468 kg/m^3)')
xlabel('Strain')
ylabel('Stress[N/mm^2]')
grid on
der_stress_40_02c=diff(stress_40_02c)/dt;
figure(50)
plot(der_stress_40_02c)
grid on
max_der_stress_40_02c=der_stress_40_02c(1);
% length(der_stress_40_02c)
for ii=2:672
    if der_stress_40_02c(ii)>max_der_stress_40_02c
        max_der_stress_40_02c=der_stress_40_02c(ii);
        pos_40_02c=ii;
    end
```

```
end
stress_40_02c=stress_40_02c(pos_40_02c:end);
stress_40_02c=stress_40_02c-stress_40_02c(1);
strain_40_02c=strain_40_02c(1:(end-pos_40_02c+1));
figure(51)
plot(strain_40_02c,stress_40_02c)
title('Sample 40__02c - Ti tube filled with aluminum foam
(approximate density 468 kg/m^3)')
xlabel('Strain')
ylabel('Stress[N/mm^2]')
grid on
% 2)Samples filled with aluminum foam (nominal density 815
kg/m^3)
% sample 40_13a
force_pos_40_13a=abs(force_40_13a);
stress_40_13a=1000*force_pos_40_13a/initial_surface;
strain_40_13a=time_40_13a*strain_rate/initial_length;
figure(53)
plot(strain_40_13a,stress_40_13a)
title('Sample 40__13a - Ti tube filled with aluminum foam
(approximate density 827 kg/m^3)')
xlabel('Strain')
ylabel('Stress[N/mm^2]')
grid on
der_stress_40_13a=diff(stress_40_13a)/dt;
figure(54)
plot(der_stress_40_13a)
grid on
max_der_stress_40_13a=der_stress_40_13a(1);
% length(der_stress_40_13a)
for ii=2:663
    if der_stress_40_13a(ii)>max_der_stress_40_13a
        max_der_stress_40_13a=der_stress_40_13a(ii);
        pos_40_13a=ii;
    end
end
stress_40_13a=stress_40_13a(pos_40_13a:end);
stress_40_13a=stress_40_13a-stress_40_13a(1);
strain_40_13a=strain_40_13a(1:(end-pos_40_13a+1));
figure(55)
plot(strain_40_13a,stress_40_13a)
title('Sample 40__13a - Ti tube filled with aluminum foam
(approximate density 827 kg/m^3)')
xlabel('Strain')
ylabel('Stress[N/mm^2]')
```

```
grid on
%sample 40_13b
force_pos_40_13b=abs(force_40_13b);
stress_40_13b=1000*force_pos_40_13b/initial_surface;
strain_40_13b=time_40_13b*strain_rate/initial_length;
figure(56)
plot(strain_40_13b,stress_40_13b)
title('Sample 40__13b - Ti tube filled with aluminum foam
(approximate density 838 kg/m^3)')
xlabel('Strain')
ylabel('Stress[N/mm^2]')
grid on
der_stress_40_13b=diff(stress_40_13b)/dt;
figure(57)
plot(der_stress_40_13b)
grid on
max_der_stress_40_13b=der_stress_40_13b(1);
for ii=2:846
    if der_stress_40_13b(ii)>max_der_stress_40_13b
        max_der_stress_40_13b=der_stress_40_13b(ii);
        pos_40_13b=ii;
    end
end
stress_40_13b=stress_40_13b(pos_40_13b:end);
stress_40_13b=stress_40_13b-stress_40_13b(1);
strain_40_13b=strain_40_13b(1:(end-pos_40_13b+1));
figure(58)
plot(strain_40_13b,stress_40_13b)
title('Sample 40__13b - Ti tube filled with aluminum foam
(approximate density 838 kg/m^3)')
xlabel('Strain')
ylabel('Stress[N/mm^2]')
grid on
% sample 40_13c
force_pos_40_13c=abs(force_40_13c);
stress_40_13c=1000*force_pos_40_13c/initial_surface;
strain_40_13c=time_40_13c*strain_rate/initial_length;
figure(59)
plot(strain_40_13c,stress_40_13c)
title('Sample 40__13c - Ti tube filled with aluminum foam
(approximate density 760 kg/m^3)')
xlabel('Strain')
ylabel('Stress[N/mm^2]')
grid on
der_stress_40_13c=diff(stress_40_13c)/dt;
```

```
figure(60)
plot(der_stress_40_13c)
grid on
max_der_stress_40_13c=der_stress_40_13c(1);
% length(der_stress_40_13c)
for ii=2:735
    if der_stress_40_13c(ii)>max_der_stress_40_13c
        max_der_stress_40_13c=der_stress_40_13c(ii);
        pos_40_13c=ii;
    end
end
stress_40_13c=stress_40_13c(pos_40_13c:end);
stress_40_13c=stress_40_13c-stress_40_13c(1);
strain_40_13c=strain_40_13c(1:(end-pos_40_13c+1));
figure(61)
plot(strain_40_13c,stress_40_13c)
title('Sample 40__13c - Ti tube filled with aluminum foam
(approximate density 760 kg/m^3)')
xlabel('Strain')
ylabel('Stress[N/mm^2]')
grid on
%% 3)Empty titanium samples untreated
% sample E40_01
force_pos_E40_01=abs(force_E40_01);
stress_E40_01=1000*force_pos_E40_01/initial_surface;
strain_E40_01=time_E40_01*strain_rate/initial_length;
figure(63)
plot(strain_E40_01,stress_E40_01)
title('Sample E40__01 - Empty Ti tube untreated')
xlabel('Strain')
ylabel('Stress[N/mm^2]')
grid on
der_stress_E40_01=diff(stress_E40_01)/dt;
figure(64)
plot(der_stress_E40_01)
grid on
max_der_stress_E40_01=der_stress_E40_01(1);
for ii=2:795
    if der_stress_E40_01(ii)>max_der_stress_E40_01
        max_der_stress_E40_01=der_stress_E40_01(ii);
        pos_E40_01=ii;
    end
end
stress_E40_01=stress_E40_01(pos_E40_01:end);
stress_E40_01=stress_E40_01-stress_E40_01(1);
```

```
strain_E40_01=strain_E40_01(1:(end-pos_E40_01+1));
length(strain_E40_01)
length(stress_E40_01)
figure(65)
plot(strain_E40_01,stress_E40_01)
title('Sample E40__01 - Empty Ti tube untreated')
xlabel('Strain')
ylabel('Stress[N/mm^2]')
grid on
% sample E40_02
force_pos_E40_02=abs(force_E40_02);
stress_E40_02=1000*force_pos_E40_02/initial_surface;
strain_E40_02=time_E40_02*strain_rate/initial_length;
figure(66)
plot(strain_E40_02,stress_E40_02)
title('Sample E40__02 - Empty Ti tube untreated')
xlabel('Strain')
ylabel('Stress[N/mm^2]')
grid on
der_stress_E40_02=diff(stress_E40_02)/dt;
figure(67)
plot(der_stress_E40_02)
grid on
max_der_stress_E40_02=der_stress_E40_02(1);
for ii=2:705
    if der_stress_E40_02(ii)>max_der_stress_E40_02
        max_der_stress_E40_02=der_stress_E40_02(ii);
        pos_E40_02=ii;
    end
end
stress_E40_02=stress_E40_02(pos_E40_02:end);
stress_E40_02=stress_E40_02-stress_E40_02(1);
strain_E40_02=strain_E40_02(1:(end-pos_E40_02+1));
figure(68)
plot(strain_E40_02,stress_E40_02)
title('Sample E40__02 - Empty Ti tube untreated')
xlabel('Strain')
ylabel('Stress[N/mm^2]')
grid on
% sample E40_03
force_pos_E40_03=abs(force_E40_03);
stress_E40_03=1000*force_pos_E40_03/initial_surface;
strain_E40_03=time_E40_03*strain_rate/initial_length;
figure(69)
plot(strain_E40_03,stress_E40_03)
```

```
title('Sample E40__03 - Empty Ti tube untreated')
xlabel('Strain')
ylabel('Stress[N/mm^2]')
grid on
der_stress_E40_03=diff(stress_E40_03)/dt;
figure(70)
plot(der_stress_E40_03)
grid on
max_der_stress_E40_03=der_stress_E40_03(1);
for ii=2:634
    if der_stress_E40_03(ii)>max_der_stress_E40_03
        max_der_stress_E40_03=der_stress_E40_03(ii);
        pos_E40_03=ii;
    end
end
stress_E40_03=stress_E40_03(pos_E40_03:end);
stress_E40_03=stress_E40_03-stress_E40_03(1);
strain_E40_03=strain_E40_03(1:(end-pos_E40_03+1));
figure(71)
plot(strain_E40_03,stress_E40_03)
title('Sample E40__03 - Empty Ti tube untreated')
xlabel('Strain')
ylabel('Stress[N/mm^2]')
grid on
% 4)Empty titanium samples simulated foam
% sample ET40_01
force_pos_ET40_01=abs(force_ET40_01);
stress_ET40_01=1000*force_pos_ET40_01/initial_surface;
strain_ET40_01=time_ET40_01*strain_rate/initial_length;
figure(73)
plot(strain_ET40_01,stress_ET40_01)
title('Sample ET40__01 - Empty Ti tube untreated')
xlabel('Strain')
ylabel('Stress[N/mm^2]')
grid on
der_stress_ET40_01=diff(stress_ET40_01)/dt;
figure(74)
plot(der_stress_ET40_01)
grid on
max_der_stress_ET40_01=der_stress_ET40_01(1);
for ii=2:768
    if der_stress_ET40_01(ii)>max_der_stress_ET40_01
        max_der_stress_ET40_01=der_stress_ET40_01(ii);
        pos_ET40_01=ii;
    end
```

```
end
stress_ET40_01=stress_ET40_01(pos_ET40_01:end);
stress_ET40_01=stress_ET40_01-stress_ET40_01(1);
strain_ET40_01=strain_ET40_01(1:(end-pos_ET40_01+1));
length(strain_ET40_01)
length(stress_ET40_01)
figure(75)
plot(strain_ET40_01,stress_ET40_01)
title('Sample ET40__01 - Empty Ti tube untreated')
xlabel('Strain')
ylabel('Stress[N/mm^2]')
grid on
% sample ET40_02
force_pos_ET40_02=abs(force_ET40_02);
stress_ET40_02=1000*force_pos_ET40_02/initial_surface;
strain_ET40_02=time_ET40_02*strain_rate/initial_length;
figure(76)
plot(strain_ET40_02,stress_ET40_02)
title('Sample ET40__02 - Empty Ti tube untreated')
xlabel('Strain')
ylabel('Stress[N/mm^2]')
grid on
der_stress_ET40_02=diff(stress_ET40_02)/dt;
figure(77)
plot(der_stress_ET40_02)
grid on
max_der_stress_ET40_02=der_stress_ET40_02(1);
for ii=2:873
    if der_stress_ET40_02(ii)>max_der_stress_ET40_02
        max_der_stress_ET40_02=der_stress_ET40_02(ii);
        pos_ET40_02=ii;
    end
end
stress_ET40_02=stress_ET40_02(pos_ET40_02:end);
stress_ET40_02=stress_ET40_02-stress_ET40_02(1);
strain_ET40_02=strain_ET40_02(1:(end-pos_ET40_02+1));
figure(78)
plot(strain_ET40_02,stress_ET40_02)
title('Sample ET40__02 - Empty Ti tube untreated')
xlabel('Strain')
ylabel('Stress[N/mm^2]')
grid on
% sample ET40_03
force_pos_ET40_03=abs(force_ET40_03);
stress_ET40_03=1000*force_pos_ET40_03/initial_surface;
```

```
strain_ET40_03=time_ET40_03*strain_rate/initial_length;
figure(79)
plot(strain_ET40_03,stress_ET40_03)
title('Sample ET40__03 - Empty Ti tube untreated')
xlabel('Strain')
ylabel('Stress[N/mm^2]')
grid on
der_stress_ET40_03=diff(stress_ET40_03)/dt;
figure(80)
plot(der_stress_ET40_03)
grid on
max_der_stress_ET40_03=der_stress_ET40_03(1);
for ii=2:697
    if der_stress_ET40_03(ii)>max_der_stress_ET40_03
        max_der_stress_ET40_03=der_stress_E40_03(ii);
        pos_ET40_03=ii;
    end
end
stress_ET40_03=stress_ET40_03(pos_ET40_03:end);
stress_ET40_03=stress_ET40_03-stress_ET40_03(1);
strain_ET40_03=strain_ET40_03(1:(end-pos_ET40_03+1));
figure(81)
plot(strain_ET40_03,stress_ET40_03)
title('Sample ET40__03 - Empty Ti tube untreated')
xlabel('Strain')
ylabel('Stress[N/mm^2]')
grid on
% 6)Samples of only foam (nominal density 560 or 815 kg/m^3)
% sample 36_12b
force_pos_36_12b=abs(force_36_12b);
stress_36_12b=1000*force_pos_36_12b/initial_surface_f;
strain_36_12b=time_36_12b*strain_rate/initial_length;
figure(83)
plot(strain_36_12b,stress_36_12b)
title('Sample 36__12b - Sample of only foam(approximate density
484 kg/m^3)')
xlabel('Strain')
ylabel('Stress[N/mm^2]')
grid on
der_stress_36_12b=diff(stress_36_12b)/dt;
figure(84)
plot(der_stress_36_12b)
grid on
max_der_stress_36_12b=der_stress_36_12b(1);
for ii=2:length(der_stress_36_12b)
```

```
    if der_stress_36_12b(ii)>max_der_stress_36_12b
        max_der_stress_36_12b=der_stress_36_12b(ii);
        pos_36_12b=ii;
    end
end
stress_36_12b=stress_36_12b(pos_36_12b:end);
stress_36_12b=stress_36_12b-stress_36_12b(1);
strain_36_12b=strain_36_12b(1:(end-pos_36_12b+1));
length(strain_36_12b)
length(stress_36_12b)
figure(85)
plot(strain_36_12b,stress_36_12b)
title('Sample 36__12b - Sample of only foam(approximate density
484 kg/m^3)')
xlabel('Strain')
ylabel('Stress[N/mm^2]')
grid on
% sample 36_12c
force_pos_36_12c=abs(force_36_12c);
stress_36_12c=1000*force_pos_36_12c/initial_surface_f;
strain_36_12c=time_36_12c*strain_rate/initial_length;
figure(86)
plot(strain_36_12c,stress_36_12c)
title('Sample 36__12c - Sample of only foam(approximate density
544 kg/m^3)')
xlabel('Strain')
ylabel('Stress[N/mm^2]')
grid on
der_stress_36_12c=diff(stress_36_12c)/dt;
figure(87)
plot(der_stress_36_12c)
grid on
max_der_stress_36_12c=der_stress_36_12c(1);
for ii=2:length(der_stress_36_12c)
    if der_stress_36_12c(ii)>max_der_stress_36_12c
        max_der_stress_36_12c=der_stress_36_12c(ii);
        pos_36_12c=ii;
    end
end
stress_36_12c=stress_36_12c(pos_36_12c:end);
stress_36_12c=stress_36_12c-stress_36_12c(1);
strain_36_12c=strain_36_12c(1:(end-pos_36_12c+1));
length(strain_36_12c)
length(stress_36_12c)
figure(88)
```

```
plot(strain_36_12c,stress_36_12c)
title('Sample 36__12c - Sample of only foam(approximate density
544 kg/m^3)')
xlabel('Strain')
ylabel('Stress[N/mm^2]')
grid on
% sample 36_17a
force_pos_36_17a=abs(force_36_17a);
stress_36_17a=1000*force_pos_36_17a/initial_surface_f;
strain_36_17a=time_36_17a*strain_rate/initial_length;
figure(89)
plot(strain_36_17a,stress_36_17a)
title('Sample 36__17a - Sample of only foam(approximate density
1030 kg/m^3)')
xlabel('Strain')
ylabel('Stress[N/mm^2]')
grid on
stress_36_17a=stress_36_17a(713:end);
stress_36_17a=stress_36_17a-stress_36_17a(1);
strain_36_17a=strain_36_17a(1:(end-713+1));
length(strain_36_17a)
length(stress_36_17a)
figure(91)
plot(strain_36_17a,stress_36_17a)
title('Sample 36__17a - Sample of only foam(approximate density
1030 kg/m^3)')
xlabel('Strain')
ylabel('Stress[N/mm^2]')
grid on
% sample 36_17b
force_pos_36_17b=abs(force_36_17b);
stress_36_17b=1000*force_pos_36_17b/initial_surface_f;
strain_36_17b=time_36_17b*strain_rate/initial_length;
figure(92)
plot(strain_36_17b,stress_36_17b)
title('Sample 36__17b - Sample of only foam(approximate density
746 kg/m^3)')
xlabel('Strain')
ylabel('Stress[N/mm^2]')
grid on
stress_36_17b=stress_36_17b(611:end);
stress_36_17b=stress_36_17b-stress_36_17b(1);
strain_36_17b=strain_36_17b(1:(end-611+1));
% NB: 13308 is the point for which the slope start to be almost
constant (same consideration done for sample 36_17a)
```

```
length(strain_36_17b)
length(stress_36_17b)
figure(94)
plot(strain_36_17b,stress_36_17b)
title('Sample 36__17b - Sample of only foam(approximate density
746 kg/m^3)')
xlabel('Strain')
ylabel('Stress[N/mm^2]')
grid on
% sample 36_17c
force_pos_36_17c=abs(force_36_17c);
stress_36_17c=1000*force_pos_36_17c/initial_surface_f;
strain_36_17c=time_36_17c*strain_rate/initial_length;
figure(95)
plot(strain_36_17c,stress_36_17c)
title('Sample 36__17c - Sample of only foam(approximate density
679 kg/m^3)')
xlabel('Strain')
ylabel('Stress[N/mm^2]')
grid on
stress_36_17c=stress_36_17c(713:end);
stress_36_17c=stress_36_17c-stress_36_17c(1);
strain_36_17c=strain_36_17c(1:(end-713+1));
length(strain_36_17c)
length(stress_36_17c)
figure(97)
plot(strain_36_17c,stress_36_17c)
title('Sample 36__17c - Sample of only foam(approximate density
679 kg/m^3)')
xlabel('Strain')
ylabel('Stress[N/mm^2]')
grid on
%% 7)Comparisons
% Empty Ti samples untreated
figure(100)
plot(strain_E40_01,stress_E40_01)
title('Empty Ti samples untreated')
xlabel('Strain')
ylabel('Stress [N/mm^2]')
xlim ([0 0.054])
grid on
hold on
plot(strain_E40_02,stress_E40_02,'r')
plot(strain_E40_03,stress_E40_03,'k')
legend('Sample E40__01','Sample E40__02','Sample E40__03')
```

```
% Empty Ti samples simulated foam
figure(101)
plot(strain_ET40_01,stress_ET40_01)
title('Empty Ti samples simulated foam')
xlabel('Strain')
ylabel('Stress[N/mm^2]')
xlim([0 0.058])
grid on
hold on
plot(strain_ET40_02,stress_ET40_02,'r')
plot(strain_ET40_03,stress_ET40_03,'k')
legend('Sample ET40__01','Sample ET40__02','Sample ET40__03')
% Ti untreated Vs Ti simulated foam
figure(102)
plot(strain_E40_01,stress_E40_01)
title('Ti untreated Vs Ti simulated foam')
xlabel('Strain')
ylabel('Stress[N/mm^2]')
grid on
hold on
plot(strain_ET40_01,stress_ET40_01,'r')
legend('Sample untreated','Sample simulated foam')
close all
%Samples of only foam
figure(103)
title('Samples of only foam')
xlabel('Strain [%]')
ylabel('Stress[N/mm^2]')
grid on
hold on
plot(strain_36_17a,stress_36_17a,'m')
plot(strain_36_17b,stress_36_17b,'g')
plot(strain_36_17c,stress_36_17c)
plot(strain_36_12c,stress_36_12c,'k')
plot(strain_36_12b,stress_36_12b,'r')
legend('F_-815_-1a - Approximate density 1030 kg/m^3','F_-815_-
1b - Approximate density 746 kg/m^3','F_-815_-1c - Approximate
density 679 kg/m^3','F_-560_-1c - Approximate density 544
kg/m^3','F_-560_-1b - Approximate density 484 kg/m^3')
%Ti samples filled with aluminum foam of different approximate
density
figure(104)
title('Ti tubes filled with aluminum foam of different
approximate density')
xlabel('Strain [%]')
```

```
ylabel('Stress[N/mm^2]')
xlim([0 0.07])
grid on
hold on
plot(strain_40_01c,stress_40_01c,'k')
plot(strain_40_01b,stress_40_01b,'r')
plot(strain_40_01a,stress_40_01a)
plot(strain_40_13b,stress_40_13b,'g')
legend('FF_-560_-1c - Approximate density 400 kg/m^3','FF_-560_-
1b - Approximate density 567 kg/m^3','FF_-560_-1a - Approximate
density 712 kg/m^3','FF_-815_-1b - Approximate density 838
kg/m^3')
%Ti and Ti filled with metal foam of different density
figure(105)
title('Empty Ti tube Vs foam filled Ti tubes')
xlabel('Strain [%]')
ylabel('Stress[N/mm^2]')
xlim([0 0.07])
grid on
hold on
plot(strain_40_13b,stress_40_13b,'k')
plot(strain_40_13c,stress_40_13c,'r')
plot(strain_40_01a,stress_40_01a)
plot(strain_40_01b,stress_40_01b,'c')
% plot(strain_E40_01,stress_E40_01,'r')
plot(strain_ET40_01,stress_ET40_01,'g')
legend('FF_-815_-1b - Approximate density 838 kg/m^3','FF_-815_-
1c - Approximate density 760 kg/m^3','FF_-560_-1a - Approximate
density 712 kg/m^3','FF_-560_-1b - Approximate density 567
kg/m^3','ET_-2 - Empty Ti tube termically treated')
%% C) Stress/M
initial_length=0.07;                          %[m]
r=0.020;                                      %[m]
r_f=0.018;                                    %[m]
rho_Ti=4540;                                  %[kg/m^3]
rho_f1=838;                                   %[kg/m^3]
rho_f2=760;                                   %[kg/m^3]
rho_f3=712;                                   %[kg/m^3]
rho_f4=567;                                   %[kg/m^3]
V_Ti=pi*(r^2-r_f^2)*initial_length;
V_foam=pi*(r_f^2)*initial_length;
M_Ti=V_Ti*rho_Ti;
M_s1=V_Ti*rho_Ti+V_foam*rho_f1;
M_s2=V_Ti*rho_Ti+V_foam*rho_f2;
M_s3=V_Ti*rho_Ti+V_foam*rho_f3;
```

```
M_s4=V_Ti*rho_Ti+V_foam*rho_f4;
y_40_13b=stress_40_13b/M_s1;
y_40_13c=stress_40_13c/M_s2;
y_40_01a=stress_40_01a/M_s3;
y_40_01b=stress_40_01b/M_s4;
y_ET40_01=stress_ET40_01/M_Ti;
figure(106)
title('Empty Ti tube Vs foam filled Ti tubes')
xlabel('Strain [%]')
ylabel('Stress/M [N/(kg*mm^2)]')
xlim([0 0.07])
grid on
hold on
plot(strain_40_13b,y_40_13b,'k')
plot(strain_40_13c,y_40_13c,'r')
plot(strain_40_01a,y_40_01a)
plot(strain_40_01b,y_40_01b,'c')
plot(strain_ET40_01,y_ET40_01,'g')
legend('FF_-815_-1b - Approximate density 838 kg/m^3','FF_-815_-
1c - Approximate density 760 kg/m^3','FF_-560_-1a - Approximate
density 712 kg/m^3','FF_-560_-1b - Approximate density 567
kg/m^3','ET_-2 - Empty Ti tube termically treated')
```

Bibliography

[1] Lorna J. Gibson and Michael F. Ashby, *Cellular Solids*.

[2] M.F. Ashby, A.G. Evans, N.A. Fleck, L.J. Gibson, J.W. Hutchinson and H.N.G. Wadley, *Metal Foams: A Design Guide*.

[3] Andrea Villa, *Produzione di barre tubolari anti-intrusione laterali tramite schiumatura diretta.* Politecnico di Milano 2009-2010.

[4] Carolina Gabbiani, *Ottimizzazione di tubi anti-intrusione riempiti di schiuma d'alluminio.* Politecnico di Milano 2012-2013.

[5] John Banhart. *Manufacture, characterisation and application of cellular metals and metal foams.* Progress in materials science, 2001. Vol.46, pp.559-632.

[6] S. Iannace, L. Verdolotti, S. Colini, *La storia dei materiali cellulari nell'ingegneria.*

[7] M. Monno, V. Mussi and D. Negri, *Aluminum foam/steel interface formed during foaming process in air or argon flow: a micro structural comparison.*

[8] M. Monno, V. Mussi, D. Negri A. Rota and S. Valeri, *On the influence of some parameters in aluminum foam/steel substrate bonding.*

[9] M. Yan, Z. Fan, *Durability of materials in ,molten aluminum alloys*. 2001 Kluwer Academic Publishers.

[10] V. C. Srivastava, K. L. Sahoo. *Processing, stabilization and applications of metallic foams. Art of science.* Materials Science-Poland, Vol. 25, No. 3, 2007.

[11] I.W. Hall, M. Gauden, C.-J.Yu, *Crushing of aluminum closed cell foams: density and strain rate effects*. Scripta Materialia. 2000.Vol.43, pp.515-521.

[12] A. Paul, U. Ramamurty, *Strain rate sensitivity of a closed-cell aluminum foam*. Materials Science and Engineering, 2000.

[13] J. Banhart, J. Baumeister, *Deformation characteristics of metal foams.* Journal of materials science, 1998. Vol.33, pp. 1431-1440.

[14] Yishan Pan, Xiangfeng Lv, Zhonghua Li, Xiaochun Xiao, *Study on Dynamic Energy Absorption Ability of Closed-cell Si-Al Foam Metals Considering Geometry Size.* Tech Science Press, 2011, Vol.6, pp. 127-132.

[15] G.J. Davies, Shu Zhen. *Metallic foams: their production, properties and applications*. Journal of Materials Science, 1983. Vol.18, pp. 1899-1911.

[16] Chin-Jye Yu, Harald H. Eifert, John Banhart, Joachim Baumeister, *Metal foaming by a powder metallurgy method: Production, properties and applications.* Mat Res Innovat (1998) 2:181-188.

[17] J. Baumeister, J. Banhart, M. Weber, *Aluminium foams for transport industry*. Materials & Design, Vol. 18, Nos. 4/6, pp. 217-220, 1997.

[18] J. Baumeister, M. Monno, M. Goletti, V. Mussi and J. Weise, *Dynamic Behavior of Hybrid APM and Aluminum Foam Filled Structures*. Metals 2012, 2, 211-218.

[19] I.S. Golovin, H.R. Sinning, *Damping in some cellular metallic materials.* Journal of Alloys and Compounds.

[20] I.S. Golovin, H.-R. Sinning, J.Goken, W.Riehemann. *Fatigue-related damping in some cellular metallic materials.* Materials Science and Engineering.

[21] T. J. Lu, J. M. Ong, *Characterization of close-celled cellular aluminum alloys*. Journal of material science 36 (2001) 2773-2786.

[22] G. Bertolino, A. Gruttadauria, P. Arneodo Larochette, E.M. Castrodeza, A. Baruj, H.E. Troiani, *Cyclic pseudoelastic behavior and energy dissipation in as-cast Cu-Zn-Al foams of different densities.* Intermetallics 19 (2011) 577-585.

[23] J. Banhart, W. Brinkers, *Fatigue behavior of aluminum foam.* Journal of materials science letters 18 (1999) 617-619.

[24] N. Kulkarni, H. Mahfuz, S. Jeelani, L.A. Carlsson. *Fatigue crack growth and life prediction of foam core sandwich composites under flexural loading*. Composite Structures 59 (2003) 499-505.

[25] A.-M. Harte, N.A. Fleck and M.F. Ashby. *Fatigue failure of an open cell and a closed cell aluminum alloy foam.* Acta mater, Vol. 47, No. 8, pp. 2511-2524, 1999.

[26] B. Zettl, H. Mayer, S.E. Stanzl-Tschegg, H.P. Degischer. *Fatigue properties of aluminum foams at high numbers of cycles.* Materials Science and Engineering A292 (2000) 1-7.

[27] M.D. Ingraham, C.J. DeMaria, K.A. Issen, D.J. Morrison. *Low cycle fatigue of aluminum foam.* Materials Science and Engineering A504 (2009) 150-156.

[28] O.B. Olurin, N.A. Fleck and M.F. Ashby, *Indentation resistance of an aluminium foam.* Scripta mater, 43 (2000) 983-989.

[29] S. Golovin and H.-R. Shinning. *Special features of static and cyclic deformation of highly cyclic deformation of highly porous metallic materials.* Metal Science and Heat Treatment, Vol. 44, Nos. 5-6, 2002.

[30] D. Lehmus, C. Marschner, J.Banhart, *Influence of heat treatment on compression fatigue of aluminum foams.* Journal of materials science 37 (2002) 3447-3451.

[31] V.S. Deshpande, N.A. Fleck, *High strain rate compressive behaviour of aluminium alloy foams.* International Journal of Impact Engineering 24 (2000) 277-298.

[32] T. Mukai, T. Miyoshi, S. Nakano, H. Somekawa, K. Higashi, *Compressive response of a closed-cell aluminum foam at high strain rate.* Scripta Materialia, 2006. Vol.54, pp.533-537.

[33] C.M. Cady, G.T. Gray III, C. Liu, C.P. Trujillo, B.L. Jacquez, and T. Mukai, C*ompressive properties of a closed-cell aluminum foam as a function of strain rate and temperature*. Shock Compression of Condensed Matter, 2001.

[34] V. Mussi, *Schiume metalliche per la progettazione meccanica.*

[35] Lorenzo Peroni, Massimiliano Avalle, Marco Peroni. *The mechanical behaviour of aluminium foam structures in different loading conditions.* International Journal of Impact Engineering, 2008. Vol.35, pp.644–658.

[36] M. Kedadouche, M. Thomas, A. Tahan. *Empirical Mode Decomposition of Acoustic Emission for Early Detection of Bearing Defects.*

[37] M. Kedadouche, M. Thomas and A. Tahan, *Cyclostationarity applied to acoustic emission and development of a new indicator for monitoring bearing defects*. 3ième Congrès International sur l'Ingénierie des Risques Industriels, Reims, 3-5Juillet 2013.

[38] RILEM Technical Committee (Masayasu Ohtsu), *Recommendation of RILEM TC 212-ACD: acoustic emission and related NDE techniques for crack detection and damage evaluation in concrete.*

[39] Z. Rahman, H. Ohba, T. Yoshioka and T. Yamamoto*, Incipient damage detection and its propagation monitoring of rolling contact fatigue by acoustic emission*. Tribology International 42 (2009) 807–815.

[40] B. Muravin, *Acoustic Emission Method: History, Fundamentals and Applications.*

[41] Physical Acoustic Corporation, *PocketAE™ & Pocket AEwin User's Manual.* January 2007.

[42] Physical Acoustic Corporation, *AEwin™ SOFTWARE Installation, Operation and User's Reference Manual*, January 2007.

[43] *Instruction manual ultarprob 10000.*

[44] *http://www.muravin.com*

[45] *http://www.develop3d.com*

[46] *http://www.induceramic.com*

[47] *http://www.directindustry.com*

[48] *http://www.ecocatalysis.com*

[49] MTS System Corporation, *MTS 810 & 858 Material Testing Systems*, 2006.

[50] *http://www.betavib.com*

[51] *http://www.arcam.com*

[52] A. Bernasconi, M. Filippini, M. Giglio, A. Lo Conte, G. Petrone and M. Sangirardi, *Fondamenti di costruzione di macchine*, Seconda edizione McGraw-Hill, 2006.

[53] M. Huang, L. Jiang, P.K. Liaw, C.R. Brooks, R. Seeley, D.L. Klarstrom, *Using Acoustic Emission in Fatigue and Fracture Materials Research*, JOM November 1998, vol. 50, no. 11.

[54] Z. Kral, W. Horn and J. Steck, *Crack Propagation Analysis Using Acoustic Emission Sensors for Structural Health Monitoring Systems*, The Scientific World Journal Volume 2013, Article ID 823603, 13 pages.

[55] *http://asm.matweb.com*

[56] *http://www.matweb.com*

[57] M. Goletti, V. Mussi, P. Albertelli, A. Rossi, M. Monno and B. Schiavi, *Design, manufacture and performance evaluation of a machine tool ram based on a steel/foam sandwich structure*.